





Hyperglycaemia Induced Immunomodulation of Macrophages in Diabetic Vascular Disease

Thesis submitted for the degree of

Doctor of Philosophy in Cardiovascular Science

University of Oxford

Laurienne Edgar

Division of Cardiovascular Medicine

Radcliffe Department of Medicine

&

Green Templeton College

Supervisors: Professor Robin Choudhury

Dr Naveed Akbar

“Around here, however, we don’t look backwards for very long. We keep moving forward, opening up new doors and doing new things, because we're curious… and curiosity keeps leading us down new paths.”

- **Walt Disney**

Abstract

The work presented within this thesis investigated the mechanisms by which diabetic hyperglycaemia progresses atherosclerosis through long lasting, pro-inflammatory modulation of disease relevant cells, specifically monocytes and macrophages and their bone marrow precursors. The mechanisms by which diabetes increases atherosclerosis and cardiovascular disease risk even after glucose normalisation remains unknown. We hypothesised that: (i) hyperglycaemia altered cellular metabolism; (ii) these changes heighten pro-inflammatory responses, which remain altered after glucose normalisation and (iii) these increase atherosclerosis *in vivo*.

Chapter 1: reviews the background to the hypotheses tested in the following experimental chapters. It explains the context of the work within the broader scientific field. Overall chapter 1 summarises the current understanding of how diabetic hyperglycaemia affects atherosclerosis and the disease relevant monocytes and macrophages. It describes how monocyte and macrophage metabolism governs downstream inflammatory gene expression and function, and importantly its involvement in inducing long-term cellular memory through epigenetic modifications and chromatin structure alterations, in a process known as trained immunity.

Chapter 2 includes a full description of the materials and methods utilised within the following studies.

Chapter 3 investigates the effect of high glucose on monocyte and macrophage metabolism, gene expression and function. Metabolomics analysis revealed that high extracellular glucose altered monocyte metabolism, in particular increasing glycolysis. High glucose driven metabolic changes subsequently increased M1 macrophage pro-inflammatory gene expression, decreased M2 anti-inflammatory gene expression and altered functions relevant to atherosclerosis by increasing monocyte adhesion to endothelium and foam cell formation.

Chapter 4 explores how *in vivo* hyperglycaemia induces pro-inflammatory memory in monocytes and macrophages and progresses atherosclerosis, despite glucose normalisation. Bone marrow derived macrophages (BMDM) from diabetic mice, grown in physiological glucose retained heightened pro-inflammatory responses, indicating hyperglycaemic memory in the HSC niche and differentiated cells. Transplantation of diabetic bone marrow into normoglycaemic, *Ldlr*$^{-/-}$ mice increased plaque burden in the aortic root and plaque lipid content, compared to *Ldlr*$^{-/-}$ mice transplanted with non-diabetic bone marrow, confirming a memory effect.

Chapter 5 examines whether hyperglycaemic memory is induced in BM progenitors through long-lasting metabolically driven epigenetic marks that alter chromatin accessibility and transcription factor binding, similar to the mechanism underlying trained immunity in other contexts, and whether these changes are relevant to human disease and can potentially be pharmacologically altered. ATAC-seq analysis on diabetic and wild-type (WT) HSCs revealed altered chromatin structure, potentially mediated through the increased histone modifications H3K27ac and H3K4me3. These histone modifications were normalised by DCA, indicating a role for glycolysis. Motif analysis revealed that binding sites for the transcription factors PU.1, CTCF and RUNX1 were significantly enriched in peaks differentially present in diabetic HSC. Genes that were differentially expressed in macrophages laser capture microdissected from human atherosclerotic plaque macrophages displayed a disproportionately higher representation of RUNX1 controlled genes in plaques from patients with diabetes, indicating its role in human disease. RUNX1 inhibition prevented generation and downstream presentation of hyperglycaemic memory in BMDM in an *in vitro* model of hyperglycaemic memory.

Chapter 6 summarises the major findings, discusses study limitations and directions for future work. Diabetic hyperglycaemia altered HSC and macrophage metabolism to induce epigenetic changes which increased their pro-inflammatory responses and exacerbated atherosclerotic disease *in vivo*. PU.1, CTCF and RUNX1 have been previously associated to chromatin

priming elements. This novel demonstration of immunological memory may help to explain why targeting elevated glucose is often ineffective in reducing cardiovascular risk in diabetes.

Acknowledgements

All of the work presented here has been made possible through the generous funding provided by the British Heart Foundation 4-year doctoral training programme, the Dorothy Field Trust, and through the Novo Nordisk Foundation Tripartite Immunometabolism Consortium (TrIC) grant. I would also like to acknowledge the travel grants and additional funds offered by Green Templeton College, all of which were extremely valuable throughout my DPhil.

I would like to start by giving a nod to the people who inspired me to pursue a DPhil. Firstly, my placement year supervisor Dr Peter Maier and his lab Martina and Karo, who's crazy antics in the lab and excellent teaching skills inspired my love for scientific research. Secondly, my geek squad! Your incredible friendship, the many stimulating science conversations, dragging me through every revision period and lab practical sessions have put me where I am today.

For the duration of my DPhil, I have been fortunate to have been surrounded by an incredibly knowledgeable, friendly and talented group of lab colleagues. I have learnt so much from all of them and there have been countless laughs along the way. With a special note to Jillian, thank you for the lunchtime discussions, advice and too much boardgame fun over the last 4 years. And to Ellie, my Oxford twin! I couldn't have asked for a more hard-working and intelligent counterpart to have gone through this postgraduate journey with.

I would like to thank my primary supervisor, Professor Robin Choudhury, who truly has enabled my personal development. I am thankful for the continual dedication, time and guidance provided. His critical and innovative way of thinking have been an invaluable lesson and will continue to be instrumental in the way I tackle all future challenges. A huge thank you for allowing me to be a part of the TrIC Consortium, where I was able to meet so many interesting people, engage in fascinating discussions, see a completely different side of science and importantly eat some of the best food I've ever eaten!

Special thanks to my colleague, supervisor and dear friend, Dr Naveed Akbar. He has been the most fantastic teacher, with a huge knowledge of experimental techniques, inventive ways of tackling scientific questions and talent for communication and public outreach. He has been a source of positive energy, motivation and support which have motivated me through this DPhil. I will truly miss our daily interactions, our regular discussions on all things science and daily cake eating!

Thank you to my amazing family, Graham, Lorinda, Shené and Monique, who have always provided me with ongoing love and support and entertained my geeky science conversations without hesitation! Last but not least, I am so grateful to my husband, Will, for his support. encouragement and for caring for me through the highs and lows. I could not have done this without him or any of the people listed.

Collaborations & Contributions

Aspects of this work would not have been possible without the support and collaboration of many others. Listed below are the contributions others have made to this thesis:

- Generation of the streptozotocin, diabetic mouse model and animal husbandry were performed by Dr Ricardo Carnicer, Dr Klemen Ziberna and Ms Ritu Arya (Division of Cardiovascular Medicine, University of Oxford).
- Scanning Electron Microscopy images were acquired by Dr Errin Johnson (Dunn School of Pathology, University of Oxford)
- Bone marrow derived macrophage flow cytometry analysis was performed by Dr Thomas Cahill (Division of Cardiovascular Medicine, University of Oxford).
- Blood for peripheral blood monocyte isolation from healthy volunteers were obtained by Dr Mohammad Alkahilil (Division of Cardiovascular Medicine, University of Oxford).
- Non-targeted metabolomics mass spectroscopy was performed by Dr Héctor Gallart-Ayala and Dr Craig Wheelock (Karolinska Institute, Stockholm).
- The bone marrow transplant experiment, blood lipid measurements and flow cytometry analysis to assess engraftment were performed at The Jackson Laboratories, Bar Harbor, USA.
- Patients awaiting carotid endarterectomy were recruited and carotid plaques were collected freshly at time of surgery, by Dr Joshua Chai (Division of Cardiovascular Medicine, University of Oxford). Laser capture microdissection and RNA isolation were performed in collaboration.
- Sequencing (for the ATAC-seq) were performed by Dr Thomas Krausgruber (CeMM, Vienna). Microarray sequencing was performed by Cambridge Genomic Services (Department of Pathology, University of Cambridge). All sequencing data were analysed by Dr Madeleine Lemieux (Bioinfo, Canada).

Table of Contents

Abstract 3

Acknowledgements 6

Collaborations & Contributions 8

Table of Contents 9

Table of Figures 14

List Of Abbreviations 17

Chapter 1 : Introduction 20

Background – Global burden of diabetes and cardiovascular disease 21

Diabetic atherosclerosis and current therapeutic options 21

Atherosclerosis In Diabetes 23

Pathophysiological mechanisms of atherosclerosis and the effect of diabetes 23

Macrophages 27

Macrophage “classifications” 27

Effect of hyperglycaemia on monocytes and macrophages 30

Monocyte and macrophage metabolism 31

Innate Immune Cell Memory 40

Epigenetic memory and the role of cellular metabolism 40

Trained immunity 46

Hyperglycaemic memory 48
Hypotheses 52
Chapter 2 : Materials and Methods 53
Experimental Procedures 54
Animal handling and husbandry 54
Streptozotocin (STZ) induced diabetic mice model 54
Diabetic bone marrow (BM) transplant experiment 54
Experimental Model Details 56
Cell lines 56
BMDM Culture 56
BMDM *in vitro* memory model 59
Mouse monocyte isolation 61
HSC isolation 61
Human peripheral blood monocyte samples 62
Laser capture microdissection (LCM) isolation of human plaque macrophages 63
Method Details 64
Quantitative real-time polymerase chain reaction (qPCR) 64
Foam Cell Formation Assay 70
Monocyte and Macrophage Static Adhesion Assay 71
Immunofluorescence 73
Scanning Electron Microscopy (SEM) 74

Flow Cytometry 74
GLUT1 Surface Expression Assay 76
Aortic Root Plaque Analysis 76
Western Blot Analysis 77
Human Monocyte Metabolomics 79
Mouse Metabolite Measurements 79
Human Plaque Macrophage Microarray 80
Assay for Transposase Accessible Chromatin (ATAC)-sequencing 80
Statistical Analysis 82
Data Resources 83
Chapter 3 : Hyperglycaemic Effects on Macrophage Metabolism, Gene Expression and Function 84
Introduction 85
Hypothesis 85
Aims 85
Methods 85
Metabolism characterisation 86
GLUT1 surface expression 88
Succinate and α-KG measurements 88
BMDM gene expression 88
Static adhesion assay 88

Foam cell assay 89
Results 89
High glucose alters monocytes and macrophage metabolism 89
High glucose-induced metabolic changes alter macrophage gene expression 102
High glucose-induced metabolic changes alter monocyte and macrophage function 106
Summary 112
Discussion 112
Chapter 4 : Diabetic Hyperglycaemic Memory in Macrophages Increases Atherosclerosis 119
Introduction 120
Hypothesis 120
Aims 120
Methods 121
BMDM gene expression, static adhesion and foam cell formation assays 121
Diabetic bone marrow transplant and atherosclerosis *in vivo* 123
Results 125
Hyperglycaemic memory drives atherosclerosis 131
Summary 140
Discussion 140
Chapter 5 : Hyperglycaemia Induces Long Lasting Memory through Alterations in Chromatin Accessibility and Transcription Factor Binding 144
Introduction 145

Hypothesis 146

Aims 146

Methods 146

Western Blot 146

ATAC-seq 147

Laser Capture Microdissection (LCM) and Transcriptome Analysis of Human Carotid Plaque Macrophages 149

BMDM Memory Model 149

Results 150

Diabetic hyperglycaemic memory is induced in HSC and driven by changes in metabolism leading to epigenetic reprogramming 150

Summary 173

Discussion 173

Chapter 6 : Discussion 179

Conclusion 188

References 189

Table of Figures

Figure 1.1 **Pathogenesis of atherosclerosis**. 26

Figure 1.2 **Macrophage polarisation summary**. 29

Figure 1.3 **M1 macrophage metabolism overview**. 33

Figure 1.4 **Chromatin structure overview**..... 41

Figure 1.5 **Interplay between cellular metabolism and epigenome.** 43

Figure 1.6 **SIRT1, p66^{Shc} and Set 7 associated mechanisms of vascular hyperglycaemic memory.**..... 49

Figure 2.1 **BMDM differentiation and stimulation protocol.** 58

Figure 2.2 **In vitro BMDM hyperglycaemic memory model.** 60

Figure 2.3 **RNA Gel Electrophoresis.**..... 66

Figure 3.1 **Summary of metabolomics protocol.** 87

Figure 3.2 **Diabetic hyperglycaemia alters cellular metabolism.** 90

Figure 3.3 **BMDM characterisation**. 92

Figure 3.4 **High glucose alters mouse cell metabolism.** 95

Figure 3.5 **GLUT1 assay cell number titre**. 97

Figure 3.6 **BMDM GLUT1 surface expression**. 99

Figure 3.7 **High glucose increases succinate levels.** 101

Figure 3.8 **BMDM Housekeeping panel.** 103

Figure 3.9 **High glucose alters macrophage inflammatory gene expression**. 105

Figure 3.10 **Static adhesion monocyte time course.** 107

Figure 3.11 **DCA inhibits glucose altered monocyte adhesion to endothelial cells.** ... 109

Figure 3.12 **2-DG inhibits glucose altered monocyte adhesion to endothelial cells.** .. 110

Figure 3.13 **DCA reduces glucose enhanced BMDM foam cell formation.** 111

Figure 4.1 **Schematic of diabetic BMDM protocol.** 122

Figure 4.2 **Schematic on bone marrow (BM) transplant experimental design.** 124

Figure 4.3 **Streptozotocin-induced diabetic mouse model details.** 126

Figure 4.4 **Diabetic bone marrow derived macrophages display hyperglycaemic memory gene expression responses**. 128

Figure 4.5 **Bone marrow derived macrophages from diabetic mice manifest hyperglycaemic memory in functional responses.** 130

Figure 4.6 **Bone marrow transplant engraftment.** 132

Figure 4.7 **Bone marrow transplant lipid measurements.** 133

Figure 4.8 **Aortic root image quantification methods.** 135

Figure 4.9 **Example aortic root images.** 136

Figure 4.10 **Diabetic bone marrow drives atherosclerosis, after glucose normalisation.** 138

Figure 5.1 **ATAC-seq protocol and analysis pipeline.** 148

Figure 5.2 **HSC display increased glucose uptake and lactate production**. 151

Figure 5.3 **Epigenetic changes induced by high glucose or diabetes.** 153

Figure 5.4 **ATAC-seq Differential Peak Examples.** 158

Figure 5.5 **Top 3 transcription factor motifs identified in ATAC-seq HSC analysis**. ... 161

Figure 5.6 **LCM example carotid plaque sections.**..... 163

Figure 5.7 **RUNX1 target genes are over represented in diabetic plaque macrophages.** 166

Figure 5.8 **In vitro hyperglycaemic memory model.** 168

Figure 5.9 **RUNX1 and Glycolysis inhibition prevents generation of hyperglycaemic memory, in vitro**. 170

Figure 5.10 **RUNX1 inhibition normalises hyperglycaemic memory gene expression, in vitro.**..... 172

Figure 6.1 **Proposed mechanism underlying hyperglycaemic memory in haematopoietic stem cells (HSC) and macrophages.** 181

List Of Abbreviations

2-DG	2-deoxyglucose
ACAT	Acetyl-coenzyme A: cholesterol acyltransferase
ACC1	Acetyl-CoA carboxylase
ac-LDL	DiI-acetylated LDL
ACLY	ATP citrate lyase
ACO2	Aconitase 2
ARG1	Arginase-1
ATAC-seq	Assay for Transposase-Accessible Chromatin using sequencing
ATF-1	Cyclic AMP-dependent transcription factor-1
ATP	Adenosine triphosphate
B2M	β2 microglobulin
BCG	*Bacillus Calmette–Guérin*
BM	Bone marrow
BMDM	Bone marrow derived macrophages
CAD	Coronary artery disease
CARKL	Carbohydrate kinase-like protein
CD36	Cluster of differentiation 36
CD45	Lymphocyte common antigen
CD68	Cluster of differentiation 68
CD68-^{GFP}	C57BL/6-Tg (CD68-EGFP)1Drg/J mice
cDNA	Complementary DNA
ChrM	Mitochondrial chromosome
CIC	Mitochondrial citrate – malate exchanger
C_t	Threshold cycle
CTCF	CCCTC-binding factor (transcription factor)
CVD	Cardiovascular disease
DCA	Dichloroacetate
DE	Differentially expressed
DMEM	Dulbecco's Modified Eagle Medium
DNMT3b	DNA methyltransferase 3b
ECs	Endothelial cells
ERG	ETS-related gene
F-2,6-P_2	Fructose-2,6-bisphosphate
FA	Fatty acid
FACS	Flow associated cell sorting
FAD	Flavin adenine dinucleotide
FAO	Fatty acid oxidation
FBS	Foetal bovine serum
FDR	False discovery rate
Fe^{2+}	Iron
FIZZ1	Resistin-like molecule-α
FRiP	Fraction of reads in called peak
G-1,3-P_2	D-glycerate 1,3-bisphosphate
G-3-P	Glyceraldehyde 3-phosphate

G-6-P	Glucose-6-phosphate
GAL3	Galectin-3
GAPDH	Glyceraldehyde 3-phosphate dehydrogenase
GFP	Green fluorescent protein
GLUT	Glucose transporter
H3K27ac	Histone 3 acetylation at lysine reside 27
H3K4me3	Histone 3 trimethylation at lysine reside 4
HAT	Histone acetyltransferase
HbA1c	Haemoglobin A1c
HDAC	Histone deacetylase
HDL	High density lipoprotein
HDM	Histone demethylase
HIF1-α	Hypoxia-inducible factor-1α
HK	Hexokinase
HO-1	Haem oxygenase 1
HMT	Histone methyltransferase
HSC	Haematopoietic stem cells
ICAM-1	Intercellular adhesion molecule
IFNγ	Interferon γ
IL-1	Interleukin-1
IL-10	Interleukin-10
IL-1β	Interleukin-1β
IL-4	Interleukin-4
IL-6	Interleukin-6
iNOS	Inducible nitric oxide synthase
IRG1	Cis-aconitic acid decarboxylase
JMJD	JmjC domain demethylase
LCM	Laser capture microdissection
LDH	Lactate dehydrogenase
LDLR	Low density lipoprotein receptor
Ldlr$^{-/-}$	B6.129S7-Ldlrtm1Her/J mice
LPS	Lipopolysaccharide
LSD1	Lysine-specific HDM
MCP-1	Monocyte chemoattractant protein 1
M-CSF	Macrophage colony stimulating factor
MMe	Metabolically active macrophage
MSEA	Metabolite set enrichment analysis
mTOR	Mammalian target of rapamycin
NAD^+	Nicotinamide adenine dinucleotide
NADPH	Nicotinamide adenine dinucleotide phosphate
NEFA	Non-esterified fatty acids
NF-κB	Nuclear factor κ-light-chain-enhancer of activated B cells
NFE2L2	Nuclear factor erythroid-derived 2-like 2
NO	Nitric oxide
O-GlcNAc	N-acetylglucosamine
OPD	o-Phenylenediamine dihydrochloride reagent
ORO	Oil Red O

oxLDL	Oxidised low-density lipoprotein
OXPHOS	Oxidative phosphorylation
PBS	Phosphate buffered solution
PBS-T	PBS plus 0.1% tween-20
PEP	Phosphoenolpyruvate
PFA	Paraformaldehyde
PFK_2	Phosphofructokinase-2
PGE_2	Prostaglandin E2
PHD	Prolyl hydroxylase
PKM2	Pyruvate kinase M2
PPP	Pentose phosphate pathway
PU.1	ETS-family transcription factor
QC	Quality control
qPCR	Quantitative real-time polymerase chain reaction
RBC	Red blood cell
ROS	Reactive oxygen species
RPMI	Roswell Park Memorial Institute medium
RUNX1	Runt-related transcription factor 1
S7P	Sedoheptulose-7-phosphate
SD	Standard deviation
SDH	Succinate dehydrogenase
SEM	Scanning electron microscopy
sEND.1	Skin derived endothelial cells
SIRT1	Sirtuin 1
SLC3A2	Glutamine transporter
STZ	Streptozotocin
TCA	Tricarboxylic acid
TET	Ten-eleven demethylase
TLR4	Toll-like receptor 4
TNF-α	Tumour necrosis factor-α
TR	Thioredoxin reductase 1
TRIG	Triglycerides
$uPFK_2$	Ubiquitous phosphofructokinase-2
VCAM-1	Vascular cell adhesion protein -1
WT	Wild-type
YM1	Chitinase-like 3
ZNF263	Zinc finger protein 263 (transcription factor)
α-KG	α-ketoglutarate

Chapter 1 : Introduction

Background – Global burden of diabetes and cardiovascular disease

Diabetes is a chronic disease, caused by an inability of the pancreas to produce insulin (type 1) or failure of the body to react to insulin (type 2). Around 3.7 million adults within the United Kingdom are diagnosed with diabetes, and it is estimated that a further 1 million people are living with undiagnosed type 2 diabetes [1]. As the body is no longer able to regulate blood sugar levels, all forms of diabetes are characterised by episodes of hyperglycaemia, with a fasting plasma glucose ≥ 7 mM [2,3]. It is a serious condition that is estimated to have a global prevalence of over 425 million adults. With an aging population and increasing levels of obesity it is predicted to steadily rise by 48 % to 629 million by 2045 [3].

The primary cause of morbidity and mortality in patients with diabetes are cardiovascular diseases (CVDs) such as myocardial infarction and stroke, of which the major underlying cause is atherosclerosis [4]. Patients with diabetes show an increased atherosclerotic burden, indicating an accelerated form of the disease, which leads to a 2-3 times increased CVD risk and a 60 % higher risk of mortality from heart disease [5,6].

The incidence of CVDs differ between patients with type 1 and type 2 diabetes, principally due to key differences in their pathogenesis [7]. As type 1 diabetes is caused by an autoimmune destruction of the pancreatic β-cells it primarily presents during childhood and adolescence, resulting in hyperglycaemia occurring much earlier in life than those with type 2 diabetes [8]. In general, this results in CVD occurring much earlier in patients with type 1 diabetes compared to type 2. Type 1 diabetes also affects equal rate of women as men under the age of 40 years old [9], whereas women with type 2 diabetes are at a higher risk of CVD than men [10].

Diabetic atherosclerosis and current therapeutic options

Plaques in patients with diabetes often display more advanced and unstable traits such as a larger lipid rich necrotic core and inflammatory cell accumulation [11], however the exact mechanisms underlying this enhanced pathology have yet to be fully defined and hence

treatment options are often non-specific. Current treatment targets, recommended by both The National Institute for Health and Care Excellence [12] and American Diabetes Association [13], for diabetes and the reduction of associated complications focuses on lowering blood pressure, cholesterol and blood glucose.

Primary atherosclerotic and cardiovascular disease treatment for patients with or without diabetes are lipid lowering drugs such as the hydroxymethylglutaryl-CoA reductase inhibitors - statins. Statins reduce low density lipoprotein (LDL) cholesterol by ~50 % which reduced major adverse outcomes that are associated with atherosclerosis, for example myocardial infarction and stroke by ~30 % for moderate intensity statin and by ~45 % for high-intensity statin treatment [14]. Although statin treatment has been shown to significantly reduce diabetic cardiovascular events, patients with diabetes still exhibit an increased risk compared to those without diabetes [15,16]. This highlights that there are multiple factors that need to be targeted to treat diabetic CVD risk. It must be noted that recent reports have highlighted that statin treatment may be accelerating the development of diabetes [17,18], however there is still a net benefit for being on statins. It does highlight the complicated interplay between lipid lowering and glucose metabolism.

Hyperglycaemia is a cardinal feature in both type 1 and type 2 diabetes and is known to exacerbate atherosclerosis progression and retard plaque regression [19], and treatments have largely focused on lowering blood glucose. Intensive glucose lowering therapy is effective in patients with type 1 diabetes, but the effect is deferred for several years [20] and temporally disconnected from the control of blood glucose [21]. In type 2 diabetes, glucose reduction has no effect [22-24] or modest [25,26] effects on atherosclerosis-related vascular outcomes. The persisting risk of cardiovascular complications, even after glucose normalisation, have been termed the ‘legacy effect’ or ‘metabolic memory’ [22,23,27], but the underlying mechanisms remain unclear. Understanding this paradigm could aid in the development of novel therapeutics with increased efficacy in eradicating diabetic vascular complications and ultimately shift the way

diabetes and its associated complications are treated. In order to begin to unravel these, we must understand the mechanisms and cells involved in the development and progression of atherosclerosis; how hyperglycaemia affects these aspects and potential mechanisms of hyperglycaemic memory.

Atherosclerosis In Diabetes

Pathophysiological mechanisms of atherosclerosis and the effect of diabetes

Atherosclerosis is a chronic pathological inflammatory process of the arterial wall, found in medium and large arteries (Figure 1.1). It is thought that the primary event in atherosclerosis is endothelial damage, endothelial cell activation and dysfunction. This leads to an increased permeability allowing for the accumulation of LDL within the subendothelial layer [28]. LDL particles are retained through interactions with extracellular matrix proteins, chiefly proteoglycans. This has been shown to be a key event in atherogenesis as proteoglycan-bound LDL molecules have an increased susceptibility to atherogenic modifications, in particular oxidation (oxLDL) [29]. In various diabetic animal models hyperglycaemia alters proteoglycan expression levels to enhance their ability to capture LDL [30].

The accumulation and retention of oxLDL particles activates endothelial cells (ECs) and leads to an increase in surface adhesion molecule expression, such as vascular cell adhesion protein -1 (VCAM-1) and intercellular adhesion molecule-1 (ICAM-1); the release of chemokines, e.g. monocyte chemoattractant protein-1 (MCP-1), as well as pro-inflammatory cytokines e.g. interleukin-1β (IL-1β) and tumour necrosis factor-α (TNF-α) [31,32]. Vascular smooth muscle cells, ECs and macrophages are the atherosclerotic cells to produce pro-atherogenic cytokines such as IL-1β [33], with macrophages being the predominant cell to secrete TNF-α [34]. These factors recruit blood mononuclear leukocytes, in particular monocytes, to the site of injury. Increased expression of molecules that attract monocytes or augment their transmigration across the endothelial barrier will enhance plaque formation and

progression [35]. Long-term exposure of high glucose, both *in vitro* [36] and *in vivo* [37], have been shown to increase EC VCAM-1 expression and subsequent monocyte adhesion.

Once adhered, monocytes are able to transmigrate [38] into the sub-endothelial layer where they come into contact with multiple cytokines, such as macrophage colony stimulating factor (M-CSF), IL-1β and TNF-α, which enable them to differentiate into macrophages. The number of macrophages within the plaque and their inflammatory status has been directly linked to plaque burden and CVD risk [39,40]. Interestingly, diabetic hyperglycaemia pathologically affects macrophage plaque content and increased haemoglobin A1c (HbA1c), a measurement of glycated haemoglobin used to monitor glycaemic control from the previous three months, is associated with heightened plaque macrophage content; independent of other risk factors such as lipid levels [11].

Differentiated macrophages have an increased expression of various scavenger receptors, including cluster of differentiation 36 (CD36), scavenger receptor- A1 and scavenger receptor-B1. These receptors are key to the pathogenesis of atherosclerosis as they recognise modified LDL particles, after which macrophages internalise the particles [41]. An increased uptake of modified LDL particles causes macrophages to develop into foam cells [42]. Once internalised by the macrophage, modified-LDL is incorporated into an intracellular lysosome which possesses enzymes that hydrolyse the LDL into free cholesterol and free fatty acids. These are then transported to the cytosol where the enzyme acetyl-coenzyme A: cholesterol acyltransferase (ACAT) catalyses cholesteryl ester formation and storage. An accumulation of cholesteryl esters gives the foam cells their characteristic “foamy” appearance [43].

During atherosclerosis, macrophages are bombarded with modified-LDL particles and their cholesterol uptake and processing machinery can become overloaded. This can lead to the ineffective conversion of toxic free cholesterol to inert cholesteryl esters by ACAT and hence increased cytosolic concentrations of free cholesterol [44]. The toxicity of free cholesterol can lead to endoplasmic reticulum stress and an increased production of reactive oxygen species

(ROS) [45], which can mediate inflammatory responses and result in apoptotic cell death. In these circumstances, macrophages are able to recognise and clear apoptotic debris through the process of efferocytosis. It has been proposed that during atherosclerosis modified LDL outcompetes apoptotic debris for clearance and may be the reason for decreased efferocytosis efficiency seen in atherosclerosis [46]. The build-up of apoptotic bodies, from increased cell death and defective efferocytosis, leads to secondary necrosis of surrounding cells to form the necrotic core, also referred to as a lipid core due to the large, acellular, lipid rich region it represents [47,48]. A necrotic core is a prominent feature of an advanced atherosclerotic lesion. It is thought to represent a feature which is responsible for plaque instability and acute thrombosis [49]. Atherosclerotic plaques in diabetes have been shown to have an enlarged necrotic core [50].

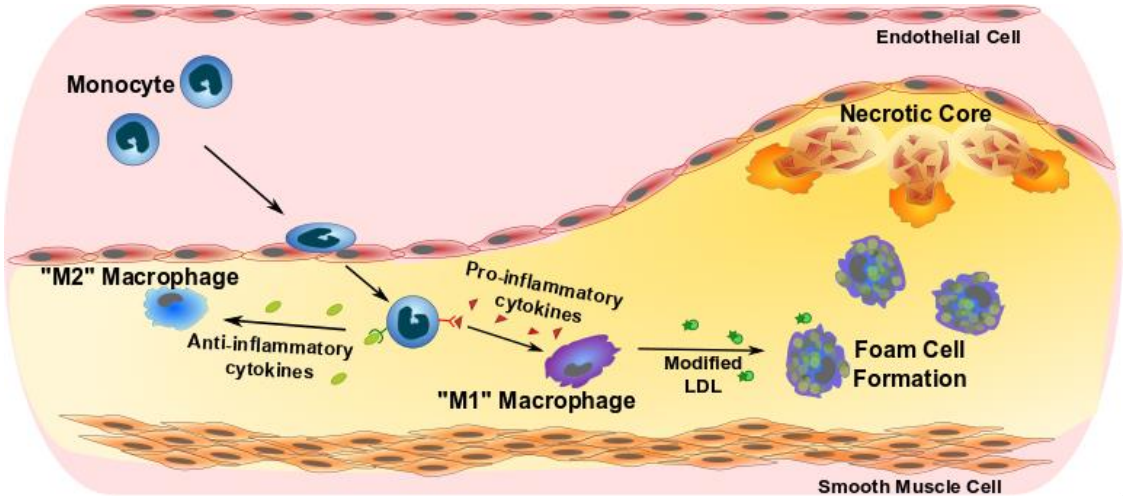


Figure 1.1 ***Pathogenesis of atherosclerosis****.*

Longitudinal illustration of a vessel, demonstrating the importance of monocytes and macrophages in the generation and progression of atherosclerosis. Circulating monocytes adhere to activated endothelium, transmigrate and in the contact of anti-inflammatory or pro-inflammatory cytokines differentiate into M2 and M1 macrophages, respectively. In the presence of modified low-density lipoproteins (LDL) macrophages form foam cells. In advanced plaques, cell death leads to the development of a necrotic core.

Macrophages

Macrophage "classifications"

As macrophages have been shown to play a critical role in all stages of atherosclerosis, they are widely regarded as therapeutic targets [44]. They are innate immune cells, heterogeneous in nature and display functional diversity and plasticity in response to their microenvironmental cues [51]. *In vitro*, macrophages have been subtyped by their opposing inflammatory phenotypes, namely a "pro-inflammatory" M1 or "tissue-reparative" M2 state and as summarised in Figure 1.2. M1 macrophages are polarised in the presence of inflammatory cytokines such as interferon-γ (IFNγ), TNF-α, interleukin-1 (IL-1), interleukin-6 (IL-6) or the activation of toll-like receptor 4 (TLR4) with lipopolysaccharide (LPS). Whereas, the M2 phenotype occurs in the presence of anti-inflammatory associated cytokines such as interleukin-4 (IL-4) or interleukin-13. Each phenotype is associated with the induction of opposing and specific inflammatory gene expression and functions, for example M1 polarisation increases expression of IL-6, iNOS and TNF-α and M2 expressing arginase-1 (ArgI) or murine specific resistin-like molecule-α (FIZZ1) and chitinase-like 3 (YM1) [52,53].

As well as specific gene and protein expression patterns, M1 and M2 macrophages are associated with opposing functional responses as well. M1 macrophages are induced through specific toll-like receptor activation, such as LPS activating TLR4, or similarly through recognition of bacteria by pattern recognition receptors [54]. M1 responses are therefore often associated with intracellular killing methods of bacterial pathogens, such as acidified phagosomal elimination [55]. M2 macrophage responses are grouped together due to their ability to antagonise inflammatory responses. IL-4 stimulated M2 macrophages have been described to be involved in killing of parasitic pathogens [56]. This is again different to interleukin-10 (IL-10) stimulated M2 macrophages, which are involved in immunoregulation responses and reparative matrix deposition [57]. Factors that alter the M1 / M2 macrophage balance can consequently have a dramatic effect on overall inflammation and its resolution.

Plaque macrophages come into contact with a wide variety of stimuli and therefore their phenotypes and functions are likely to be highly complex. Other than the “typical” M1 and M2 macrophage phenotypes, other subsets described include M(Hb), Mhem or Mox which occur in the presence of haemoglobin, haem or oxidised phospholipids respectively [58]. Like the M1 and M2 subsets, these have distinct intracellular signalling pathways, cytokine and gene expression profile, these are summarised on Figure 1.2.

Recent proteomic analyses of macrophage cell membranes following exposure of cells to high levels of glucose, palmitate and insulin have also revealed a further pro-inflammatory subset of macrophages termed metabolically active (MMe). These are specifically described in adipose tissue [59,60], however is important as it not only emphasises (i) the need to consider other functional macrophage phenotypes without being restricted by the M1 and M2 paradigm [54], and (ii) demonstrates how the availability of glucose and other metabolic factors are able to drive a distinct macrophage phenotype.

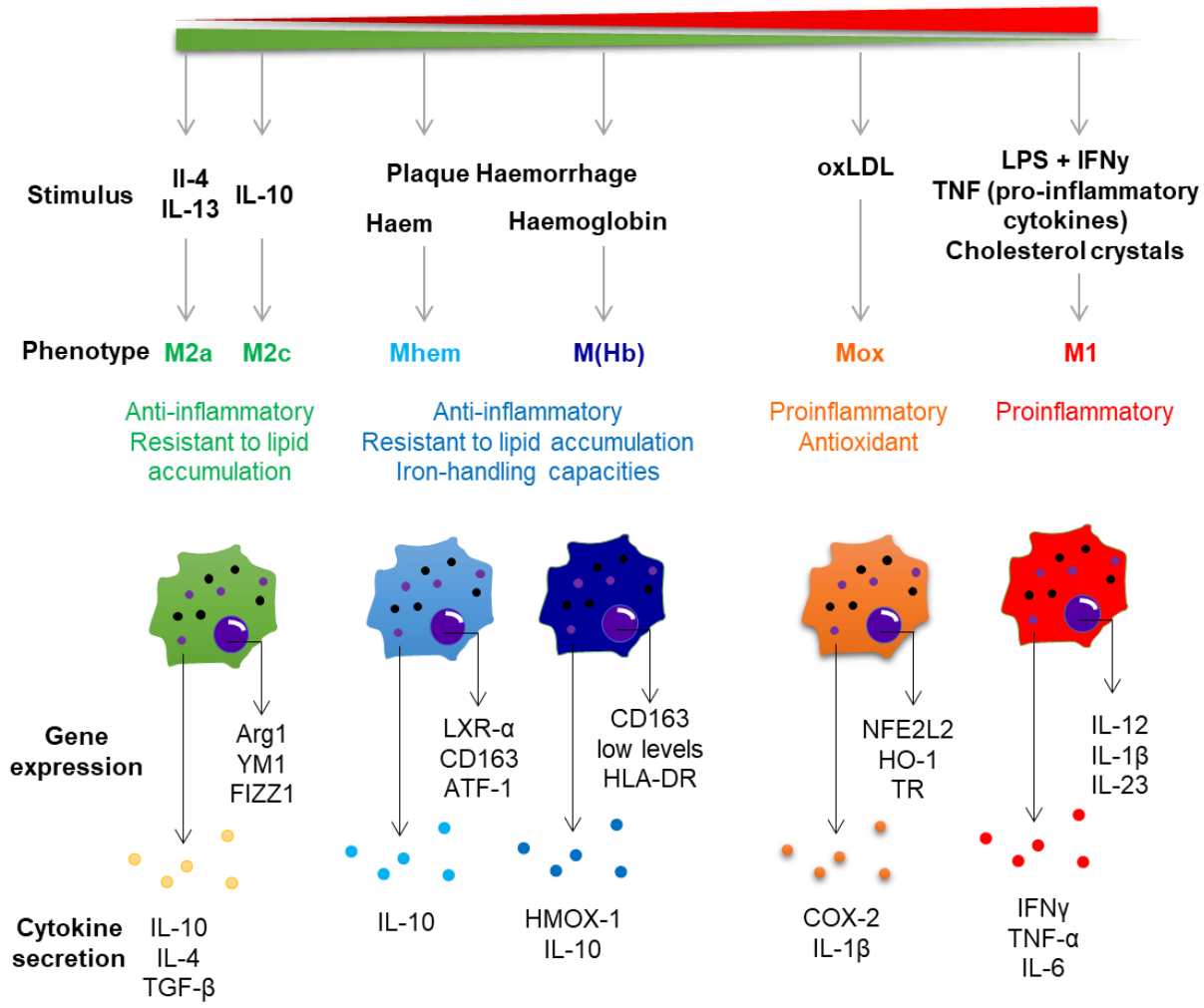


Figure 1.2 ***Macrophage polarisation summary****.*

Macrophages are polarised into a reparative associated M2 phenotype in the presence of interleukin - 4 (IL-4), -13 (IL-13) or - 10 (IL-10). In contrast, in the presence of lipopolysaccharide (LPS) and interferon-γ (IFNγ) or tumour necrosis factor-α (TNF-α) they polarise into pro-inflammatory associated M1 macrophages. Stimuli present in atherosclerotic plaques are also able to cause differentiation into distinct phenotypes, including Mhem, M(Hb) or Mox which occur in the presence of haem, haemoglobin or oxidised LDL (oxLDL), respectively. Each have a distinct profile of secreted cytokines and gene expression. Figure adapted from Martinez, F. O. and Gordon, S [54] and Chinetti-Gbaguidi, G.et al. [58].

Effect of hyperglycaemia on monocytes and macrophages

There is strong evidence that long-term hyperglycaemia leads to low-grade, chronic inflammation and this underlies the development of diabetic cardiovascular complications and can be seen by the inflammatory status of diabetic monocytes and macrophage [61,62]. Mechanisms which stimulate an inflammatory environment within and around an atherosclerotic lesion, such as increasing the M1 macrophage content, promote accelerated atherosclerosis. This may be a mechanism by which diabetes is enhancing atherogenesis.

The number of monocytes and macrophages and their inflammatory status have been shown to influence atherosclerosis [44]. Patients with type 2 diabetes have been shown to have an increased number of circulating monocytes [63], which are primed to a more pro-inflammatory state. Monocytes in diabetes express higher levels of pro-inflammatory cytokines such as TNF-α and IL-6 [64]. This is corroborated in murine studies, which show increased levels of circulating, pro-inflammatory associated Ly6-C^{hi} monocytes in the presence of diabetes [65]. Monocytes from type 2 diabetic patients, both *ex vivo* [66] and *in vivo* [67], have also been shown to have increased inflammasome activity which leads to increased IL-1β and interleukin-18 secretion. This pro-inflammatory state is not only seen at a monocyte level, but atherosclerotic plaques from diabetic mice and humans also show an increased M1 macrophage content [11,68]. Diabetes, furthermore, promotes the M1 phenotype in murine macrophages and attenuates the ability for IL-4 to stimulate an M2 phenotype [19,69].

Diabetes influences monocyte and macrophage function. Monocytes isolated from patients with both type 1 and type 2 diabetes exhibit an increased adhesion to activated endothelial cells [70,71]. It is important to note, that one study, in particular, showed that poor glycaemic control was directly linked to higher binding of diabetic monocytes to endothelial cells [72]. Diabetes also affects macrophage phenotype and function in relation to wound healing. Macrophages within wounds should be predominately anti-inflammatory, however pro-

inflammatory macrophages dominate diabetic wounds, which leads to impaired wound healing and adversely impact amputations associated with diabetic peripheral vascular disease [73].

Taken together, these findings highlight a key role of diabetic hyperglycaemia in activation of innate immune cells. Diabetes is often accompanied by other co-morbidities such as hyperlipidaemia, high blood pressure and obesity-driven inflammation. In order to determine the precise role of hyperglycaemia in perpetuating the pro-inflammatory and disease modifying cellular phenotypes described, experimental *in vitro* cell culture studies are used. Multiple studies have highlighted the role of high glucose in inducing pro-inflammatory gene expression in monocytes [74-76] as well as the adhesion of THP-1 monocyte cell line to endothelial cells [77]. High glucose has also been shown to increase the lectin-like oxidized LDL receptor-1 in human monocyte-derived macrophages, which in turn enhanced foam cell formation [78]. The mechanisms underlying the enhanced pro-inflammatory responses caused by a high glucose environment require further investigation. Understanding pathways that regulate monocyte and macrophage activation status may provide further insight.

Monocyte and macrophage metabolism

In monocytes and macrophages, recent reports describe how cellular energetic pathways are governed by an interplay between cell-intrinsic and environmental stimuli which, in turn, dramatically affect immune-related function, cell phenotype and gene expression [79]. Macrophage metabolic studies have focused on how opposing altered metabolic profiles are required for M1 and M2 polarisation. M1 macrophages rely on glucose as a primary metabolic substrate and shift to an aerobic glycolytic profile, which mirrors the Warburg effect seen in cancer cells. This is in stark contrast to M2 cells which primarily utilise fatty acid oxidation (FAO) and oxidative phosphorylation (OXPHOS) to generate a long-term adenosine triphosphate (ATP) production solution for sustained, tissue reparative and anti-inflammatory associated responses. Reviewed below are the metabolic changes involved in M1 pro-inflammatory macrophage polarisation and responses.

M1 macrophage polarisation, just like the Warburg effect, involves an increase in glycolysis, a dysregulated tricarboxylic acid (TCA) cycle, an increase in the pentose phosphate pathway (PPP), nucleotide synthesis (purine and pyrimidine metabolism) and increased fatty acid (FA) synthesis (summarised in Figure 1.3) [80].

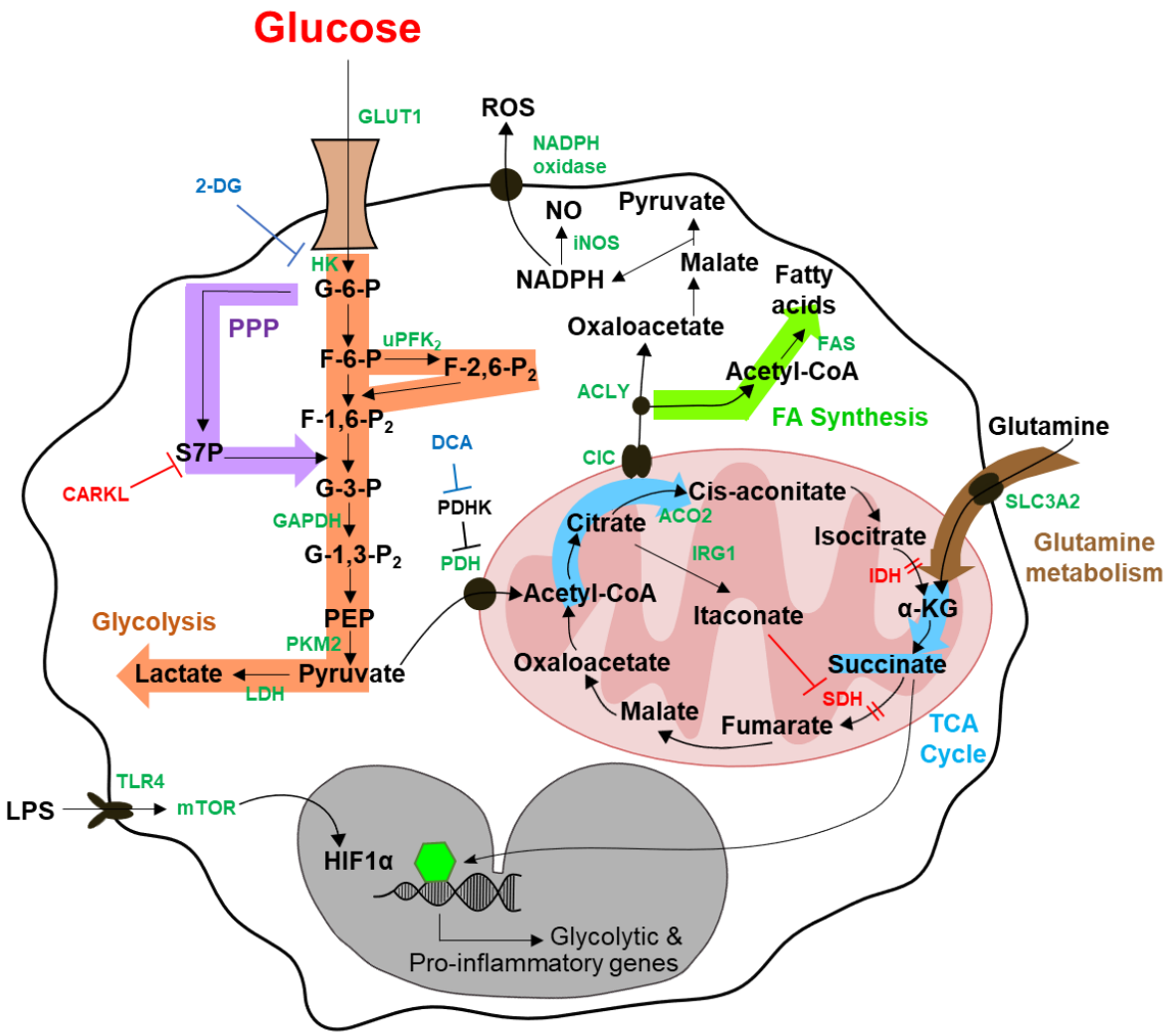


Figure 1.3 ***M1 macrophage metabolism overview****.*

M1 macrophage is characterised by a metabolic shift that increases the conversion of glucose to lactate through glycolysis (orange) and increased flux through the pentose phosphate pathway (PPP, purple). Lipopolysaccharide (LPS) decreases carbohydrate kinase-like protein (CARKL) expression, subsequently increasing sedoheptulose-7-phosphate (S7P) levels, which drive glycolytic flux. M1 macrophages also display a broken tricarboxylic acid (TCA) cycle (blue) at isocitrate dehydrogenase (IDH) and succinate dehydrogenase (SDH) leading to the accumulation of citrate and succinate. Accumulated citrate is either converted by cis-aconitic acid decarboxylase (IRG1) into itaconate to inhibit SDH or exported out the mitochondria into the cytoplasm through citrate-malate exchanger (CIC). Here it aids in increase fatty acid (FA) synthesis, nitric oxide (NO) from inducible nitric oxide synthase

(iNOS) and reactive oxygen species (ROS) from nicotinamide adenine dinucleotide phosphate (NADPH) oxidase. Succinate can stabilise hypoxia inducible factor 1-α (HIF1-α) to induce pro-inflammatory gene expression and expression of glycolytic enzymes to further upregulate glycolysis. HIF1 α is further upregulated by LPS – toll-like receptor 4 (TLR4) driven mechanistic target of rapamycin (mTOR) activation. Pharmacological inhibitors of glycolysis can be used to interrogate macrophage metabolism, like 2-deoxyglucose (2-DG), which inhibits hexokinase (HK) or dichloroacetate (DCA) which pyruvate dehydrogenase kinase (PDHK) to remove its inhibition on pyruvate dehydrogenase (PDH) and increase lactate conversion into acetyl-coA and into the TCA cycle. Figure adapted from Geeraerts, X. et al. [81]

Through integrated metabolomics and genomic studies, it has been shown that LPS stimulation changes the expression of various glycolytic enzymes that leads to the accumulation of specific metabolites. LPS stimulation increases the expression of the glucose transporter (GLUT) isoform primarily used by macrophages, GLUT1, which leads to an increase in glucose uptake. The role for GLUT1 in the development and progression of atherosclerosis is unclear, as atherosclerotic prone *Ldlr*$^{-/-}$ mice transplanted with GLUT1 overexpressing bone marrow see an alteration in metabolic activity, but no effect on atherosclerotic burden [82]. This in stark contrast to another study showing atherosclerotic prone *ApoE*$^{-/-}$ mice transplanted with GLUT1 knockout bone marrow show the expected decreased glucose uptake and also display slowed atherosclerosis progression and decreased plaque burden [83]. It is important to note that macrophages that genetically overexpress GLUT1 show an increase in glucose uptake, increased glycolytic flux and importantly show an increase in M1 associated proinflammatory responses, such as heightened IL-6 and TNF-α gene expression and secretion [84]. This illustrates the key link between metabolic phenotype and cellular inflammatory state, even in the absence of stimulation. The first rate limiting enzyme, hexokinase (HK), is also upregulated and allows for the heightened irreversible conversion of glucose to glucose-6-phosphate (G-6-P). Increased G-6-P levels aid in increasing flux through the glycolytic and PPP. The PPP pathway provides metabolites required for purine and pyrimidine metabolism, which aid in increasing nucleotide synthesis required for biosynthesis in the activated cells. The PPP pathway is an oxidative branch of the glycolysis pathway, that also aids in the production of nicotinamide adenine dinucleotide phosphate (NADPH). NADPH predominantly is required to maintain the cellular redox state and, in an M1 macrophage setting, is utilised by iNOS to produce NO and NADPH oxidase to produce ROS for pathogen killing. The final aspect of aerobic glycolysis that is increased is the expression of lactate dehydrogenase (LDH), which causes a rise in pyruvate conversation to lactate. The build-up of lactate is a key hallmark of the Warburg effect.

It has been shown that macrophage activation by LPS and M1 polarisation are dependent on glycolysis, as glycolytic inhibition prevents their inflammatory responses. Hence, a lot of work has gone into studying the molecular pathways that control this metabolic switch. LPS treated macrophages activate mammalian target of rapamycin (mTOR), through TLR-4 activation, which boosts expression and activity of hypoxia-inducible factor-1α (HIF1-α). HIF1-α is a particularly significant protein in controlling macrophage metabolic profile, as it not only promotes the switch to glycolysis under low oxygen conditions, but also similarly is activated in macrophages under normoxic conditions to promote glycolysis. For example, HIF1-α increases expression of its target genes which include glycolytic machinery like GLUT1 and LDH as well as inflammatory genes such as IL-1β.

M1 polarisation causes a switch from liver isoform of phosphofructokinase-2 (PFK_2) to the more active, ubiquitous PFK_2 ($uPFK_2$) isoform. This leads to an increased build-up of the metabolite fructose-2,6-bisphosphate (F-2,6-P_2), which helps to drive forward glycolytic flux. Additionally, it has been noted that LPS drives downregulation of the enzyme carbohydrate kinase-like protein (CARKL), leading to a build-up of the PPP metabolite sedoheptulose-7-phosphate (S7P), which again aids in driving glycolytic flux. Although not fully understood, it has been shown that the genetic silencing of CARKL increases glycolysis (increase in extracellular acidification rate) and decreases oxygen consumption upon LPS stimulation, highlighting its role as a metabolic switch. This is in direct contrast to cells that have been manipulated to overexpress CARKL, which have an increased oxygen consumption and a dampened inflammatory response to LPS [85].

Another enzyme linked to the mechanism linking inflammation and metabolism is glyceraldehyde 3-phosphate dehydrogenase (GAPDH). GAPDH is predominately considered to be a glycolytic enzyme that catalyses the conversion of glyceraldehyde 3-phosphate (G-3-P) to D-glycerate 1,3-bisphosphate (G-1,3-P_2), however it has recently been described to have post-transcriptional regulatory properties. GAPDH can translocate to the nucleus and bind to

TNF-α mRNA [86] and prevent downstream translation. However, when glycolysis is increased after activation, GAPDH is required and no longer binds to TNF-α mRNA and therefore the repression is removed, and TNF-α expression levels increase. GAPDH has also been shown to repress expression of other inflammatory cytokines, such as IFNγ and IL-6, and may be doing so via a similar mechanism [87].

While the glycolytic pathway and PPP are increased, M1 polarisation also leads to the TCA cycle being broken at two points, overall decreasing OXPHOS, and the downregulation of FAO. The disrupted TCA cycle leads to the accumulation of the metabolites citrate, itaconate and succinate. Citrate has been shown to be a significant metabolite involved in innate cell metabolic reprogramming and downstream macrophage effector functions [88]. The accumulation of citrate is thought to be due to LPS driven inhibition of isocitrate dehydrogenase (IDH), which normally catalyses the conversion of isocitrate to α-ketoglutarate (α-KG), but its decreased presence leads to an accumulation of citrate. From here, citrate takes 2 paths: exportation out of the mitochondria or irreversible conversion into the metabolite itoconate. Firstly, LPS, IFNγ and TNF-α, through NF-κB signalling, have been shown to increase the mitochondrial citrate – malate exchanger (CIC; solute carrier family 25 A1; SLC25A1) expression, which leads to increased exportation of citrate to the cytosol in exchange for malate. Once in the cytosol, citrate is able to indirectly regulate HIF1-α-regulated gene expression by inhibiting HIF asparaginyl hydroxylase, which prevents the detrimental hydroxylation of HIF1-α to increase its stability and activity [89]. As previously mentioned, HIF1-α regulated genes include inflammatory genes as well as glycolytic enzymes which aid in driving aerobic glycolysis.

Cytosolic citrate is also broken back down into its precursors oxaloacetate and acetyl-CoA by ATP citrate lyase (ACLY), an enzyme whose expression is also positively regulated by LPS and IFNγ stimulation. Another role for ACLY is the transcriptional regulation of genes encoding for glycolytic machinery, such as LDH and HK. The genetic silencing of ACLY has been shown

to decrease expression of its regulated genes and glucose consumption. Cytosolic oxaloacetate is involved in the production of inflammatory macrophage ROS, as it is converted into malate and then pyruvate by malic enzyme, with NADPH as the by-product generated. NADPH is importantly required in the future generation of NO by iNOS and NADPH oxidase derived ROS. iNOS-derived NO is also able to act as a co-factor for nitrosylation, notably nitrosylation of electron transport chain complexes have been shown to regulate them and aid in decreasing OXPHOS further [90,91]. Cytosolic citrate derived acetyl-CoA is essential for fatty acid synthesis. Acetyl-CoA can be irreversibly converted by acetyl-CoA carboxylase (ACC1) to malonyl-CoA and further adapted into fatty acids, the predominant one being prostaglandin E2 (PGE_2). The generated lipids help with the increased biosynthetic demand of an activated macrophage, and as in the case of PGE_2, can act as potent inflammatory mediators in their own right [92]. Acetyl-CoA is not only a *de novo* lipogenesis substrate, but is a key regulating co-factor for protein acetylation, importantly histone acetylation, which epigenetically affects gene expression. Histone modifications and epigenetics are described fully in a following "Innate Immune Cell Memory" section, but a noteworthy mention here is that histone acetylation has been shown to be important in macrophage IL-6 production and downstream inflammation [93]. These data highlight the key role citrate has in linking glucose metabolism, fatty acid synthesis and epigenetic reprogramming.

Other than exportation out of the mitochondria, the increased levels of mitochondrial citrate can be converted into cis-aconitate by aconitase 2 (ACO2) and then into itaconate by cis-aconitic acid decarboxylase (CAD or IRG1). IRG1 is one of the most highly induced enzymes in LPS and IFNγ activated macrophages and leads to the large accumulation of itaconate. Recently, itaconate has emerged as a regulator of macrophage anti-inflammatory responses by enabling the anti-inflammatory transcription factor nuclear factor erythroid 2–related factor 2 [94]. Although anti-inflammatory in nature, with relevance to M1 inflammatory responses, *Irg1*$^{-/-}$ bone marrow derived macrophages (BMDM) stimulated with LPS show decreased itaconate

and succinate levels [95], highlighting itaconate inhibitory role on succinate dehydrogenase (SDH) which leads to increased succinate levels.

Succinate has been shown to be increased in diabetes, obesity [96,97] and inflammation [98], highlighting its potential pathological role. LPS stimulated macrophages show a significant increase in succinate levels, partially caused by a lack of SDH activity but it has also been proposed to be due to an increased glutamine metabolism. Glutamine is taken up into the cell through the glutamine transporter (solute carrier family 3 A2; SLC3A2) and converted through anaplerosis into α-KG and then into succinate. The ratio of α-KG to succinate produced through glutaminolysis is important, as a high α-KG : succinate ratio promotes M2 macrophage polarisation, whereas a low ratio intensifies the pro-inflammatory M1 responses [99]. The accumulation of succinate in M1 macrophages can then exert pro-inflammatory downstream effects firstly, through acting as a rate-limiting substrate for protein succinylation. Succinylation is the addition of a succinyl group to protein lysine residues, although the effect of this modification on protein function is not fully understood, one recent example has illustrated that an increase in succinylation of the glycolytic enzyme pyruvate kinase M2 (PKM2, the enzyme responsible for the conversion of phosphoenolpyruvate (PEP) to pyruvate), after LPS stimulation, leads to an increase in its tetramer to dimer formation. This structural change increases its nuclear translocation, where it is able to affect inflammatory gene expression, for example by forming a transcriptional complex with HIF1-α which directly binds to the IL-1β promoter to drive expression [100] or by phosphorylating signal transducer and activator of transcription 3, which promotes IL-6 and IL-1β expression [101,102]. Of particular note, PKM2 in its dimer form has been shown to be increased in monocytes and macrophages from patients with coronary artery disease (CAD), which has been linked to an increased glycolytic flux, ROS production and inflammatory IL-6 and IL-1β expression [103]. Succinate, itself, can further potentiate HIF1-α gene expression by inhibiting prolyl hydroxylase (PHD) enzymes, stopping their hydroxylating and destabilising activity over HIF1-α.

Overall, this section describes the crucial link between metabolism and macrophage gene expression, function and inflammatory status. Understanding the regulatory mechanisms underlying immunometabolism and how the availability of metabolic substrates, for example excess glucose in diabetes, affects these processes may provide novel therapeutic targets for such diseases.

Innate Immune Cell Memory

Changes in metabolism have already been shown to induce long-term cellular memory through epigenetic modifications and chromatin structure alterations [104]. Trained immunity in monocytes, i.e. immunological memory of past insults, have previously been shown with respect to β-glucan [105,106] and *Bacillus Calmette–Guérin* (BCG) [107,108]. Understanding such pathways may provide further insight into mechanisms underlying hyperglycaemic memory in innate immune cells.

Epigenetic memory and the role of cellular metabolism

Epigenetics is defined as “the study of heritable traits in gene expression that are not due to changes in the DNA sequence” [109]. These traits are often chemical modifications that occur directly to the DNA or to the proteins that are associated with DNA and determine DNA structure.

The organisation and spatiotemporal regulation of DNA structure is an important mechanism of transcriptional regulation. Within a cell, DNA is packaged up and condensed into chromosomes. Chromosomes are formed by the coiling of chromatin, which is formed when double stranded DNA interacts with structural proteins, known as histones, to form the chromatin subunit known as a nucleosome. This process is depicted in Figure 1.4. There are four, highly conserved core histone proteins: H2A, H2B, H3 and H4. Each nucleosome is formed in eukaryotes by DNA, the length of 146 nucleotide pairs long, wrapping itself 1.62 times around an octamer of histones; the octamer formed from a pair of each core histone

protein [110]. Nucleosomes are connected and stabilised by a short DNA fragment, known as a linker DNA, and a linker histone, either H1 or H5. Although primarily thought to be only involved in DNA structure, linker histones have been shown to be dynamic in binding capacity and therefore may play a further role in transcriptional regulation [111], although this requires further study to fully understand.

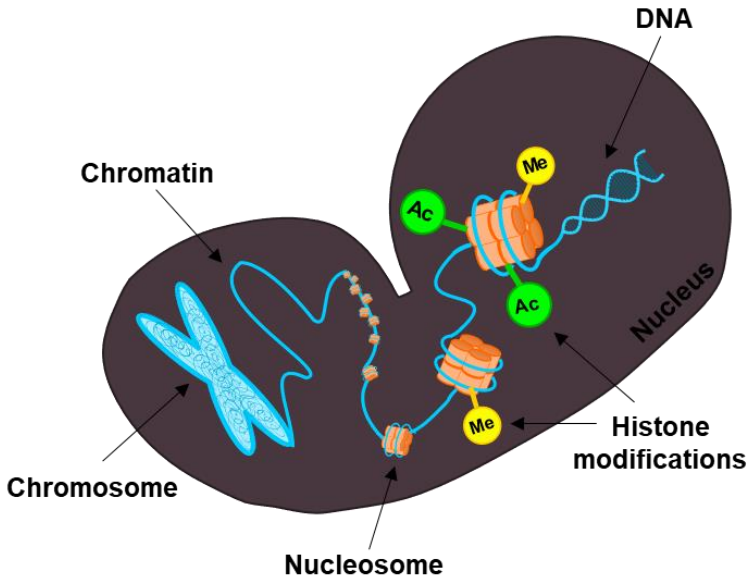


Figure 1.4 ***Chromatin structure overview****.*

DNA is coiled around 8 histones (orange) to form a nucleosome. Nucleosomes are the subunit that make up chromatin. The tightness of DNA-histone interactions, and therefore openness of the chromatin structure, are controlled by histone epigenetic modifications like acetylation (Ac) or methylate (Me). Chromatin continues to condense and coil to form chromosomes

The interactions that bind DNA and histones together are extensive. They consist of hydrogen bonds between the amino acid histone backbone and the DNA phosphodiester backbone and predominantly hydrophobic interactions between histones, rich in positively charged lysine and arginine residues, and the negatively charged DNA [112]. The interactions between negatively charged DNA and positively charged histones determine how compact the nucleosomes are formed, and therefore influence the accessibility of that DNA. For instance, the more tightly coiled the DNA is to the histone complex, the less accessible its sequence is to transcription factors and transcription machinery, hence the repression of those genes. However, the interactions are further influenced by epigenetic modifications that occur on the long N-terminal amino acid "histone tail" that protrudes out from the DNA-histone core. These modifications can alter the overall histone charge, therefore adjusting the affinity of the DNA-histone complex allowing for chromatin remodelling to occur that controls DNA structure, chromatin accessibility and downstream gene expression [113].

Histone tails are primarily lysine and arginine amino acid residues, which can be subjected to the addition of reversable post-translational modifications such as the addition of acetyl groups, known as acetylation; methylation, the addition of methyl groups or phosphorylation through the addition of a phosphorus group. The location and number of these marks dictate their effect on gene expression. The abundance of these epigenetic modifications are tightly regulated, and the interplay between cellular metabolism is illustrated in Figure 1.1Figure 1.5 and described in more detail below.

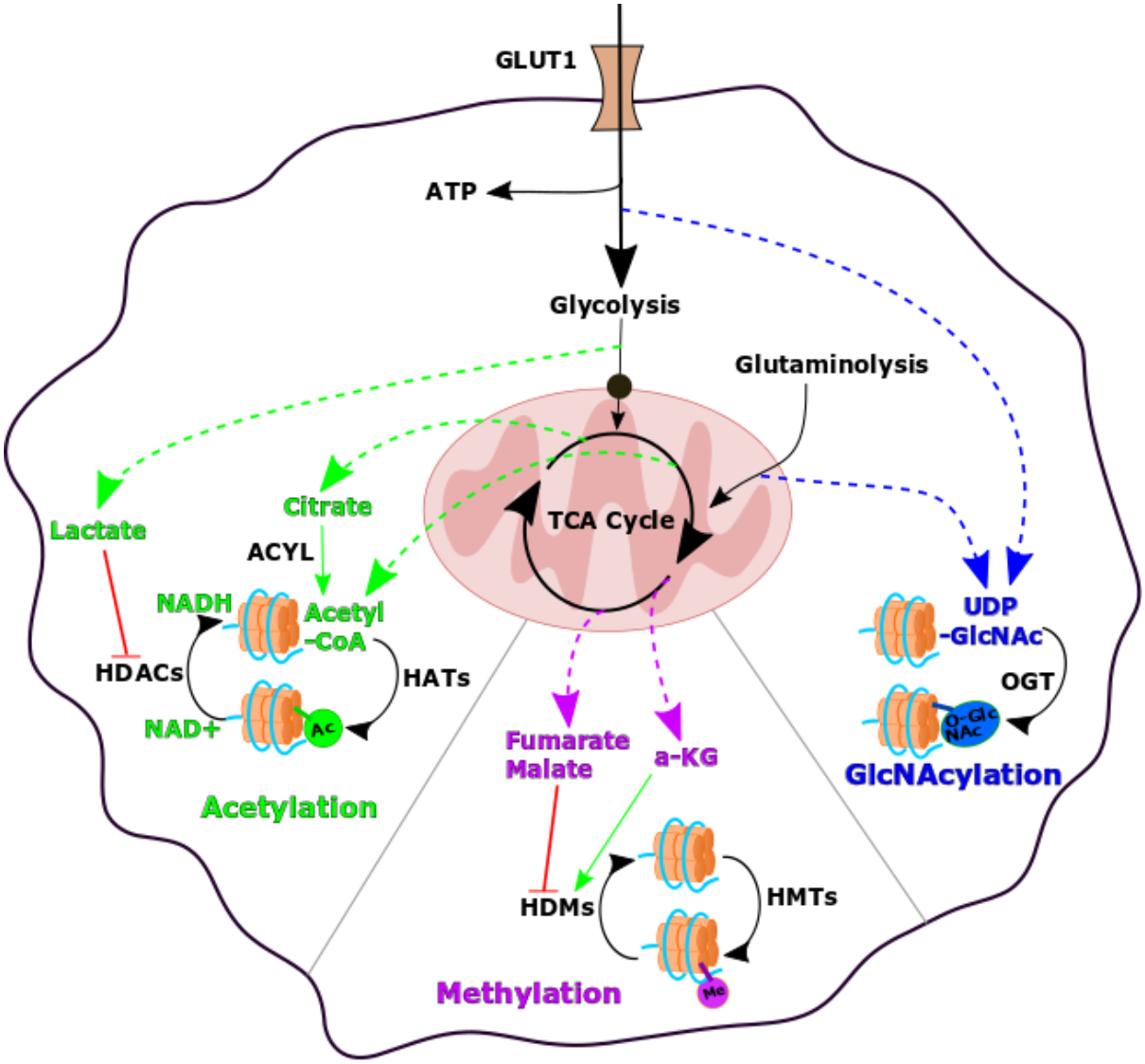


Figure 1.5 ***Interplay between cellular metabolism and epigenome.***

Histone acetylation is induced by histone acetyl transferases (HATs) and removed by histone deacetylases (HDACs). Acetyl-CoA is an essential HAT cofactor, which is produced directly from the TCA cycle, or by TCA cycle derived citrate and converted to acetyl-CoA by nuclear ATP citrate lyase (ACLY). iUDP-glucosamine (UDP-GlcNAc) derived from glucose and glutamine metabolism, is used by the enzyme O-GlcNAc transferase (OGT) to induce the epigenetic mark O-linked N-acetylglucosamine group (O-GlcNAc). Histone methylation is increased by histone methyltransferase (HMT) and removed by histone demethylases (HDMs). TCA metabolite α-KG stabilises certain HDMs, however structurally similar fumarate and malate inhibit histone demethylase enzymes, overall increasing histone methylation status. Figure adapted from Kinnaird, A. et al [114].

Histone acetylation of a lysine residue removes a positive charge and is therefore associated with destabilisation and opening of the chromatin and enhanced transcriptional activity. The addition or removal of these marks are very dynamic and are controlled by specialist enzymes. The group of enzymes governing histone acetylation levels are acetyltransferases (HATs) or opposingly deacetylases (HDACs) [115].

Histone acetylation is an essential switch for regions of chromatin accessibility, with hyperacetylation of histones H3 and H4 increasing chromatin openness [116]. The metabolite acetyl-CoA is an essential, rate-limiting co-factor for HATs. Relatively high levels of ACLY are present in the nucleus, which leads to the conversion of citrate to acetyl-CoA and oxaloacetate [117], as previously described. Nuclear ACLY is important for maintaining global histone acetylation, and of relevance, ACLY-dependent histone acetylation increases according to glucose availability [118]. Under low glucose conditions, cells primarily utilised fatty acid oxidation, which resulted in mitochondrial acetyl-CoA levels increasing, whereas cytoplasmic and nucleic acetyl-CoA levels remained unchanged. Conversely, an excess of glucose led to increased nucleocytoplasmic acetyl-CoA concentrations and an accumulation of histone acetylation [118].

HDAC activity is also shown to be regulated by metabolite availability, in particular class III HDACs, known as Sirtuins 1-7, require the essential metabolite co-factor of nicotinamide adenine dinucleotide (NAD^+). NAD^+ is used as a co-enzyme, in which it accepts electrons to be reduced to NADPH. It is particularly important in the TCA cycle (Figure 1.3). When there is a favourable energetic environment, for example an abundance of glucose, there is a high NADPH : NAD^+ ratio which negatively regulates Sirtuins, leading to downregulated HDAC activity. For this reason, periods of fasting increase NAD^+ concentrations, in particular leading to increased sirtuin 1 (SIRT1) activity and decreased global histone acetylation [119]. Sirtuin deacetylase reactions are further metabolically regulated as lactate has been identified as an inhibitor [120]. Lactate is also able to endogenously inhibit all lysine deacetylases (KDAC) [114,120].

Overall, this suggests that glucose positively regulates global histone acetylation through multiple mechanisms and begins to highlight the interplay between glucose availability, metabolism and epigenetics.

Histone methylation is associated to both transcriptional activation and repression. Methylation transcriptional control is more complicated than acetylation as methylation does not infer a change in charge status, but rather directly interferes with chromatin binding complexes. Di- or trimethylation on histone 3 at the lysine residue in position 4 (H3K4), position 36 (H3K36) or position 79 (H3K79) are connected to increased transcription, whereas increased mono-, di- and trimethylation at histone 4 lysine position 9 (H3K9) or position 27 (H3K27) often indicate transcriptional repression [121]. The family of enzymes in control of histone methylation status are histone methyltransferases (HMTs) and demethylases (HDMs) [115].

Methylases are dependent on S-adenosylmethionine as a methyl donor, a metabolite product of zinc, methionine and vitamin B family metabolism. In opposition, HDM, such as JmjC domain (JMJD) and ten-eleven (TET) family of proteins, utilise iron (Fe^{2+}) and α-KG as stabilising co-factors and are regulated by variable concentrations. However, metabolites succinate and fumarate are structurally similar to α-KG and their accumulation inhibits both JMJD, TET and other α-KG dependent enzymes, leading to hypermethylation [122]. Another, structurally distinct, lysine-specific HDM (LSD1) is vital for the demethylation of H3K4me1/2 and H3K9me1/2 and regulated by the redox state of the cell, however requires flavin adenine dinucleotide (FAD) rather than NAD^+. LSD1 activity is stimulated in high concentrations of FAD. When the TCA cycle is over-active, FAD is reduced to $FADH_2$ and LSD1 activity is subsequently reduced [104].

Another epigenetic modification heavily regulated by metabolism is the addition or removal of an O-linked N-acetylglucosamine group (O-GlcNAcylation), by the enzyme O-GlcNAc transferase which utilises UDP-glucosamine (UDP-GlcNAc) derived from glucose and

glutamine metabolism. UDP-GlcNAc levels have been shown to specifically differentiate M1 and M2 macrophage metabolic profiles, with M2 characterised by higher levels [123], although its relevance to macrophage function requires further investigation.

Trained immunity

When describing memory and the immune system, it is common to think only of the adaptive immune system [124]. However, recent reports have described a memory phenotype in innate immune cells known as trained immunity [108].

The definition of trained immunity is: a primary stimulus that leads to the memory, mediated by molecular mechanisms such as epigenetic changes [125] and miRNA [126,127], whereby the cell exhibits "a heightened response to a secondary infection that can exert both toward the same microorganism or a different one (cross-protection) [107]." Although not fully characterised, the primarily mechanism believed to underpin trained immunity in macrophages is due to changes in cellular metabolism, which are relayed into the nucleus through epigenetic modifications to induce long-lasting changes in gene expression [128].

Trained immunity has previously been described in the context of β-glucan [105], *candida albicans* infection [106] and tuberculosis vaccine BCG [108]. All reported stimuli of trained immunity appear to act through receptor mediated responses to induce metabolic changes that lead to chromatin modifying epigenetic modifications in innate immune cells and their precursors. All report stimuli were shown to induce metabolic and epigenetic reprogramming in monocytes. For instance, β-glucan signals through the dectin-1 receptor, leading to the activation of HIF1-α. This in turn leads to the metabolic dysregulation, previously described, whereby aerobic glycolysis is increased, and the TCA cycle is broken leading to accumulation of citrate and fumarate. Both the accumulation of cytosolic acetyl-CoA, through citrate breakdown, and fumarate accumulation, through glutamine replenishment, inhibiting the lysine HDM KDM5 lead to the specific accumulation of the epigenetic marks H3K4me3 and H3K27ac at the

promoter sites of inflammatory cytokines such as *Il-6* and *Tnf-α* [108,125,129]. The induction of β-glucan trained immunity has been reported to also involve the metabolite mevalonate, highlighting the role of cholesterol synthesis in the induction of H3K27ac and trained immunity in macrophages [130]. Interesting, BCG is able to enter the bone marrow (BM) and by altering the inflammatory milieu, promotes myelopoiesis and educates haematopoietic stem cells (HSCs) through the induction of the epigenetic marks H3K27ac and H3K4me3 to generate trained monocytes and macrophages with enhanced pro-inflammatory responses [131].

The relevance of trained immunity has been indicated in atherosclerosis. Induction of trained immunity in monocytes through exposure to various micro-organisms resulted in macrophages with persistent pro-atherogenic and pro-inflammatory phenotype, increasing cytokine production and foam cell formation through histone methylation. Importantly, trained monocytes with the same phenotype are present in patient with established atherosclerosis [132].

Although predominantly described in response to an infection, recently trained immunity has been described in BM myeloid progenitor cells in response to a high fat "Western diet" [133]. A high fat diet *in vivo* caused changes in the chromatin landscape, indicating epigenetic reprogramming that persisted despite returning animals to a normal chow diet. Training of monocytes with oxLDL indicated a role for inflammasome activation and IL-1β in cellular reprogramming [133]. This, along with many other studies, link IL-1β to trained immunity [134]. For example, BCG vaccination leads to a significant production of IL-1β from trained monocytes, which strongly correlated with lower viremia after a secondary yellow fever vaccination and suggests a role for IL-1β family member in the protection of reinfection [135]. All of these data suggest that changes in a metabolic environment is enough of a stimulus to induce a trained immunity phenotype and requires further investigation.

Hyperglycaemic memory

Diabetic hyperglycaemic memory has been described for over 20 years [136,137]. Multiple studies that have identified a correlation between the extent of hyperglycaemic memory and epigenetic modifications [138-141]. However, previous studies providing mechanistic insight have predominantly focused on persistent endothelial cell dysfunction [142]. Some of these are illustrated in Figure 1.6 and described below.

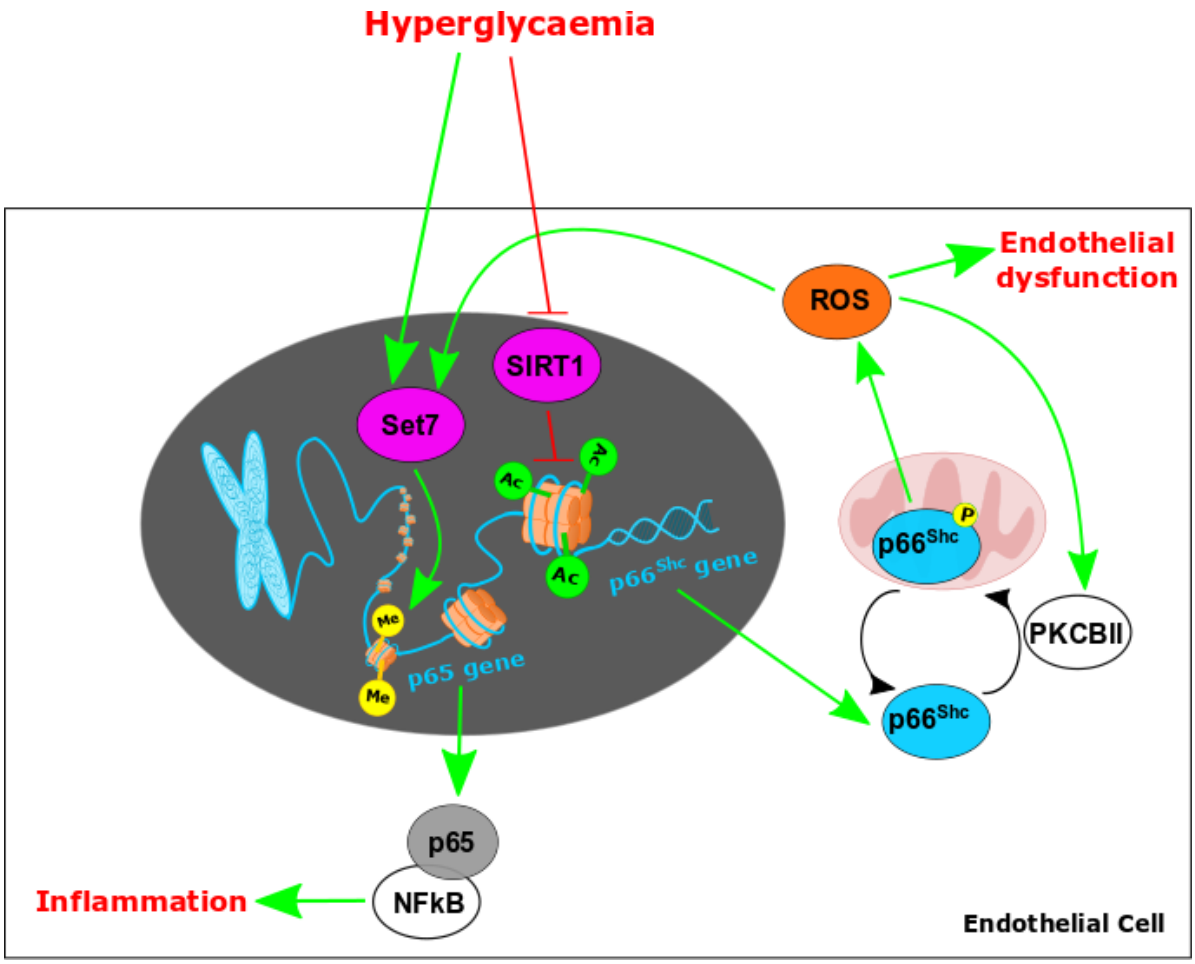


Figure 1.6 ***SIRT1, p66^{Shc} and Set 7 associated mechanisms of vascular hyperglycaemic memory.***

Hyperglycaemia upregulates the methyltransferase enzyme Set7, inducing hypermethylation, especially H3K4me3, at p65 promoter, subsequently increasing its gene expression, NFκB activation and vascular inflammation. Hyperglycaemia decreases SIRT1 deacetylation activity, causing hyperacetylation at p66^{Shc} promoter and its heightened gene expression. PKCβII activates p66^{Shc} through phosphorylation, causing its translocation to the mitochondria and increasing associated ROS production. Subsequent reactive oxygen species (ROS) generation both maintains PKCβII activity and increases Set7 activity to continue driving p65 expression and consequent inflammation. SET7, PKCβII and p66^{Shc} upregulated activity persists despite glucose normalisation. Heightened mitochondrial ROS, particularly eNOS reduces NO availability, changes which underlie endothelial dysfunction. Figure adapted from Paneni, F. et al [141].

El-Osta *et al.* [138] first identified that endothelial cells exposed to transient periods of high glucose caused an increase in inflammatory nuclear factor κ-light-chain-enhancer of activated B cells (NF-κB) p65, which caused down-stream upregulation of VCAM-1, interleukin-18 and monocyte chemoattractant protein 1 (MCP-1) expression. Upregulated p65 expression were due to long-lasting epigenetic modifications at its promoter, including enrichment of H3K4me, mediated by the methyltransferase enzyme Set7, and reduction of H3K9me2 and H3Kme3 by the LSD1. These epigenetic modifications persisted after 6 days of glucose normalisation [138]. Exposure to high glucose leads to an accumulation of Set7 in the nucleus of vascular endothelial cells, which not only leads to methylation of p65 promoter, but also results in increased H3K4me1 associated IL-8 expression [143]. Set7 methyltransferase has also been identified to be of importance in monocytes [144] and pancreatic islets [145]. Set7 expression is increased in peripheral blood monocytes from patients with type 2 diabetes, which in turn display heightened Set7-depented H3K4me at the NF-κB p65 promoter [146]. Exposure of monocytes to high glucose also shown an increased Set7 recruitment and associated H3K4me at NF-κB p65 promoter and inflammatory genes such as TNF-α and cyclooxygenase-2 [147].

Pro-inflammatory gene promotors in endothelial cells were also found to be hyper-acetylated at H3K9 and H3K14, which corresponded to decreased DNA methylation [140]. Normalisation of mitochondrial superoxide production eradicated the epigenetic marks at p65 promoter, highlighting the role for ROS in the pathophysiology of vascular hyperglycaemic memory and its role in modulating chromatin remodelling enzymes [138]. The role for ROS in the development of vascular memory was further illustrated with the identification that the mitochondrial adapter protein $p66^{shc}$, a redox enzyme and regulator for mitochondrial ROS production, displays increased expression and protein phosphorylation after high glucose exposure, which subsequently leads to increased ROS production [148]. Mice deficient in $p66^{shc}$ display increased

resistance to oxidative stress and were shown to be protected from hyperglycaemic-associated endothelial dysfunction [149].

Further studies confirmed the presence of hyper-acetylation at histone 3 and decreased $p66^{shc}$ promoter methylation but reported that this may in part be also due to the decreased activity of SIRT1 [150,151]. *In vitro* overexpression of SIRT1 or activation of SIRT1 *in vivo* with the therapeutic metformin, normalised high-glucose induced metabolic memory in the vasculature by stabilising hyperglycaemic driven ROS and suppresses NF-κB activation [152]. Clinical relevance of this pathway is further demonstrated as monocytes isolated from patients with type 2 diabetes display increased $p66^{shc}$ gene expression and oxidative stress [153]. Recent work has also shown that circulating leukocytes from patients exhibiting coronary artery disease have a significantly reduced methylation at their $p66^{shc}$ promoter sites, highlighting the potential role for this pathway in the context of cardiovascular disease [154]. Although these epigenetic modifications were put down to increased DNA methyltransferase 3b (DNMT3b) activation, another chromatin modifying enzyme shown to be stimulated by hyperglycaemic associated oxidative stress [155]. DNMT3b expression is also important for macrophage inflammatory function, as macrophages exposed to the fatty acid stearate exhibit increased DNMT3b expression and a subsequent downregulated ability to polarise into an M2 phenotype [156].

Understanding genes and pathways under hyperglycaemic regulation and how this memory is generated may provide mechanistic understanding and supply us with novel targets for a more specific approach to decrease CVD risk in patients with diabetes.

Hypotheses

1. Diabetic hyperglycaemia alters monocyte and macrophage metabolism and inflammatory status.
2. These putative pro-inflammatory effects are long lasting and drive atherosclerosis *in vivo*, despite glucose normalisation.
3. Hyperglycaemic memory is induced through metabolic memory and epigenetic modifications, similar to the mechanism described in trained immunity.
4. Hyperglycaemic memory is relevant to human diabetic vascular disease.

Chapter 2 : Materials and Methods

Experimental Procedures

Animal handling and husbandry

All animal protocols were conducted in accordance with the UK Home Office, under the guidance of the operation of the Animals (Scientific Procedures) Act 1986 and as detailed in the UK Home Office project licence No. 30/3374; 27/01/2016. Wild-type (WT) C57BL/6J mice were purchased from Charles River and a breeding colony established. Mice were maintained and housed at the Functional Genetics Facility (FGF) at the Wellcome Trust Centre for Human Genetics, Oxford, in groups of 2-5 animals per cage at 20-22 °C with a 12-hour light / dark cycle with food and water *ad libitum*. Diets consisted of standard rodent chow (Special Diet Services: Rat & Mouse diet number 1 as a standard, United Kingdom).

Streptozotocin (STZ) induced diabetic mice model

C57Bl/6 male littermates were randomly assigned to control or diabetic experimental groups. Diabetes was induced through an intra-peritoneal injection of streptozotocin (STZ; Sigma-Aldrich, USA) at a low dose range (42 – 45 mg / kg / day) over five consecutive days. STZ was dissolved in 25 mM sodium citrate buffer (Sigma Aldrich, UK) (pH 4.5) immediately prior to injections, control WT mice received the equivalent volume of citrate buffer. Mice were injected between the ages of 14 - 16 weeks and regularly monitored for changes in body weight (g) and non-fasted blood glucose levels (mM). Blood glucose levels were measured using Aviva Accu-Check glucose monitor (Roche, USA) and hyperglycaemia classified as a plasma concentration >13.9 mM after 2 weeks. Mice were euthanised by cervical dislocation (Schedule 1) and tissues harvested between 6-12 weeks after the final STZ injection.

Diabetic bone marrow (BM) transplant experiment

Mouse BM transplantation experiments were performed at The Jackson Laboratory, Bar Harbor, Maine, USA, *in vivo* facility in accordance with The Institutional Animal Care and Use Committee (IACUC) regulations (AAALAC accredited facility, Project Reference 70195 IVAT).

Mice were housed in groups of 2-5 animals per cage at 20-22 °C with a 12-hour light / dark cycle with food and water *ad libitum*. Diets consisted of standard rodent chow, unless stated otherwise. Diabetes was induced in C57BL/6-Tg (CD68-EGFP)1Drg/J mice (CD68-^{GFP}) as previously described for 6 weeks. CD68-^{GFP} are transgenic mice expressing green fluorescent protein (GFP) under control of the cluster of differentiation 68 (CD68) promoter, leading to the expression of GFP in predominantly monocytes and macrophages [157]. Diabetic mice with non-fasted blood glucose levels >13.9 mM, control citrate buffer treated CD68-^{GFP} mice and B6.129S7-Ldlrtm1Her/J mice (*Ldlr*$^{-/-}$) of the same age were used as BM donors. Donor mice received 550 rads of irradiation, BM was isolated by flushing both tibias and femurs using Hank's Balanced Salt Solution (HBSS) (Sigma-Aldrich, USA), counted and 5 x10^6 viable cells intravenously injected into irradiated *Ldlr*$^{-/-}$ recipient mice (10 mice per experimental group). Five *Ldlr*$^{-/-}$ mice were not irradiated and served as unmanipulated controls.

After engraftment, all recipient animals were placed on a "Western" type diet (Open Source Diets® D12079B: 21 % fat, 40 % kcal) for 12 weeks. Whole blood was collected through retro-orbital bleed at 4- and 8-weeks post engraftment for flow cytometric analysis of peripheral blood mononuclear cells and to monitor engraftment. Engraftment was monitored by staining cells for lymphocyte common antigen (CD45; cluster of differentiation 45) and GFP and assessing the relative proportion of CD45+GFP+ cells among total CD45+ population. At 12 weeks, mice were euthanized via carbon dioxide inhalation, whole blood collected, and sera processed for triglycerides (TRIG), non-esterified fatty acids (NEFA), LDL and high-density lipoprotein (HDL) cholesterol measurements by The Jackson Laboratory's Clinical Chemistry Core Facility. Mice were perfused with phosphate buffered solution (PBS), followed by perfusion and fixation with 4 % paraformaldehyde (PFA) overnight. The heart and aorta were dissected and placed in 70 % ethanol for shipping and until processing.

Experimental Model Details

Cell lines

All cell lines were grown at 37°C and 5 % carbon dioxide in T75 or T175 flat bottomed flasks (Corning, UK). The fibroblast cell line, L929, were grown in Roswell Park Memorial Institute (RPMI) medium supplemented with 10 % foetal bovine serum (FBS) (Life Technologies), 2 % penicillin – streptomycin (Sigma Aldrich) and 2 mM glutamine (Life Technologies). L929 cells were grown to full confluency for 7 – 8 days and the conditioned media removed, centrifuged and the supernatant aliquoted and stored at -20 °C until required for murine BM differentiation to bone marrow derived macrophages (BMDM).

Skin derived endothelial cells (sEND.1 [158]) were cultured in 25 mM glucose Dulbecco's Modified Eagle Medium (DMEM) with 10 % FBS, 2 % penicillin – streptomycin and 2 mM glutamine until required for static adhesion assays.

BMDM Culture

BMDM were generated, as depicted in Figure 2.1, by flushing BM from murine femurs and tibias with 10 mL PBS and passed through a 70 µm filter (BD Falcon, UK) to remove any remaining bone fragments or other debris and create a single cell suspension. Cell suspensions were centrifuged at 400 *g* for 5 minutes followed by plating the isolated cell pellets in non-tissue culture treated petri-dishes (Thermo Fisher, UK) in 10 mL of differentiation media (5 mM glucose DMEM media (Sigma Aldrich, UK) supplemented with 10 % FBS, 2 % penicillin - streptomycin and 2 mM glutamine) plus 20 % L929 cell conditioned media.

Cultures were supplemented with the addition of 5 mL fresh differentiation media on day 4 and ready for positive selection on day 7. BMDM were selected through adhesion by firstly discarding the differentiation media, any remaining floating and undifferentiated cells, followed by the addition of 4 mL of 2.5 % trypsin-EDTA (Life Technologies, UK) and incubating cells for 5 minutes at 37 ºC until previously adhered cells were dislodged. Trypsin was neutralised

through the addition of 10 mL DMEM media and the solution collected and centrifuged for 400 *g* for 5 minutes to pellet the cells. Pelleted cells were plated in 8 mL of complete media (5 mM glucose DMEM media supplemented with 10 % FBS, 2 % penicillin - streptomycin and 2 mM glutamine) in new non-treated Petri-dishes for 20 minutes at 37 ºC, at this point media and any unadhered cells were discarded. All remaining attached cells were plated in 8 mL fresh complete media and considered to be BMDM, ready to use after a 24-hour rest on cell culture day 8 of culture. All further experimentation was performed in complete media unless stated otherwise.

BMDM were plated into 12-well plates (Corning Incorporated, UK) at a density of 2 x10^5 cell/ mL / well and stimulated for 16 hours with either 10 ng/mL recombinant murine IFNy (R&D Systems, UK) plus 100 ng/mL LPS (Sigma Aldrich, UK), 10 ng/mL recombinant mouse IL-4 (R&D Systems, UK) or media only control. WT BMDM were also simultaneously cultured in various glycaemic conditions (5 mM glucose complete DMEM media with the addition of glucose (1 M stock solution; D-Glucose monohydrate in PBS; Scientific Laboratory Supplies, UK) to make a final concentration of either 11 mM or 20 mM glucose) or an osmotic control condition (5 mM glucose complete DMEM media plus 15 mM mannitol (1 M stock solution; D-Mannitol in PBS; Calbiochem, UK)). STZ diabetic BMDM and control mice were stimulated in complete 5 mM glucose DMEM media. Metabolic studies were performed in the absence or presence of 10 mM dichloroacetate (DCA) (Sigma Aldrich, UK) or 1 mM 2-deoxy-d-glucose (2-DG) (Sigma Aldrich, UK) dissolved in PBS. BMDM were used for metabolite readings, gene expression analysis and functional assays such as foam cell formation and static adhesion to activated endothelium.

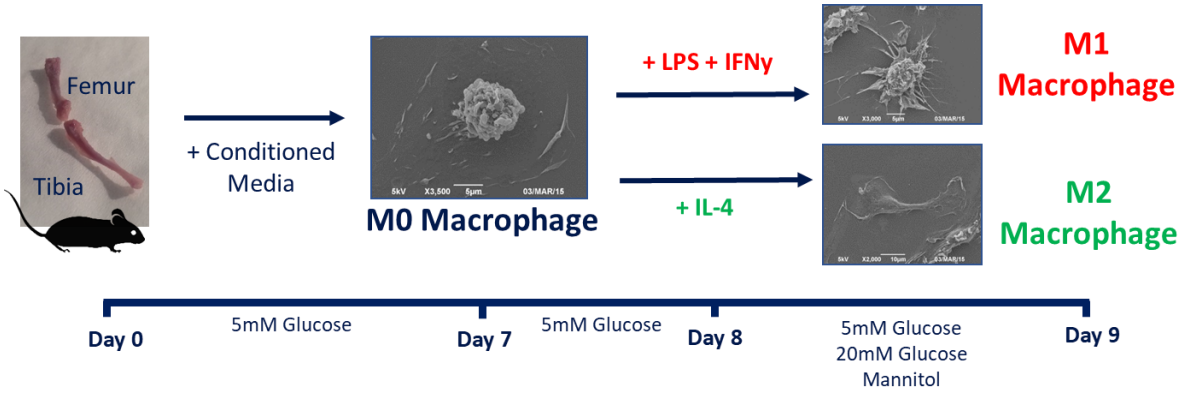


Figure 2.1 ***BMDM differentiation and stimulation protocol.***

Bone marrow was isolated from murine femur and tibias, differentiated in 5 mM conditioned media for 7 days into a basal state M0 macrophage. Macrophages were then polarised into a pro-inflammatory M1 or anti-inflammatory associated M2 macrophage in the presence of lipopolysaccharide (LPS) plus interferon-γ (IFNγ) or interleukin-4 (IL-4), respectively, overnight in varying extracellular glucose (5 mM or 20 mM) or control (5 mM glucose + 15 mM mannitol) conditions.

BMDM *in vitro* memory model

To investigate the mechanisms by which long-term inflammatory memory is induced in macrophages WT C57Bl/6 BM was differentiated into BMDM in 5 mM glucose differentiation media plus experimental conditions for a defined period of time, as illustrated by Figure 2.2. Experimental conditions included varying glycaemic conditions, 5 mM or 20 mM glucose, for 1, 2, 3, 4 or 7 days in the presence or absence of 1, 5, 10 or 20 mM DCA or 0.25, 0.5, 1, 5 or 10 µM Ro5-3335 (Merck Millipore, UK). BMDM were then positively selected by the previously described protocol and re-plated into 5 mM glucose complete DMEM media and left to incubate in physiological glucose concentration for 48 hours, to allow a period of "glucose normalisation". BMDM were then stimulated for use with 10 ng/mL IFNy plus 100 ng/mL LPS or control media for 16 hours in the absence or presence of matching concentrations of Ro5-3335 before use for gene expression analysis.

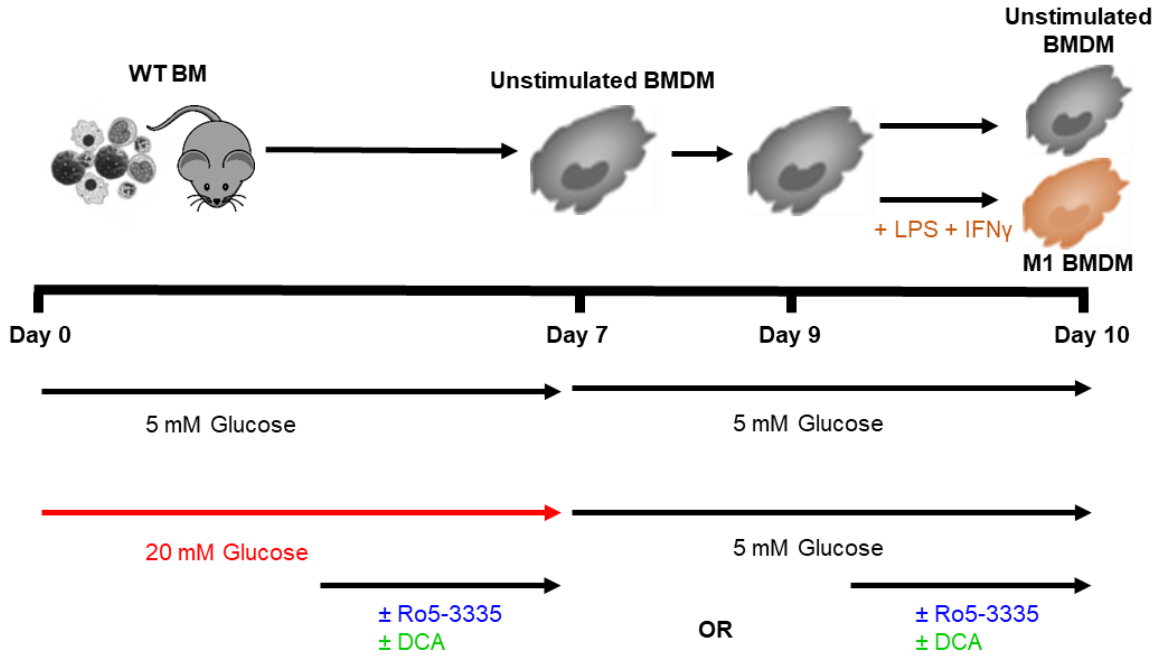


Figure 2.2 ***In vitro BMDM hyperglycaemic memory model.***

Mouse wild type (WT) bone marrow (BM) samples were differentiated into bone marrow derived macrophages (BMDM) either in 5 mM or 20 mM glucose ± the glycolytic inhibitor dichloroacetate (DCA) or the RUNX1 inhibitor Ro5-3335; followed by a period or low glucose (5 mM) for 48 hours and stimulation into a control or an M1 macrophage overnight ± DCA or Ro5-3335.

Mouse monocyte isolation

Mouse monocytes were isolated from either spleen or peripheral blood using the EasySep™ Mouse Monocyte Isolation Kit (Stemcell Technologies, Canada) according to the manufacturer's protocol. Briefly, blood was collected through terminal pentobarbital anaesthesia and cardiac puncture and placed in 50 mL ammonium chloride red blood cell (RBC) lysis buffer (1.5 mM ammonium chloride, 100 µM sodium bicarbonate, 11 µM EDTA disodium) for 5 minutes at room temperature. Spleens were dissected and minced with the back of a 1 mL syringe through a 70 µm filter to create a single cell suspension into 50 mL RBC lysis buffer. All isolated cells were subjected to the following monocyte enrichment protocol, as per the manufacturer's instructions.

Samples were centrifuged for 5 minutes at 400 *g* to pellet cells. Cells were washed once with 5 mL PBS, re-centrifuged and then resuspended in 500 µL isolation buffer (PBS + 2 % FBS + 1 mM EDTA (Life Technologies, UK)) in a 5 mL polystyrene round-bottom flow associated cell sorting (FACS) tube (Life Technologies, UK). 50 µL/mL rat serum was added to the sample plus 100 µL/mL antibody selection cocktail and incubated for 5 minutes at 4 °C. EasySep™ magnetic particles were then added at 75 µL/mL of sample, mixed and incubated at 4 °C for 5 minutes. Once the sample was bought up to a total volume of 2.5 mL with the addition of more isolation buffer, it was placed in the EasySep magnet and incubated at room temperature for 2.5 minutes to separate beads and unwanted bound cells. The desired enriched monocyte cell suspension was poured out into a new tube and centrifuged to pellet desired cells. Isolated monocytes were used for gene expression analysis and static adhesion assay.

HSC isolation

An enriched HSC fraction was isolated from BM by removing lineage committed cells using the MagniSort Mouse Hematopoietic Lineage Depletion Kit (ThermoFisher Scientific, UK), according to the manufacturer's description. Briefly, BM from each mouse's femurs and tibias

were flushed and incubated for 10 minutes at room temperature with biotin conjugated antibody solution in a 5 mL FACS tube. Antibody solution consisted 1.2 mL 10 % bovine serum albumin (BSA; Sigma-Aldrich, UK)-PBS plus 75 µL of each antibody against CD3, CD4, B220, Ter119 and Gr1 which bind and enable removal of mature T cells, B cells, natural killer cells, dendritic cells, monocytes, granulocytes and erythroid cells. After antibody incubation time, 200 µL MagniSort™ Streptavidin Negative Selection Beads (Invitrogen, UK) beads were added, allowed to incubate at room temperature for 5 minutes and placed in the EasySep magnet for 5 minutes. The depleted, HSC enriched solution was then poured off and collected in a fresh 5 mL falcon tube and centrifuged for 5 minutes at 400 *g* to pellet desired cells.

HSCs were cultured in 5 mL FACS tubes in complete 5 mM DMEM media (or with the addition of 15 mM glucose or 15 mM mannitol for indicated WT stimulations) with the addition of 10 ng/mL recombinant mouse IL-1β (R&D Systems, UK) for 16 hours for western blot or 6 hours for assay for transposase-accessible chromatin using sequencing (ATAC-seq) analysis.

Human peripheral blood monocyte samples

All clinical investigations were conducted in accordance with the Declaration of Helsinki and samples stored under the UK Human Tissue Act (2004). The Oxfordshire Research Ethics Committee (REC reference 15/NW/0972) approved the human clinical cohort protocols used for blood isolation. All healthy volunteers provided informed consent to participate.

Peripheral venous blood, 15-30 mL, was obtained from healthy volunteers by Dr Mohammad Alkhalil, in k2-ethylenediaminetetraacetic acid (K2-EDTA) coated tubes (BD Vacutainer, New Jersey) and processed within 1 hour. Plasma and a mononuclear cell enriched fraction were obtained through density centrifugation by centrifuging whole blood on Accuspin Histopaque-1077 columns (Sigma-Aldrich, USA) according to the manufacturer's instructions. Plasma was made platelet-poor through centrifugation for 10 minutes at 5000 *g* and then frozen and stored in 500 µL aliquots at -80 ºC.

The mononuclear cell enriched fraction was taken forward for monocyte isolation using the negative selection bead isolation kit: EasySep human monocyte enrichment kit without CD16 depletion (Stemcell Technologies, Canada), following the manufacturer's protocol. Briefly, cells were resuspended at a concentration of 5 x 10^7 cells/mL in isolation buffer (described above) plus 50 µL/mL antibody enrichment cocktail and incubated at 4 ºC for 10 minutes. EasySep D Magnetic particles were added at 50 µL/mL and after a final 5-minute incubation at 4 ºC, the total volume was brought up to 2.5 mL with isolation buffer and the unwanted cells, conjugated to the magnetic beads, are separated using the EasySep Magnet. Desired, enriched monocytes were poured into a fresh tube and pelleted by centrifuging for 5 minutes at 400 *g* before use. Human monocytes were cultured and stimulated in complete 5 mM glucose DMEM media in 5 mL FACS tubes, plus either a pro-inflammatory stimulus (100 ng/mL LPS + 10 ng/mL recombinant human IFNy (Life Technologies, UK)) or an anti-inflammatory stimulus (10 ng/mL recombinant human IL-4 (Life Technologies, UK)) for 6 hours. Cells were centrifuged for 5 minutes at 400 *g* and cell pellets lysed for RNA or human monocytes were cultured and stimulated in complete 5 mM glucose complete DMEM media supplemented with 15 mM glucose or mannitol osmotic control in 5 mL FACS tubes for 12 hours. The media and lysate of these cells were used for metabolomics analysis, as described below.

Laser capture microdissection (LCM) isolation of human plaque macrophages

The UK National Research Ethics Service (REC reference 09/H0606/95) approved the human clinical cohort protocols for carotid plaque collection and processing. All patients provided informed consent and willingness to participate in the following described study. Patients awaiting carotid endarterectomy were recruited and carotid plaques were collected freshly at time of surgery. Explanted carotid plaques were washed in ice-cold sterile PBS and snap-frozen in OCT and stored at -80ºC until processed.

LCM was carried out using a PALM Microbeam LCM system (Carl Zeiss GmbH, Germany) using an adapted “guide slide” approach [159]. Carotid plaque samples were freshly sectioned at 15 µm. Guide slides consisted of 3 consecutive sections: the first section stained with Masson-Goldner staining kit protocol (according to the manufacturer’s description; Sigma Aldrich, UK), to aid in determination of micro-anatomical locations. and the next 2 to follow were immune-stained for either macrophages (CD68) or smooth muscle cells (α-actin), following the same protocol described for aortic root sections. The subsequent sections (up to 15) were cut onto LCM membrane slides (ThermoFisher Scientific, UK) and cresyl violet stained ready for immediate processing. Macrophage cell clusters were identified manually, based on the guideslide staining using PALM RoboSoftware (version 4.5, Carl Zeiss GmbH, Germany). A total combined area of interest (AOI) between 3 – 5 x10^6 µm^2 were laser-captured on a Zeiss PALM AdhesiveCap™ (Carl Zeiss GmbH, Germany). Cells were immediately lysed and snap-frozen on dry ice and stored at -80ºC until the RNA was extracted using the RNEasy micro kit (Qiagen, UK), according to the manufacture’s protocol.

Method Details

Quantitative real-time polymerase chain reaction (qPCR)

qPCR was used to quantify gene expression in mouse and human cells. Full method details are described below. In summary, RNA was first isolated, then reverse transcribed into its complementary DNA (cDNA) sequence ready for quantification of a desired gene transcript through the PCR amplification with sequence specific Taqman DNA probes labelled with a fluorescent reporter to allow detection upon hybridization with their complementary sequence.

RNA isolation

Both human and mouse cell RNA was isolated using the RNeasy Plus mini kit (Qiagen, UK). Monocytes in suspension were centrifuged at 400 g for 5 min and the cell pellet lysed in 300 µL RLT lysis buffer (from RNeasy Plus mini kit). Adherent BMDM were first washed in PBS,

followed by the addition of 300 µL RLT lysis buffer and scraped with a pipette tip to dislodge and lyse cells. All RLT-cell samples were snap frozen on dry ice and stored at -80 ºC until further isolation.

RNA was extracted according the manufacturer's instructions. RNA was eluted in 25 µl RNAse-free water. Final RNA yield and purity determined by A260/A280 (nm) ratio, measured using a nanodrop 100 spectrophotometer (Thermo Fisher Scientific). All RNA taken forward for qPCR analysis had an A260/A280 ratio between 1.8 – 2.15, indicating a high purity RNA sample.

Quality of RNA with a nanodrop determined concentration below 15 ng/ µL was also assessed through gel electrophoresis. A denaturing 2.5 % TAE buffer (2.0 M Tris Acetate + 100 mM Na-EDTA, National Diagnostics, USA) -agarose gel was prepared by dissolving 2.5 mg Hi-Res Standard Agarose (AGTC Bioproducts, UK) in 100 mL 1x TAE buffer plus 1 µl 10,000x GelRed Nucleic Acid Gel Stain (Biotium, USA) and allowed to set in a gel mould until firm to the touch. Intact RNA, mixed at a 1:4 dilution with 6x Blue Gel Loading Dye (New England Biolabs, USA), along with a 1 kb DNA Ladder (New England BioLabs, UK) was run for 30 minutes at 200 mV to allow the 18S and 28S rRNA bands to separate. An example gel is shown (Figure 2.3) and demonstrates the correct 2:1 ratio of 28S:18S band intensity that indicates intact and high-quality RNA.

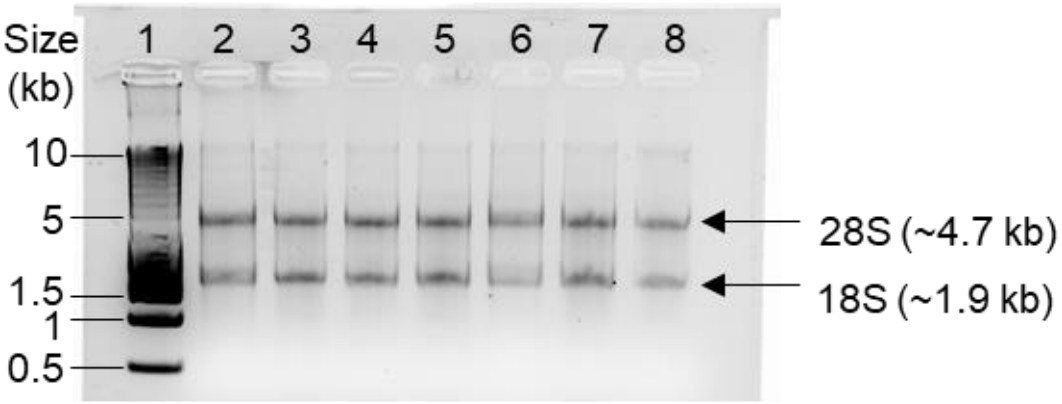


Figure 2.3 ***RNA Gel Electrophoresis.***

Mouse bone marrow derived macrophages (BMDM) were run on a 1.5 % agarose gel to allow 28S and 18S strands to separate and visualise RNA quality. Lane 1 shows a 1 kilobase (kb) ladder used as reference. Lanes 2 – 8 represent individual mouse BMDM, all stimulated with LPS + IFNy.

Complementary DNA (cDNA) synthesis

Isolated RNA samples were reverse transcribed into cDNA using the QuantiTect Reverse Transcription Kit (Qiagen, UK) on a 96 Well Thermal Cycler (Veriti, Thermo Fisher Scientific) according to the manufacturer's instructions. Firstly, to ensure that any remaining contaminating genomic DNA was eliminated, gDNA wipeout buffer was added to the RNA (RNA concentrations were standardised for each complete experiment; ranging between 10 pg – 1 µg for all data shown here) and incubated for 2 minutes at 42 °C. Afterwards, RNA samples were reverse transcribed into cDNA through the addition of a pre-prepared mastermix of Quantiscript Reverse Transcriptase, Quantiscript RT Buffer and Reverse Transcriptase Primer Mix and incubating at 42 °C for 15 minutes. Lastly, the reverse transcriptase was denatured through a 3-minute incubation at 95 °C, after which the synthesised cDNA was stored at -80 °C until use.

Real-time qPCR

All qPCR reactions were performed using the TaqMan Gene Expression Assay system (ThermoFisher Scientific) according to the manufacturer's descriptions. TaqMan Universal Master Mix II with UNG (Applied Biosystems, UK) contains a DNA polymerase that uses sequence-specific primers and a TaqMan probe (probes used are detailed in Table 2.1**Error! Reference source not found.**) to amplify target cDNA in order to detect the probe-specific gene of interest is present and at what quantity.

Reagent	Company	Identifier
Mouse B2M Taqman assay	Applied Biosystems	Cat# 4331182; Assay ID: Mm00437762_m1
Mouse IL-6 Taqman assay	Applied Biosystems	Cat# 4331182; Assay ID: Mm00446190
Mouse iNOS (Nos2) Taqman assay	Applied Biosystems	Cat# 4331182; Assay ID: Mm00440502
Mouse TNF Taqman assay	Applied Biosystems	Cat# 4331182; Assay ID: Mm00443260
Mouse IL1b Taqman assay	Applied Biosystems	Cat# 4331182; Assay ID: Mm00434228_m1
Mouse YM1 (Chil3) Taqman assay	Applied Biosystems	Cat# 4331182; Assay ID: Mm00657009
Mouse FIZZ1 (Retnla) Taqman assay	Applied Biosystems	Cat# 4331182; Assay ID: Mm00556208
Mouse β-actin (Acta2) Taqman assay	Applied Biosystems	Cat# 4331182; Assay ID: Mm00607939_s1
Mouse Cyclophilin Taqman Assay	Applied Biosystems	Cat# 4331182; Assay ID: Mm01273726_m1
Mouse GAPDH Taqman Assay	Applied Biosystems	Cat# 4331182; Assay ID: Mm99999915_g1

Table 2.1 ***qPCR Primer Details.***

The Taqman oligonucleotide probes are sequence-specific and constructed to contain a bound fluorescent reporter dye at the 5' end and a quencher at the 3' end. qPCR reactions start with a rise in temperature to denature the double stranded cDNA. The reaction temperature is then lowered which if the probe's target sequence is present in the cDNA, allows it to anneal. The taq DNA polymerase uses unlabelled primers present in the Master Mix and the template DNA to synthesise a new strand. The polymerases' endogenous 5' nuclease activity cleaves annealed probes to remove them from the template strand and consequently separate the quencher from the reporter dye end, leading to an increased reporter dye signal. With each temperature PCR cycle, additional reporter dye molecules are released and causes an accumulation of fluorescence intensity signal that appears on the linear, exponential phase of a qPCR amplification plot. The number of cycles it takes for a probes amplification curve to cross the automatic threshold (determined automatically by the software as 10 standard deviations above the mean baseline fluorescence) gives you a threshold cycle (C_t) value. This value is relative to the starting concentration of the target cDNA: the higher the starting copy number, the earlier the fluorescence signal intensity surpasses the significance cycle threshold and the lower the C_t value. The C_t value for the gene of interest was then normalised to the C_t of the house-keeping gene β2 microglobulin (B2M) – to give a ΔC_t value per replicate per gene of interest. Each sample replicate ΔC_t values were then averaged and qPCR data are expressed per sample as the relative fold gene expression: $2^{-\Delta Ct}$.

For reaction, a master mix containing 0.5 µL gene of interest specific Taqman primer (Table 2.1), 3.5 µL RNA-free water and 5 µL Taqman universal master mix II with UNG per reaction was prepared. Next, 1 µL of cDNA at 5 ng/µL was pipetted into a 384-well MicroAmp reaction plate (Applied Biosystems, UK) followed by 9 µL master mix / well. Plates were then sealed with an a MicroAmp Clear Adhesive Film (Applied Biosystems, UK), centrifuged at 2000 *g* for

2 minutes and run on a QuantStudio 7 Flex Rea-Time PCR System (Applied Biosystems by Life Technologies) under the following conditions:

Stage Name	Temperature	Time	No. Cycles
Holding Stage	50°C	2 min	1
	95°C	10 min	
Cycling Stage	95°C	15 sec	40
	60°C	1 min	

Data was collected using QuantStudio Real-Time PCR Software, exported as an excel file and analysed using GraphPad Prism (v5.01; GraphPad Software).

Foam Cell Formation Assay

The ability for macrophages to take up modified lipid and retain it to for foam cells was assessed using WT or STZ BMDM cultured with DiI-acetylated LDL (ac-LDL) (Bioquote Limited, USA), according to a protocol developed within the group and previously described [160]. WT BMDM stimulations were performed in complete DMEM media with either 5 mM, 20 mM glucose or mannitol, whereas all STZ BMDM, or corresponding citrate WT control BMDM, stimulations were carried out in 5 mM glucose complete DMEM media. Positively selected BMDM were grown onto 10 mm glass cover slips (VWR International, USA) in 12-well plates (Corning Incorporated, UK). BMDM were either used as controls and left unstimulated or stimulated into a pro-inflammatory state with LPS + IFNγ for 16 hours. Media was removed, and cells were washed with PBS to remove any remaining cytokine stimulus, followed by the addition of 25 µg/mL ac-LDL ± 10 mM DCA. After 48 hours all media and remaining ac-LDL were removed, cells washed 3 times with PBS and fixed with 4 % PFA (Alfa Aesar, UK) for 15 minutes at room temperature.

To quantify the amount of lipid up take BMDM were stained with the lipid soluble dye Oil Red O (ORO) (Sigma-Aldrich, UK). ORO stock solution and working solution were prepared each time. ORO stock solution was prepared by dissolving 250 mg ORO powder into 30 mL 99 % Triethylphosphate (Sigma Aldrich, UK) and 20 mL distilled water (dH_2O). A working solution was then prepared by mixing ORO stock solution: dH_2O at a ratio of 3:2 with agitation it on a roller for 5 minutes and then passed through a 0.45 µm filter to remove any undissolved powder.

PFA was removed and safely discarded. Fixed BMDM were dH_2O washed and then incubated in 500 µL/well working ORO solution for 20 minutes at room temperature. Cells were then washed with dH_2O three times to remove any unabsorbed ORO and mounted on polysine coated microscope slides (VWR International, USA) with glycerol mounting medium with DAPI and DABCO (Abcam, UK) to fluorescently label nuclei blue. Slides were air dried and imaged on the same day using a bright-field light microscope (Leica DM 2500 LED Optical Microscope) with 5x, 10x, 20x and 100x magnification. Phase contrast images were captured to image the ORO stained lipid and fluorescent DAPI images captured at the matching locations. Lipid was quantified using phase contrast images, nuclei cell count gained from DAPI images and merging of matching phase contrast and DAPI images were all performed using ImageJ software. Four DAPI and four matching ORO images were taken per cover slip. Per set of DAPI and ORO images, the area of lipid quantified was divided by the cell count. Data displayed was the average of all four image values from one cover slip to give the amount of lipid area per cell per sample.

Monocyte and Macrophage Static Adhesion Assay

sEND.1 cells were grown to confluency on 10 mm glass cover slips in 12-well plates and activated by 10 ng/mL recombinant mouse TNF-α (R&D Systems, UK) for 16 hours in complete 25 mM glucose DMEM media. Monocytes and macrophages were stimulated in complete DMEM media, with WT monocytes cultured in various glycaemic and control

conditions, and STZ macrophages in 5 mM glucose, normoglycaemic conditions. BMDM were left unstimulated or LPS + IFNγ stimulated in the presence or absence of the glycolytic inhibitors 10 mM DCA or 1 mM 2-DG for 16 hours before use. Murine monocytes, after fresh isolation, were stimulated under similar conditions as BMDM but in 5 mL FACS tubes and the addition of 50 µM β-mercaptoethanol (Sigma Aldrich, UK) to prevent adhesion and differentiation. After stimulation, BMDM were dislodged into solution with trypsin, centrifuged for 5 minutes at 400 *g* and the pellet PBS washed. Monocytes were centrifuged for 5 minutes at 400 *g* and their cell pellet PBS washed. From this point both cell types were treated the same. Cells were then fluorescently labelled green using the lipophilic PKH67 fluorescent cell linker kit (Sigma Aldrich, UK) according to the manufacturer's instructions.

Briefly, a PKH67 working solution was prepared by mixing Diluent C and concentrated PKH67 at a ratio of 1 mL Diluent C: 4 µL PKH67. Cells were resuspended in 200 µL Diluent C and mixed with 200 µL PKH67 working solution / sample. After a 5-minute incubation at room temperature, each sample reaction was neutralised with 400 µL assay media (DMEM media, 0.1 % BSA, 2 % penicillin – streptomycin and 2 mM glutamine). Samples were centrifuged at 400 *g* for 5 minutes and cells resuspended in 1 mL assay media. Cells were counted on an automated cell counter (Countess II FL Automated Cell Counter, Thermo Fisher Scientific) and added to sEND.1 cell cover slips at a density of 50 000 cells / 500 µL assay buffer. After a 1-hour incubation at 37 ºC, media and remaining floating cells were removed and cover slips washed with PBS to allow for only adhered monocytes or macrophages to remain. Coverslips were fixed and mounted using the same method as the foam cell assay. Cover slips were allowed to air dry and imaged on the same day. DAPI images, to confirm endothelial monolayer presence, and PKH67 green images at the matching location were captured using a bright-field light microscope (Leica DM 2500 LED Optical Microscope) at x10 and x20 magnification. The number of adhered cells, from PKH67 green images, were quantified using

ImageJ software. The data displayed is the average of quantified adhered cells from 4 images per sample.

Immunofluorescence

Unstimulated BMDM used for immunofluorescence were plated onto 13 mm diameter glass cover slips (VWR International, UK) and allowed to adhere for 12 hours. All media was removed, cells were washed in PBS and fixed in 4 % PFA for 15 minutes at room temperature. Glass cover slips were washed in PBS three times for 5 minutes and blocked to reduce non-specific background staining cover slips with DAKO protein block (DAKO, UK) for 30 minutes at room temperature. Primary antibodies for macrophage markers Galectin-3 (GAL3; goat anti-galectin 3, VWR International, UK), CD68 (rat IgG2a anti-CD68; AbD Serotec, UK), CD11b (rat IgG2b anti-CD11b; BD Pharmingen, UK) and F4/80 (rat IgG2b anti-F4/80; AbD Serotec, UK) or isotype control antibodies for rat IgG2a (LEAF™ Purified Rat IgG2a, κ Isotype Ctrl Antibody; BioLegend, UK) or rat IgG2b (Rat IgG2b, κ Isotype Control; BD Pharmingen, UK) were diluted to 1 µg/mL in PBS. DAKO block was then removed, and without washing, primary antibodies were added (with the exception of the negative control cover slip that received no primary antibody) and incubated for 1 hour at room temperature. Primary antibodies were then removed, and cover slips watched three times for 5 minutes each before the corresponding secondary antibody (diluted 1:400 in PBS) was added and incubated for 1 hour at room temperature. Secondary antibodies (anti-goat A_{488} or anti-rat A_{488}, Life Technologies, UK) were removed, cells washed in PBS and stained for mounted on polysine slides (VWR International, UK) using DAPI mount (DAPI ProLong Gold antifade reagent with DAPI; Life Technologies, UK) to co-stain the nuclei. Fluorescent images were taken on Leica DM 2500 LED Optical Microscope.

Scanning Electron Microscopy (SEM)

BMDM were grown in a 12-well cell culture plate in 5 mM glucose DMEM and either left unstimulated or stimulated with LPS plus IFNγ or IL-4 overnight. Media was removed, and cells were washed with ice cold PBS to remove residual media. Samples were then incubated in a primary fixative (2.5 % glutaraldehyde in PBS) for 1 hour at room temperature. Cells were washed three times in PBS, followed by an incubation in a secondary fixative (1% OsO_4 in PBS) for 1 hour at 4 ºC. Cells were washed three times in water, followed by dehydration in increasing concentrations of ethanol (50 %, 70 %, 90 % then 95%) for 5 minutes each at room temperature and a final 20-minute incubation in 100 % ethanol at room temperature. Cells were dried in the fume hood by quickly adding 0.5 mL hexamethyldisilazane (HMDS) for three minutes. HMDS was then removed and the sample plate left open overnight in the fume hood for HMDS fumes to evaporate. Samples were then mounted on carbon adhesive tape on SEM stubs and sputter-coated with 10 – 15 nm thickness of gold. SEM images were acquired on a JEOL 6390 SEM.

Flow Cytometry

Flow cytometry was performed on unstimulated WT M0 BMDM. BMDM were resuspended in 500 µL 2 % FBS/PBS plus 1 % mouse Fc receptor block (Miltenyi Biotec, UK) for 5 minutes on ice. Samples were then incubated for 20 minutes at room temperature, protected from light, with the antibodies summarised in Table 2.2. Samples were then rinsed with 1 mL of 2 % FBS-PBS, centrifuged at 350 g for 7 minutes and resuspended in 200 µL 2 % FBS/PBS. 7-AAD viability stain (eBioscience, UK) was added to a final concentration of 1 % 5 minutes before flow cytometry. Samples were then run on a FACSAria III (BD Biosciences, UK) and analysed of FlowJo software (FlowJo, LLC v10.2, Treestar, Inc.).

Target	Clone	Isotype	Supplier; Cat #	Fluorophore	Dilution
CD45	30-F11	Rat IgG2b, κ	Biolegend 103124	AF647	1:200
CD11b	M1/70	Rat IgG2b, κ	Biolegend 101206	FITC	1:100

Table 2.2 ***Antibodies for flow cytometry***

GLUT1 Surface Expression Assay

To quantify surface expression of GLUT1, after performing a cell titration to determine correct cell number, BMDM were plated at 5000 cells / well in a 96 well plate in 5 mM complete DMEM media. Cells were then stimulated in 5 mM glucose, 20 mM glucose or an osmotic control (5 mM glucose plus 15 mM mannitol) with 100 ng/mL LPS + 10 ng/mL IFNγ or 10 ng/mL IL-4 for 0.5, 1, 2, 4, 6 or 24 hours. At the correct time point, media was removed, cells were washed three times with PBS and then fixed with 3 % PFA for 5 minutes at room temperature. PFA was then neutralized with 125 mM glycine for 10 minutes at 4 ºC. Cells were washed three times with PBS, followed by blocking with 10 % goat serum + 3 % BSA in PBS for 45 minutes at 4 ºC. Blocking buffer is removed, and without washing, primary rabbit anti-GLUT1 (Abcam PLC, UK) was added at a concentration of 1:400 in PBS and incubated overnight at 4 ºC.

Cells were washed with PBS three times before the secondary anti-rabbit-HRP conjugate (Insight Biotechnology Limited, UK) was added at a 1:1000 dilution in PBS for 1 hour at room temperature. Cells were washed and 200 µl of o-Phenylenediamine dihydrochloride (OPD) reagent (0.4 mg/mL OPD dissolved in 0.05 M phosphate-citrate buffer (pH 5.0) plus 0.0004 % hydrogen peroxide) for 10 minutes at room temperature. Finally, 50 µl / well of 3 M HCl was added, incubated for 10 minutes at room temperature before 150 µl of the supernatant was moved into a new 96 well plate and absorbance measured at 492 nm. Background readings were measured from wells without cells and this subtracted from cell measurements. Data was then normalised to corresponding 5 mM glucose readings and displayed as fold change.

Aortic Root Plaque Analysis

To quantify plaque burden PFA fixed aortic roots were placed in optimal cutting medium (OCT) and sectioned on a plane parallel to the atria. In order to quantify plaque area, plaque lipid content and collagen content, sections were Masson-Goldner trichrome stained (Merck, UK). Briefly, sections were re-fixed in Bouins solution at room temperature for 1 hour, washed in

running water for 5 minutes and then subjected to the Masson-Goldner staining kit protocol from the second 70% ethanol incubation according to the manufacturer's protocol. Xylene-wet slides were then mounted with Neo-Mount and sealed with cover glass. Plaque characteristics were quantified on Image Pro Plus software version 6.0 (Media Cybernetics, Silverspring, MD). Masson trichrome stained aortic root sections were used to quantify plaque area by masking plaque area; collagen by masking green stained collagen within the plaque area and necrotic area by masking the white area within the plaque area [161].

Immunofluorescence was performed on adjacent sections. Sections were stained for macrophage content using GFP (rabbit anti-GFP, Invitrogen, UK), the macrophage marker GAL3 or α-actin to quantify smooth muscle cells (rabbit anti-smooth muscle cell α-actin; Abcam PLC, UK). For immunofluorescence staining, sections were rehydrated with PBS for 5 minutes at room temperature and blocked for 1 hour with DAKO blocking buffer. Anti-GAL3 and anti-GFP primary antibodies were diluted to 1 µg/mL in DAKO and added to sections overnight at 4 ºC. Secondary antibodies (anti-rabbit A_{488} or anti-goat A_{594}; Life Technologies, UK) were diluted 1:200 in DAKO and added for 1 hour at room temperature and then DAPI mounted. Fluorescent images were analysed using Image J software. Nuclear stained (DAPI) images were used to ascertain aortic root structure and outline plaque area borders. Plaque borders were combined with immunofluorescence stained images where either α-actin or GAL3 were masked to quantify intra-plaque actin content or macrophage content, respectively.

Western Blot Analysis

WT or STZ HSC cultured in 5 mM or 20 mM glucose ± 10 ng/mL IL-1β ± 10 mM DCA and WT or STZ BMDM cultured in 5 mM glucose ± 10 ng/mL IFNγ plus 100 ng/mL LPS were used for protein analysis. Cells were washed in ice-cold PBS and lysed in RIPA lysis buffer (150 mmol/L NaCl, 1.0% IGEPAL® CA-630, 0.5% sodium deoxycholate, 0.1% SDS, 50 mmol/L Tris, pH 8.0) supplemented with protease and phosphatase inhibitors (Complete protease

inhibitor cocktail, Roche, UK). Protein concentration was determined by bicinchoninic acid assay (BCA) assay (Pierce BCA Protein Assay Kit, ThermoFisher Scientific, UK) according to assay instructions.

20 µg of protein alongside a rainbow protein molecular weight ladder (FisherScientific, UK) were loaded and run on an SDS-PAGE gel (4-12 % Bis-Tris Gel, Life Technologies, UK) for separation by gel electrophoresis, at 120 mV for 60 minutes at room temperature. Proteins were transferred onto a nitrocellulose membrane (Bio-Rad, UK) by cutting the gel, loading it into a cassette with the nitrocellulose membrane in NuPage transfer buffer (25 mM Tris-Base, 192 mM glycine, 20 % methanol; Life Technologies, UK) for 120 minutes at 120 mV at 4 ºC. Successful transfer was confirmed with a 1-minute ponceau stain (Ponceau S solution; Sigma Aldrich, UK) with the appearance of protein bands.

Ponceau was washed away with PBS plus 0.1% tween-20 (PBS-T; Sigma Aldrich, UK) and membranes incubated in 5 % milk dissolved in PBS-T for 1 hour at room temperature to block non-specific protein binding. Membranes were probed with primary antibodies overnight at 4 ºC diluted in 5 % milk-PBS-T for rabbit anti-H3K4me3 (1:2500 dilution; Abcam PLC, UK), rabbit anti-H3K27ac (1:2500 dilution; Abcam PLC UK) and mouse anti-β-actin (1:5000 dilution; Abcam PLC, UK). Membranes were washed three time for 5 minutes at room temperature in PBS-T, followed by incubation with secondary antibodies anti-mouse IgG conjugated to HRP (1:25,000; Promega, UK) or anti-rabbit IgG conjugated to HRP (1:50,000; Promega, UK) for 1 hour at room temperature diluted in 5 % milk-PBS-T. After 3 washes in PBS-T, membranes were developed using the chemiluminescent substrate SuperSignal West Dura Extended Duration Substrate (Thermo Scientific, UK), according to manufacturer's instructions, for 2 minutes and immediately detected by chemiluminescence on a Biorad Image Station (ChemiDoc MP System, Biorad). Protein expression was quantified by densitometry of each band using Image Lab software (Biorad). Data shown represents H3K4me3 and H3K27ac protein quantification after normalisation to the matching β-actin quantification values.

Human Monocyte Metabolomics

Isolated human monocytes were cultured at a density of 3.5 x10^5 cells / sample in complete 5 mM glucose DMEM media, media supplemented with glucose to make a final concentration of 20 mM glucose or media with 15 mM mannitol in 5 mL FACS tubes for 12 hours. Cell lysates were prepared by extraction with ice cold methanol for 20 minutes on dry ice and snap frozen in liquid nitrogen. On the day of analysis, samples were vortexed and then centrifuged at 10,000 *g* for 10 minutes. A pooled quality control (QC) sample was prepared by mixing 60 µL of each sample extract and analysed periodically throughout the overall analytical run to confirm method performance. Samples were filtered using a 0.1 µm Ultrafree-MC centrifugal filter (5000 *g*, 3 minutes) and then transferred to LC-MS vials. Non-targeted metabolomics analyses were performed as previously described [162]. Briefly, samples were analysed on a Thermo Ultimate 3000 UHPLC coupled to a Q-Exactive Orbitrap using polarity switching (positive-negative) acquisition operating at a mass resolving power of 70,000 FWHM. Hydrophilic compounds were chromatographically separated on a Merck Sequant ZIC-HILIC column (150 × 4.6 mm, 5 µm particle size) and hydrophobic compounds using a Thermo Accucore aQ RP C18 column (150 × 2.1 mm, 2.7 µm particle size). Metabolites were identified using an in-house database [162]. Metabolite set enrichment analysis (MSEA) and metabolic pathway analysis was performed on all metabolite measurements using MetaboAnalyst online software (v4.0) [163].

Mouse Metabolite Measurements

For metabolite measurements, BMDM (at a density of 5x10^5) and HSC (at a density of 1x10^6) were cultured in 5 mM, 20 mM glucose on control conditions (5 mM glucose + 15 mM mannitol) ± 100 ng/mL LPS plus 10 ng/mL IFNγ or 10 ng/mL IL-4 in the presence or absence of 10 mM DCA or 1 mM 2-DG. Culture supernatants were run on the ABX Pentra 400 (Horiba) to measure glucose (ABX Pentra Glucose PAP CP, Horiba, UK) and lactate (ABX Pentra Lactic Acid, Horiba) levels, according to the manufacturer's instructions. Measurements were

normalised to glucose and lactate concentrations present in control complete cell culture media that was incubated under the same conditions, but not in the presence of cells.

Human Plaque Macrophage Microarray

Isolated plaque macrophage RNA concentrations were determined using the Agilent RNA 6000 Pico LabChip on the Agilent Bioanalyzer 2100 (Agilent Technologies, USA). Samples with an RNA integrity number (RIN) >5 were taken forward to RNA amplification, biotinylation and gene expression microarray analysis. These samples were submitted to Cambridge Genomic Services (Department of Pathology, University of Cambridge, UK) for further processing. Amplification and biotinylation was performed using Ovation Pico WTA V2 kit (Nugen Technologies Inc, USA) and then hybridization was carried out in random order on two Illumina Human HT12 v4.0 BeadChips (Illumina, USA) to minimise batch / chip variation. Illumina Beadarrays were firstly processed with the Bioconductor beadarray package (v.2.24.0) [164,165] using normal exponential normalization. Probe sets were collapsed per gene based on maximum interquartile range to avoid extreme values but capture variability across all samples. Unannotated and control probe sets were excluded from further analysis. Genes that were differentially expressed (DE) comprised of a final list of 21,036 genes was assessed using the Bioconductor limma package (v.3.30.13) [166] to compare diabetic to control, adjusting for symptomatic / asymptomatic status. Given the availability of orthogonal data sets and $n \geq 8$ samples per group, we used a relatively lenient adjusted p-value < 0.2 with no fold change cut off to select genes to pursue.

Assay for Transposase Accessible Chromatin (ATAC)-sequencing

WT or diabetic isolated HSC, stimulated with IL-1β or unstimulated control cells in 5 mM glucose DMEM media, were used for ATAC-seq analysis according to previously described protocol [167]. Briefly, nuclei from 50,000 cells per replicate were isolated and lysed (10 mM Tris-Cl (pH 7.4), 10 mM NaCl, 3 mmol/L $MgCl_2$, 0.05% NP-40) on ice. Immediately, isolated nuclei

were put through transposition reaction using Tn5 transposase and TD buffer (Illumina, USA) for 30 minutes at 37ºC. Following DNA purification with the MinElute PCR Purification Kit (Qiagen, UK) eluting in 11 µl, 1 µl of the eluted DNA was used in a quantitative PCR reaction to estimate the optimum number of amplification cycles. Library amplification (NEBNext High Fidelity 2x PCR master mix, New England Biolabs, USA) was followed by SPRI size selection to exclude fragments larger than 1,200 bp. DNA concentration was measured with a Qubit fluorometer (Life Technologies) and library size distribution was assessed using Bioanalyser DNA High-Sensitivity chip (Agilent, UK). Library amplification was performed using custom Nextera primers [167]. Libraries were sequenced by the Biomedical Sequencing Facility (BSF) at CeMM using the Illumina HiSeq 3000/4000 platform and the 50-bp single-read configuration.

ATAC-seq data reads were controlled for quality and trimmed of any remaining adapters with Trim Galore (v.1.8) and FastQC (v.0.11.3). Reads were then aligned to the mouse genome (Mm10) with Bowtie (v.2.2.6) in "--sensitive-local" mode. Aligned reads were filtered to remove low quality matches (MAPQ ≤ 10) or reads mapping to mitochondrial sequences. On average, 16 million uniquely mapped reads (13.4-24.6 million representing 60% of total) were retained per sample. Alignment start positions were shifted in a strand-aware manner (+4bp, -5bp, 30) prior to peak calling with MACS2 (v.2.1.1, 58) with the following settings: --nomodel --extsize 147 -q 0.01 -m 5 50 -s 50 --call-summits. Differentially bound regions were identified using DiffBind (v.2.4.8, 59,60) with peak centering (summits=100) and edgeR.

Pathway analysis was then performed on peaks enriched in diabetic samples (FDR≤0.1), by inputting the peak chromosome location into Genomic Regions Enrichment of Annotations Tool (GREAT; v3.0) [168], which predicts functions of cis-regulatory regions by firstly, assigning gene annotations of the two nearest genes (within 1000 kb regulatory domain), and then predicting the biological pathways those genes were involved in and whether any are significantly enriched (FDR<0.05). Differential peak regions were then analysed using MEME-

ChIP (v4.12.0) [169,170], which performs comprehensive motif analysis to identify any known or unknown binding motifs are enriched (enriched motifs E<0.05, minimum width = 6, minimum number of sites = 3).

RUNX1 target identification: MEME-ChIP of ATAC-seq regions identified RUNX1 as a potential regulator in both IL-1β and unstimulated diabetic HSC. MEME GOMo (v.4.12.0) [171] was used to scan Mouse and Human promoters (-1000, +200) for the consensus RUNX1 motif (MA002.2). In addition to Gene Ontology enrichment analysis, GOMo returns a list of genes identified as targets. These hits were restricted to conserved promoters bound in both Mouse and Human with empirical p-value < 0.05 or 0.01. Mouse Genome Informatics (MGI) identifiers were converted to Mouse Ensembl IDs on the MGI website (http://www.informatics.jax.org/batch), then to Human Ensembl ID and gene symbol using the Ensembl BioMart interface (http://www.ensembl.org/index.html). For p-value < 0.05, 1,300 target genes were converted of which 1,251 were represented on the arrays; for p-value < 0.01, there were 355 converted and 347 on the arrays. Over-representation of RUNX1 target genes among the DE genes was assessed by Fisher's Exact Test as implemented in R (https://www.r-project.org/). The pheatmap package (v.1.0.8; https://cran.r-project.org/web/packages/pheatmap/index.html) was used to generate a heat map of DE genes, with row-normalised log2 values shown for DE genes. Both genes and samples were clustered by Pearson's correlation.

Statistical Analysis

All non-sequencing data statistical analysis was performed in GraphPad Prism software. Data were analysed for parametric distribution by Shapiro-Wilk normality test. Comparisons between two groups were calculated by two-tailed Student’s t tests or Mann-Whitney U test for parametric or non-parametric data, respectively. Comparisons between multiple groups were calculated by one-way (or Kruskal-Wallis test with Dunn’s Post Hoc analysis for non-parametric data) or two-way ANOVA with Bonferonni post-hoc analysis and significance

represented on the graph by *p<0.05, **p<0.01 or ***p<0.001. At a value of p<0.05 the null hypothesis was rejected. Data are reported as mean ± standard deviation, for parametric data, or median ± interquartile range for non-parametric data. Number of replicates (n) and other statistical details can be found in the figure legends. For both *in vivo* and *in vitro* experiments, n= number of individual animals or individual volunteers. Fold changes are calculated as average test condition value divided by average control value.

Data Resources

The ATAC-sequencing (GSE120518) and bead array data (GSE118481) generated during this study are available at the Gene Expression Omnibus (GEO) data repository.

Chapter 3 : Hyperglycaemic Effects on Macrophage Metabolism, Gene Expression and Function

Introduction

High glucose is known to increase monocyte and macrophage pro-inflammatory gene expression [77] and functions, such as adhesion [36], migration [172] and foam cell formation [173]; however, the underlying mechanisms have not been fully described. Pro-inflammatory macrophages primarily utilise glucose as their metabolic substrate, due to their preferential switch to aerobic glycolysis [80]. It is not fully understood how increasing concentrations of glucose, for example those that occur during diabetes, might affect macrophage metabolism and in turn their inflammatory status. Understanding this may provide mechanistic insight into the pro-inflammatory effects of hyperglycaemia and high extracellular glucose.

Hypothesis

High glucose alters monocyte and macrophage cell metabolism and these change in turn affect inflammatory gene expression and function.

Aims

To understand how diabetic hyperglycaemia alters monocyte and macrophage metabolism and inflammatory function, the influence of the following was investigated:

- High glucose on monocyte and macrophage metabolism and whether metabolic changes are consistent between human and mouse cells
- High glucose driven metabolic changes on monocyte and macrophage inflammatory gene expression and functions relevant to atherosclerosis, such as adhesion to activated endothelial cells and foam cell formation

Methods

The methods description below is intended to provide an overview of experimental techniques used in this chapter. Full experimental and reagent details are described in *Materials and Methods* (Chapter 2).

Metabolism characterisation

Non-targeted metabolomics was performed on healthy volunteer human monocytes, as summarised in Figure 3.1. To interrogate whether previously described metabolic pathways or externally defined metabolite sets were altered in this dataset, pathway analysis and MSEA were performed, respectively on MetaboAnalyst [163]. Glucose and lactate levels for WT C57Bl/6 BMDM were measured using an enzymatic colorimetric assay performed on an ABX Pentra Analyser. Measurements were taken from media supernatants obtained from WT BMDM cultured in varying glucose and control conditions (5 mM, 20 mM glucose or mannitol); with or without LPS and IFNγ (M1 stimulation) or IL-4 (M2 stimulation) and in the presence of the glycolytic inhibitors DCA or 2-DG for 18 hours.

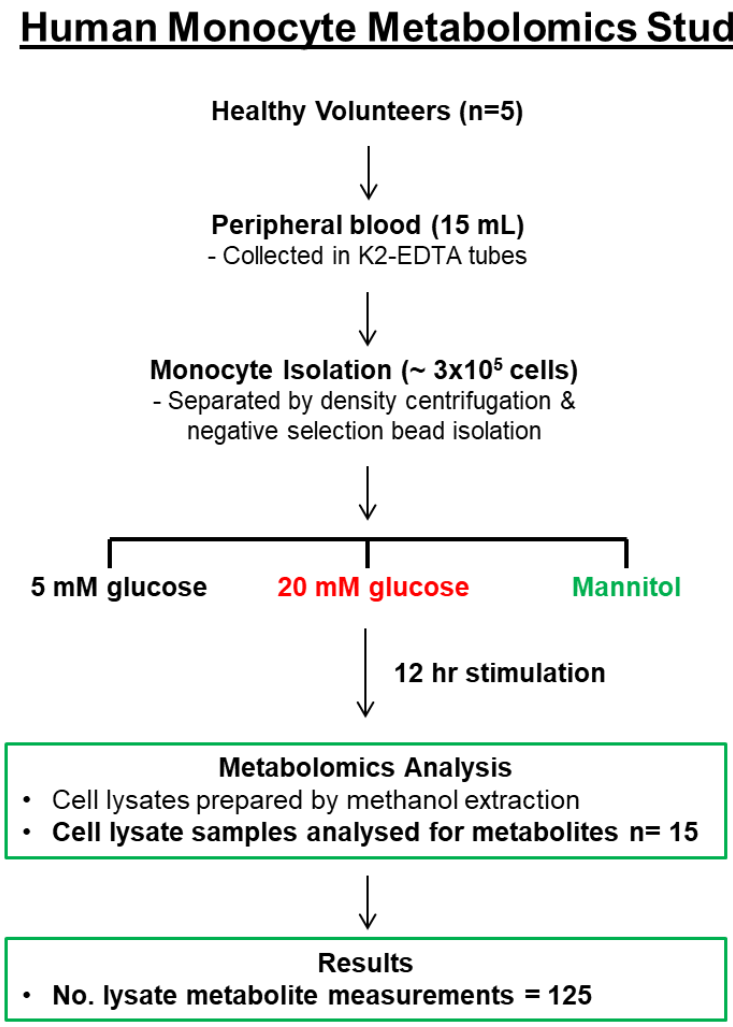


Figure 3.1 ***Summary of metabolomics protocol.***

Peripheral blood monocytes were isolated and cultured in various glucose (5 mM and 20 mM) and osmotic control (5 mM glucose + 15 mM mannitol) conditions and their cell lysates sent for metabolomics analysis at The Karolinska Institute, Stockholm.

GLUT1 surface expression

WT C57Bl/6 BMDM were cultured in varying glucose and control conditions; with or without LPS and IFNγ for varying times. After desired incubation time cells were fixed with PFA. This was followed by an incubation with rabbit anti-GLUT1 at 1:400 at 4 ºC overnight. After its removal and 3x PBS washing, cells were incubated with anti-rabbit-HRP (1:1000 dilution) for 1 hour at room temperature. GLUT1 surface expression was assessed colorimetrically through the addition of OPD reagent for 10 minutes at room temperature and absorbance measured at 492 nm (A_{492}). Data shown represents test well A_{492} with background A_{492} values removed and normalised to the corresponding 5 mM glucose value.

Succinate and α-KG measurements

WT C57Bl/6 BMDM were cultured in varying glucose and control conditions; with or without LPS and IFNγ or IL-4. Succinate and α-KG were measured in cell lysates using the colorimetric succinate assay kit (Abcam, ab204718) or colorimetric alpha ketoglutarate assay kit (Abcam, ab83431), respectively.

BMDM gene expression

WT C57Bl/6 BMDM were cultured in varying glucose and control conditions; with or without LPS and IFNγ or IL-4 and in the presence of the glycolytic inhibitors DCA or 2-DG for 18 hours. Cell lysate mRNA isolated, converted to cDNA and used for qPCR (normalised to B2M housekeeper gene expression).

Static adhesion assay

WT C57Bl/6 mouse peripheral blood monocytes were isolated; left unstimulated or stimulated with LPS plus IFNγ in varying glucose and control conditions with or without DCA or 2-DG for 18 hours; fluorescently labelled green using PKH67 and added to TNF-α stimulated sEND.1 endothelial cells for 1 hour. Unadhered cells were then removed, cover slips washed, PFA

fixed and nuclear (DAPI) stained. Four images per cover slip were taken and the number of adhered monocytes quantified, per image, and averaged to provide the data points shown.

Foam cell assay

WT C57Bl/6 BMDM were cultured in varying glucose and control conditions; with or without LPS plus IFNγ ± DCA and DiI-ac-LDL for 48 hours. Cells were then washed, PFA fixed and lipid and nucleus stained with ORO and DAPI, respectively. Four images per cover slip were taken and the amount of lipid per image quantified and normalised to the number of cells. All four values were averaged to provide the data points shown.

Results

High glucose alters monocytes and macrophage metabolism

A total of 125 metabolites measurements were identified in primary human monocytes cell lysate samples. Pathway analysis (Figure 3.2 A) revealed significant changes in the TCA cycle (FDR=0.002) and pyruvate metabolism (FDR=0.005) for high glucose (20 mM), treatment denoted by increased pyruvate, lactate, malate and succinate levels (Figure 3.2 C-F), as compared to physiological glucose (5 mM) and osmotically matched conditions (5 mM glucose + 15 mM mannitol). MSEA (Figure 3.2 B) showed enhancement of the Warburg pathway (FDR=0.04).

a

Metabolic Pathway Analysis	KEGG Pathway ID	p-value	FDR
Citrate cycle (TCA cycle)	HSA0020	3.00E-05	2.14E-03
Pyruvate metabolism	HSA00620	1.10E-04	4.57E-03
Glyoxylate and dicarboxylate metabolism	HSA00630	4.30E-04	1.17E-02
Alanine, aspartate and glutamate metabolism	HSA00250	2.57E-03	5.15E-02
Glycolysis or Gluconeogenesis	HSA00010	4.28E-03	6.85E-02

b

Metabolite Set Enrichment Analysis	Pathway ID	p-value	FDR
Warburg Effect	SMP00654	5.50E-04	4.38E-02

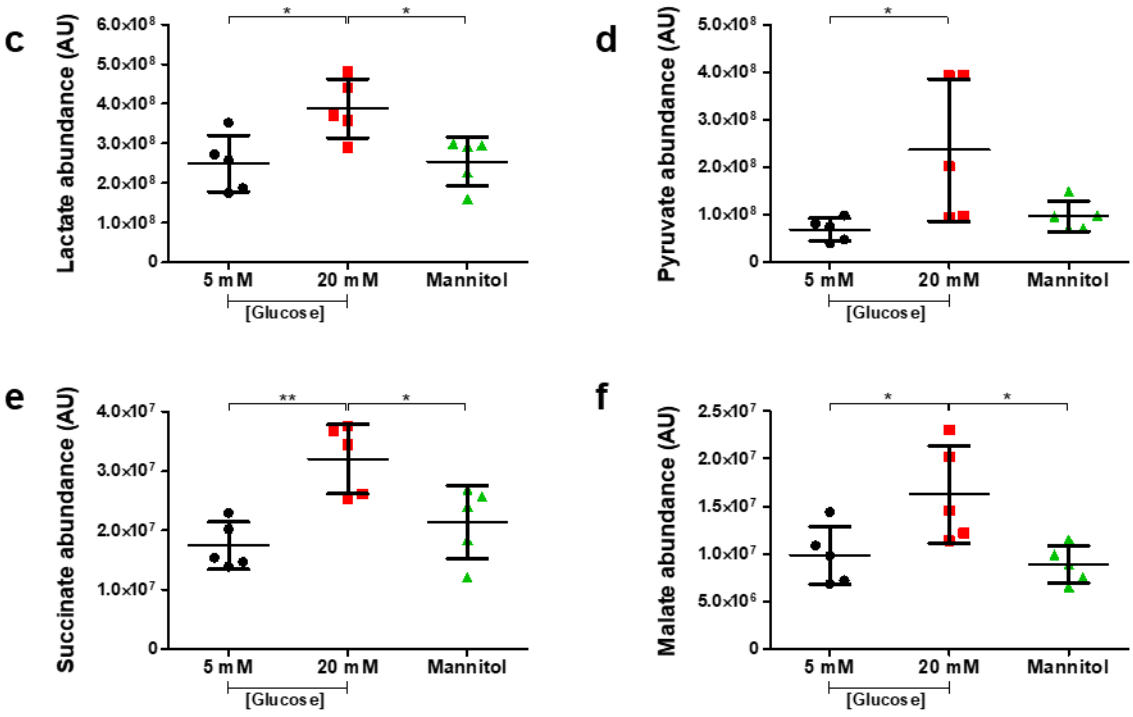


Figure 3.2 ***Diabetic hyperglycaemia alters cellular metabolism.***

*(a) Metabolic Pathway Analysis and (**b**) Metabolite Set Enrichment Analysis (MSEA) performed on MetaboAnalyst for human monocyte cell lysate metabolomics samples (n=5). Individual data showing measurements (AU = arbitrary units) of (c) lactate, (d) pyruvate, (e) succinate and (f) malate in various extracellular glucose or osmotic control (mannitol) conditions. AU = arbitrary units. Metabolomics data are n = 5 per condition, analysed by one-way ANOVA plus Bonferroni post-hoc test; *p<0.05, **p<0.01.*

Mouse BMDM were used as a primary cell culture system for confirmation of metabolism findings and as a versatile model for future studies. BMDM were differentiated from WT BM and can be seen to be differentiating and adhering over 7 days of culture (Figure 3.3 A). After positive selection through adherence, cells stained positive for the macrophage markers CD11b, F4/80, GAL3 and CD68 (Figure 3.3 B) and negative controls (where primary antibodies were not added to cells) or isotype controls revealed no staining (Figure 3.3 B); 98.3 % were CD45+ and 98.5 % CD45+ CD11b+, as assessed by flow cytometric analysis (Figure 3.3 C, D). Unstimulated M0 macrophages were then polarised into an M1 (with LPS plus IFNγ) or M2 (with IL-4) phenotype and were imaged using SEM (Figure 3.3 E).

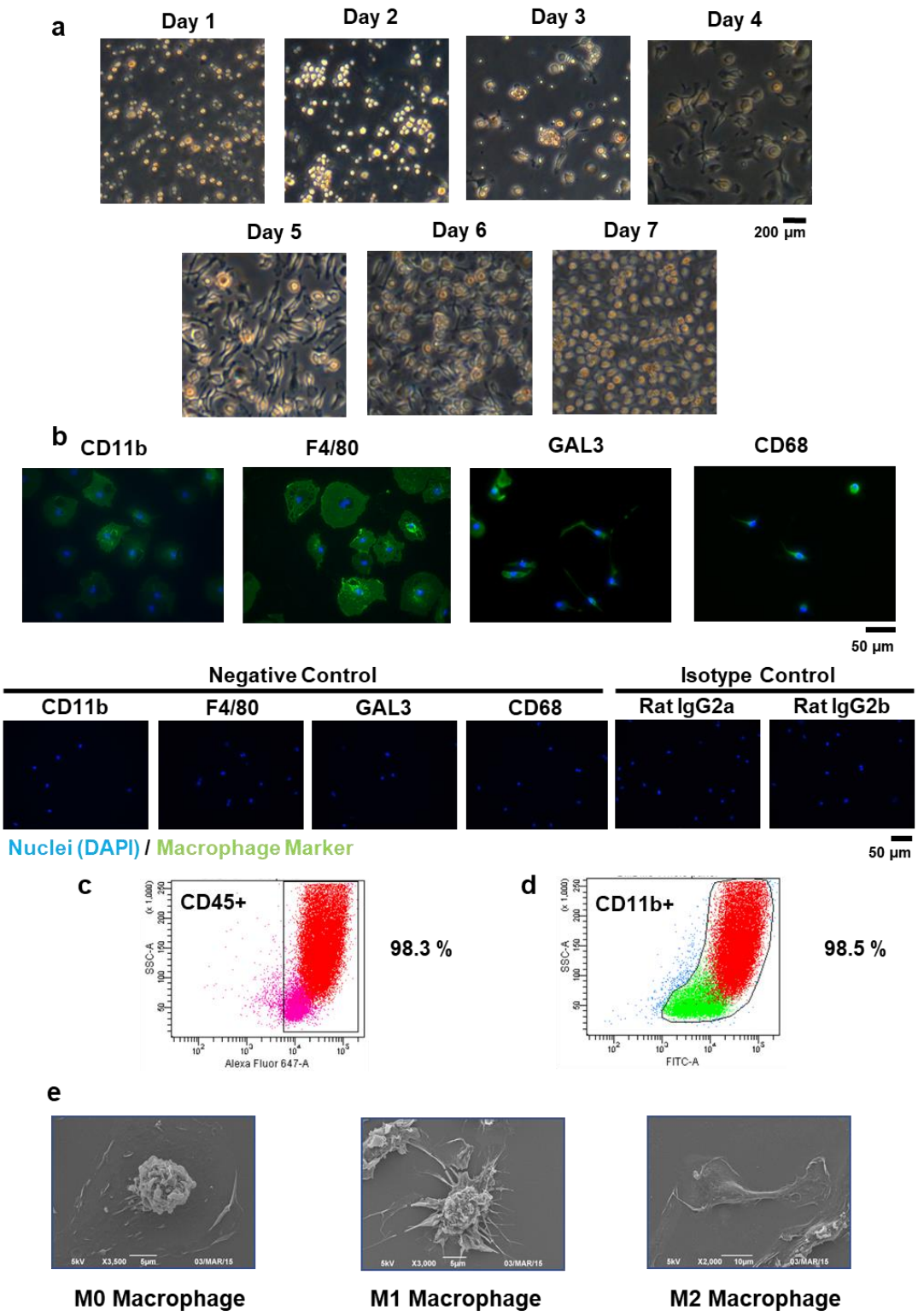


Figure 3.3 ***BMDM characterisation****.*

WT bone marrow differentiation was performed (a) over 7 days in the presence of fibroblast (L929) conditioned media. Positively selected M0 macrophages stained positive for macrophage markers (b) CD11b, F4/80, GAL3 and CD68 or negative in the presence of isotype controls or without a primary antibody (negative control); and were (c) CD45+ and (d) CD45+ CD11b+ as assessed by flow cytometry (by Dr Thomas Cahill). Scanning electron microscopy (SEM) images (performed by Dr Errin Johnson) of an (e) unstimulated M0, LPS + IFNγ stimulated M1 or IL-4 stimulated M2 macrophage.

To confirm if similar metabolic pathways and metabolites are altered by high extracellular glucose in mouse cells, metabolite measurements were taken from the supernatant of BMDM cultured in physiological (5 mM), high glucose (20 mM) or osmotic control conditions (5 mM glucose plus 15 mM mannitol), with or without M1 or M2 stimulation. High extracellular glucose conditions increased BMDM glucose consumption and lactate production ($p<0.001$), indicating increased glycolysis and lactic acid fermentation (Figure 3.4 A, B). This increase in glycolytic rate was amplified when high extracellular glucose and LPS were combined and were prevented by the glycolysis inhibitors DCA (Figure 3.4 A, B) and 2-DG (Figure 3.4 C, D).

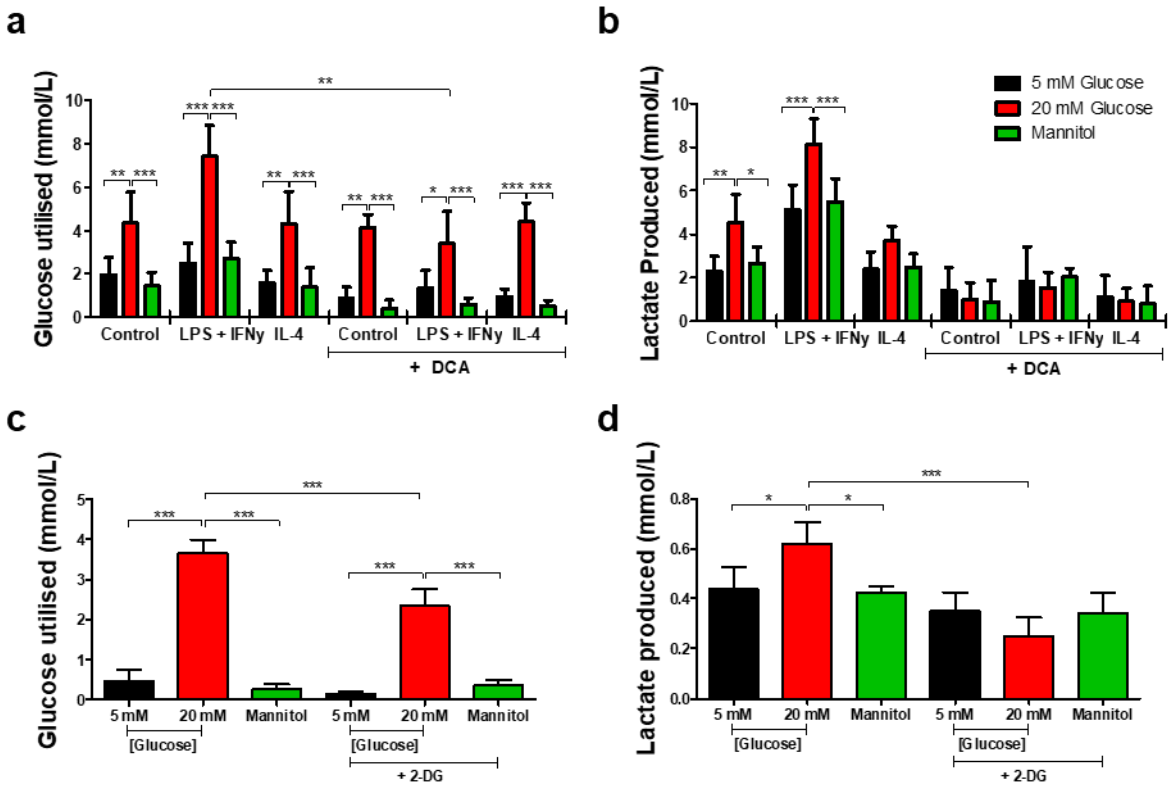


Figure 3.4 ***High glucose alters mouse cell metabolism.***

*Mouse BMDM culture supernatants indicating (a) glucose uptake and (b) lactate production in the absence or presence of dichloroacetate (DCA) or (c & d) 2-deoxyglucose (2-DG), as measured by Pentra. Sample n = 5 per condition; two-way ANOVA with Bonferroni post-hoc analysis; *p<0.05, **p<0.01, ***p<0.001. All data shown are mean ± SD.*

In order to assess BMDM GLUT1 surface expression, firstly, the optimal cell number was determined by performing the assay at varying BMDM densities (Figure 3.5). A BMDM density of 1 x10^4 was used as this was the point the signal in stimulated BMDM reached its maximal point before plateauing.

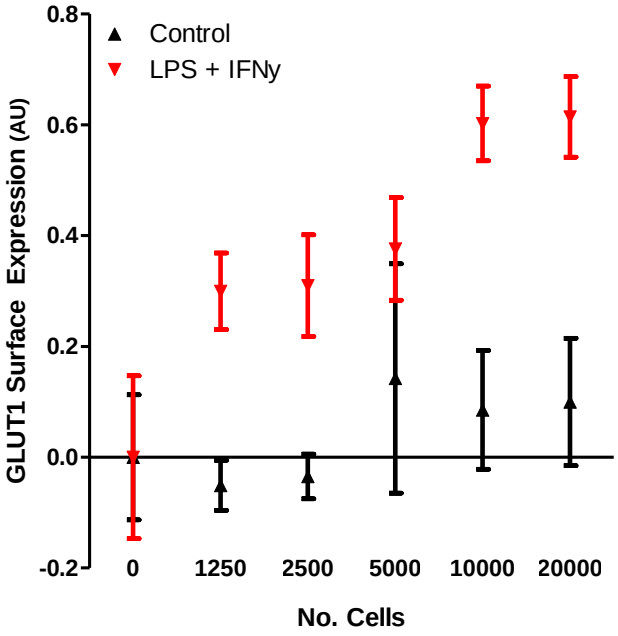


Figure 3.5 ***GLUT1 assay cell number titre****.*

Varying cell numbers were assessed for GLUT1 surface expression with or without 6-hour stimulation with LPS + IFNγ. Data shown in AU (arbitrary units) and mean ± SD, sample n=4 per condition.

Further interrogation of BMDM GLUT1 expression over time showed that high glucose caused a significant increase in its surface expression at 4 hours in unstimulated macrophages (2.8-fold; $p<0.0001$; Figure 3.6 A) and in M1 macrophages (4.5-fold, $p<0.0001$; Figure 3.6 B) which remained elevated at 6 hours (1.6-fold; $p<0.05$).

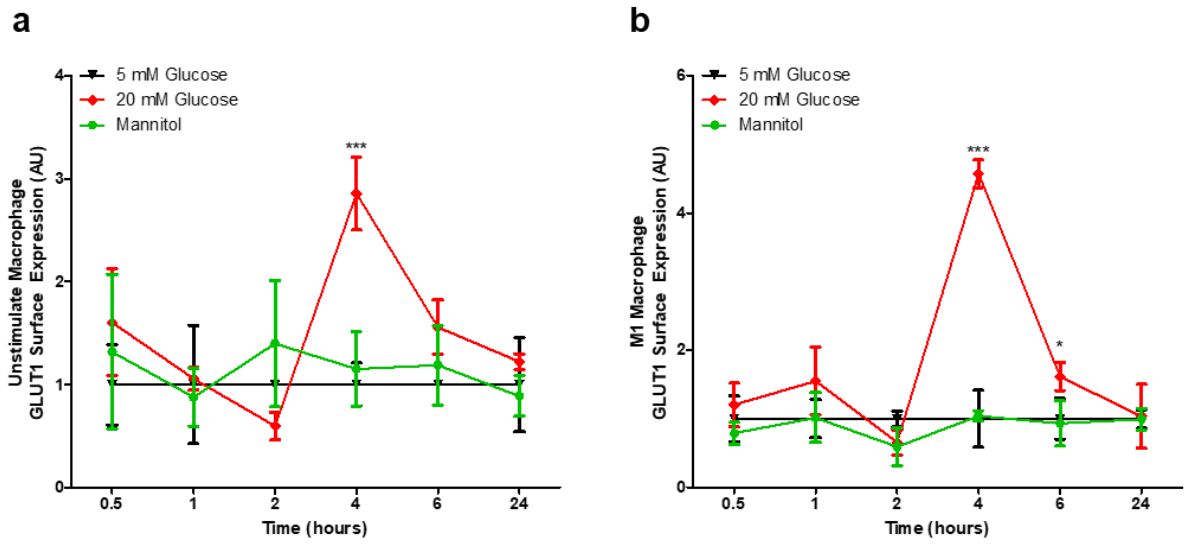


Figure 3.6 ***BMDM GLUT1 surface expression***.

*Surface expression of GLUT1 (AU= arbitrary units) in (a) unstimulated and (b) M1 (LPS + IFNy) stimulated BMDM, stimulated under various glucose or control (mannitol) conditions. Data are normalised to 5 mM glucose, sample n=4 per time point and condition, two-way ANOVA with Bonferroni post-hoc analysis; *p<0.05, ***p<0.001. Data shown as mean ± SD.*

BMDM cultured in 20 mM glucose, compared to 5 mM glucose, had increased succinate levels in both unstimulated (2.5-fold, $p<0.05$; Figure 3.7 A) and M1 stimulated states (1.9-fold, $p<0.001$; Figure 3.7 A). This leads to an increased succinate : α-KG ratio in M1 BMDM cultured in 20 mM glucose (2.2-fold, $p<0.01$; Figure 3.7 C).

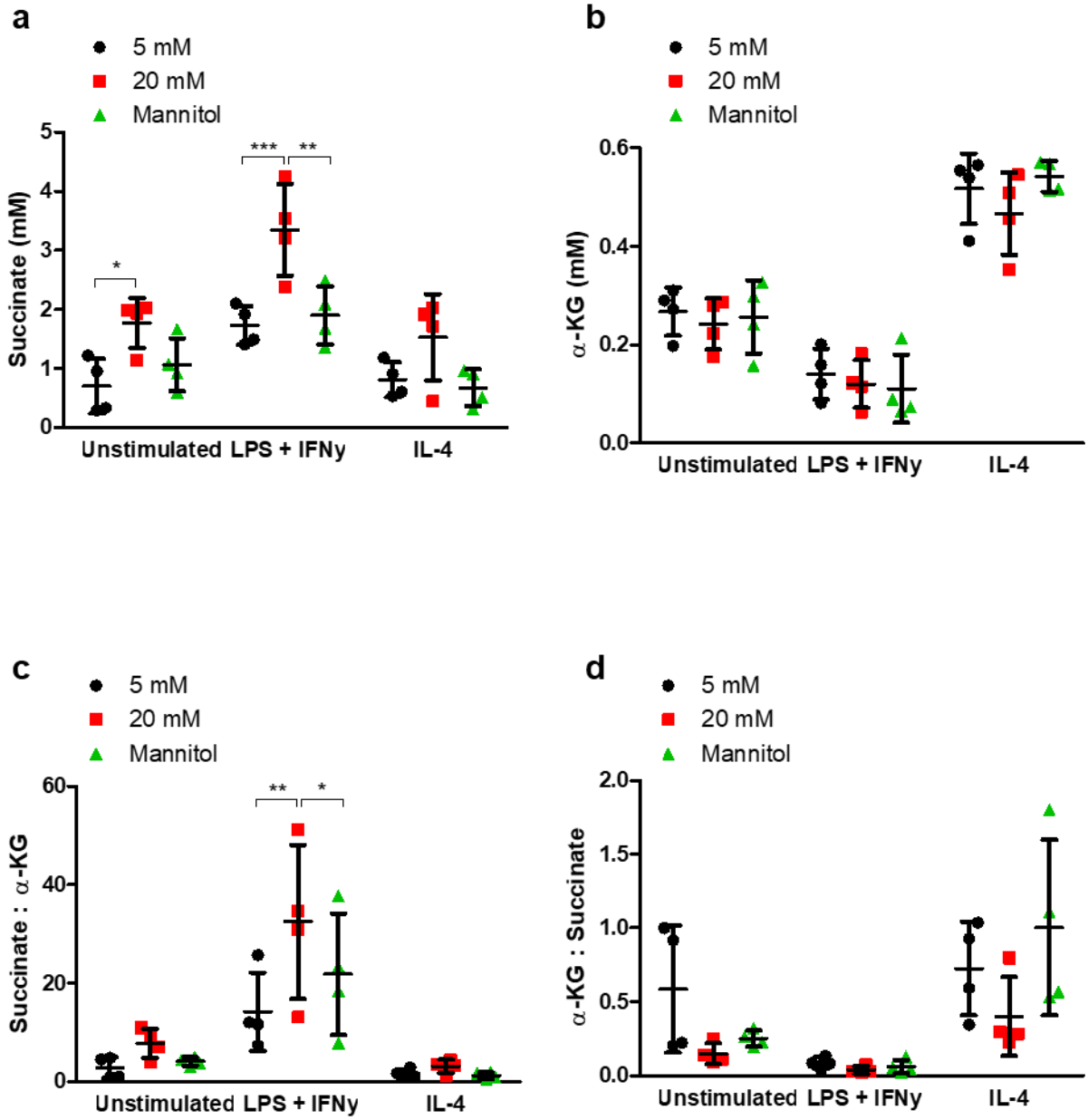


Figure 3.7 ***High glucose increases succinate levels.***

*(a) Succinate and (b) α-KG levels measured in cell lysates from BMDM cultured in 5 mM, 20 mM glucose or control (mannitol) conditions, unstimulated or M1 (LPS + IFNγ) or M2 (IL-4) stimulated. Levels used to calculate (c) succinate : α-KG and (d) α-KG : succinate ratio. Sample n=4 per condition; 2-way ANOVA with Bonferroni Post-Hoc test *p<0.05; **p<0.01; *** p<0.0001. Data shown as mean ± SD.*

High glucose-induced metabolic changes alter macrophage gene expression

For all gene expression data, the housekeeping gene *B2m* was used as was shown to be the most stable in BMDM (Figure 3.8 A) when compared to *Gapdh* (Figure 3.8 B), *Cyclophilin* (Figure 3.8 C) and smooth muscle β-*Actin* (Figure 3.8 D).

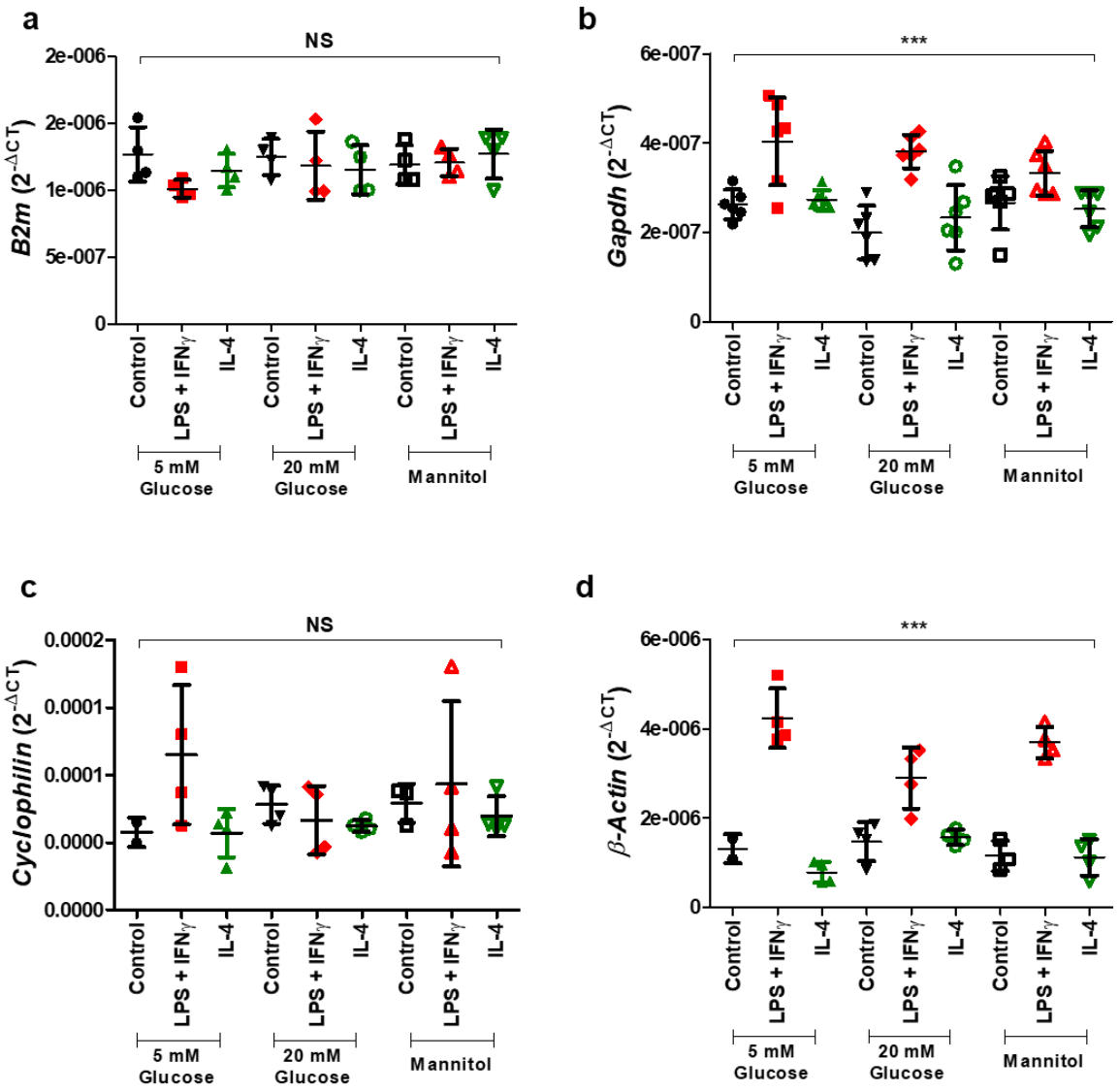


Figure 3.8 ***BMDM Housekeeping panel.***

*cDNA from unstimulated of M1 (LPS + IFNγ) or M2 (IL-4) stimulated WT BMDM were analysed for the expression of (a) B2m, (b) Gapdh, (c) Cyclophilin or (d) β-Actin. Sample n=4 per condition; 1-way ANOVA with Bonferroni Post-Hoc test *** p<0.0001. Data shown as mean ± SD.*

In BMDM, high extracellular glucose both promoted pro-inflammatory M1-associated *Il-6* (2.7 fold; $p<0.001$), *Il-1β* (1.6 fold; $p<0.05$) and *Tnf-α* (2.7 fold; $p<0.001$) expression, however *iNos* expression remained unchanged (Figure 3.9 A-D). High glucose suppressed M2-associated *Ym1* (by 75 %; $p<0.001$) and *Fizz1* (by 70 %; $p<0.001$) expression (Figure 3.9 E, F). These bi-directional changes in gene expression were restored in the presence of DCA, with the exception of *Il-1β* (Figure 3.9 A-F).

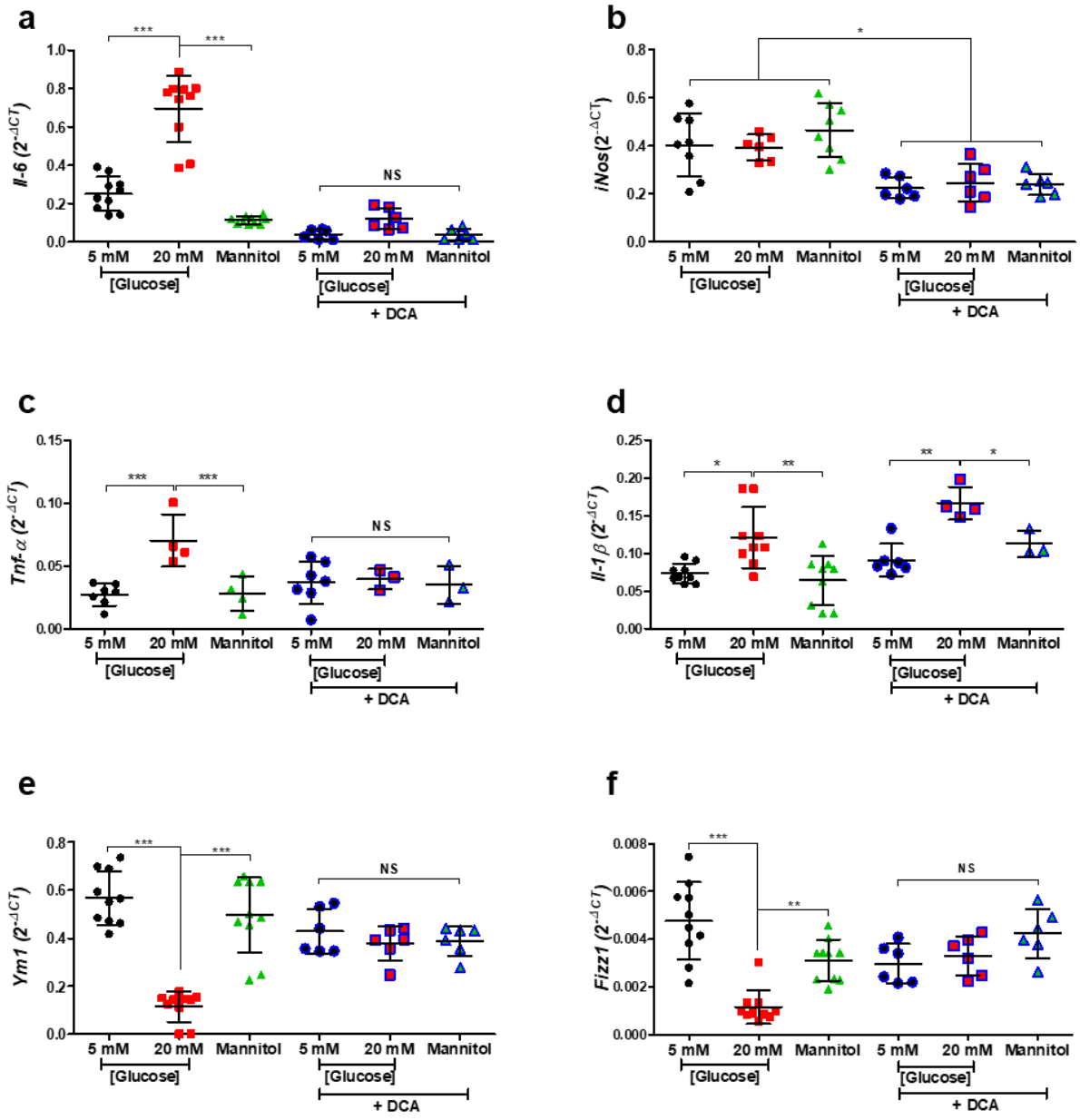


Figure 3.9 ***High glucose alters macrophage inflammatory gene expression****.*

*M1 (LPS + IFNγ stimulated) BMDM (**a**) Il-6 and (**b**) iNos gene expression in the presence or absence of dichloroacetate (DCA). M2 (IL-4 stimulated) BMDM (**c**) Ym1 and (**d**) Fizz1 gene expression. (**a-d**) qPCR data are normalised to B2m expression; n= 7-10. All data (**a-h**) are shown as mean ± SD; (**a-d**) one-way ANOVA or (**e-f**) two-way ANOVA with Bonferonni post-hoc analysis; *p<0.05, **p<0.01, ***p<0.001.*

High glucose-induced metabolic changes alter monocyte and macrophage function

Monocyte adhesion to activated endothelium was evaluated under static conditions. In pilot experiments, the assay duration with the shortest incubation time that produced the largest difference in results between unstimulated and stimulated monocytes was 1 hour (Figure 3.10), and so subsequent static adhesion assays were performed at that time point.

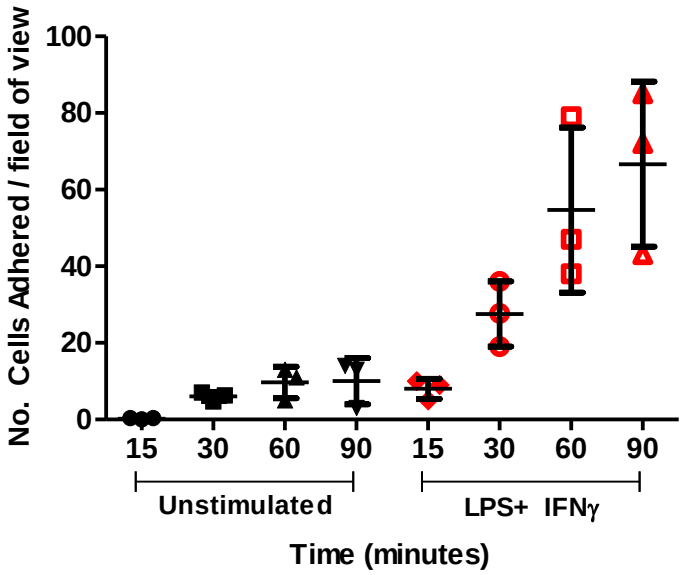


Figure 3.10 ***Static adhesion monocyte time course.***

Unstimulated or LPS + IFNγ stimulated mouse PBMC were incubated with sEND.1 endothelial cell monolayer for 15, 30, 60 or 90 mins. Data represents image quantification of PBMC adhesion. Sample n=3 per time point, data shown as mean ± SD. Each point represents an individual animal (average of 4 images).

High glucose increased mouse monocyte adhesion to activated endothelial cells (2.6 fold; $p<0.001$) and these effects were negated by the inhibition of glycolysis by DCA (Figure 3.11) and 2-DG (Figure 3.12). High glucose promoted BMDM uptake of modified-LDL to form foam cells (4.1 fold [and 2.7 fold, when M1-stimulated]; $p<0.001$ for both) (Figure 3.13) and was decreased by 30 % (and by 42 %, when M1-stimulated; $p<0.001$ for both).

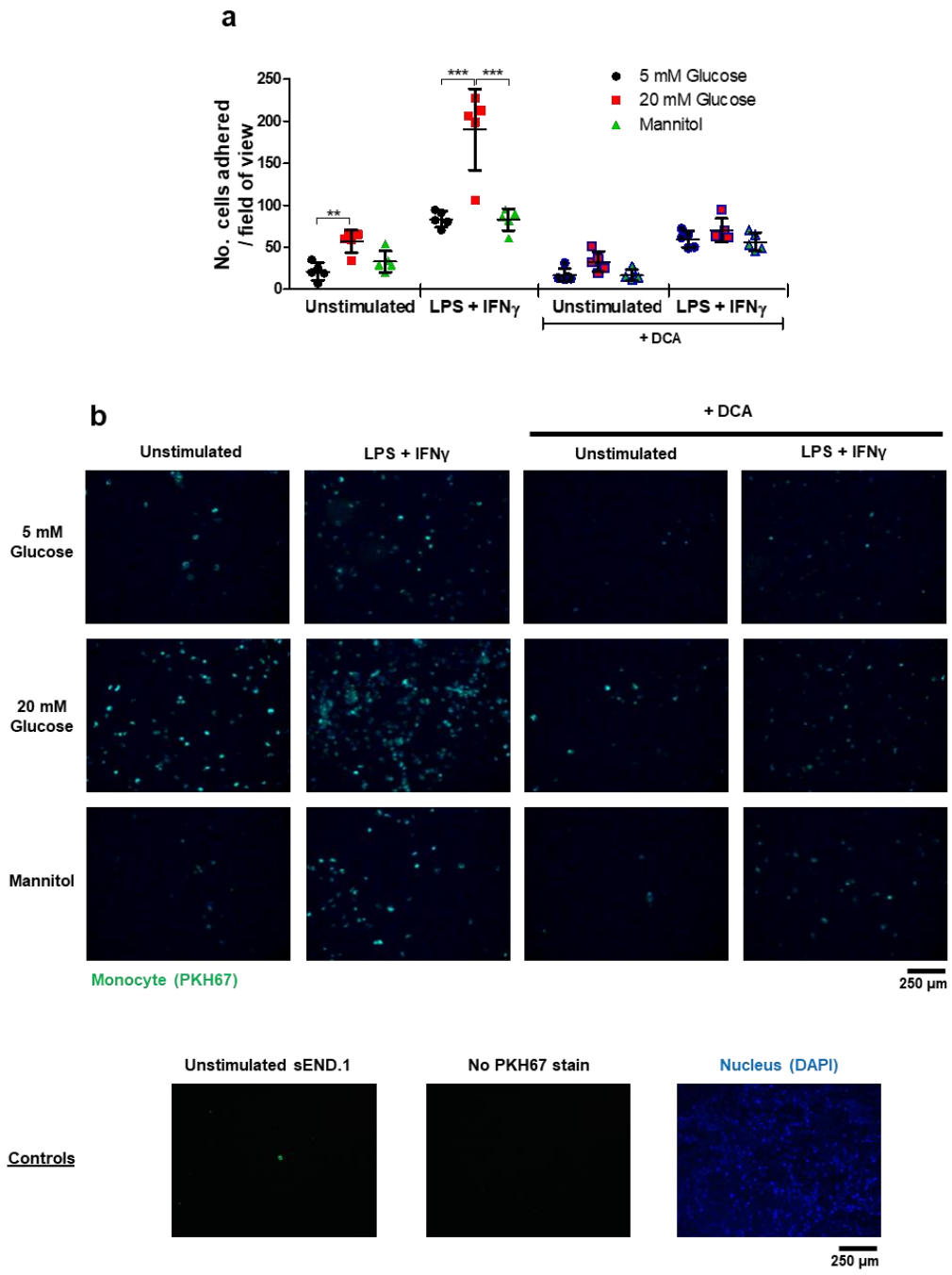


Figure 3.11 ***DCA inhibits glucose altered monocyte adhesion to endothelial cells.***

*(a) Image quantification of PBMC adhesion to endothelial cells (sEND.1), with or without dichloroacetate (DCA) glycolytic inhibition. Representative (b) static adhesion images of fluorescently PKH67 labelled monocytes to endothelial cells or DAPI nuclear staining. All data (a) are shown as mean ± SD; 2-way ANOVA with Bonferonni Post-Hoc analysis; **p<0.01, ***p<0.001 and each point represents an individual animal (average of 4 images).*

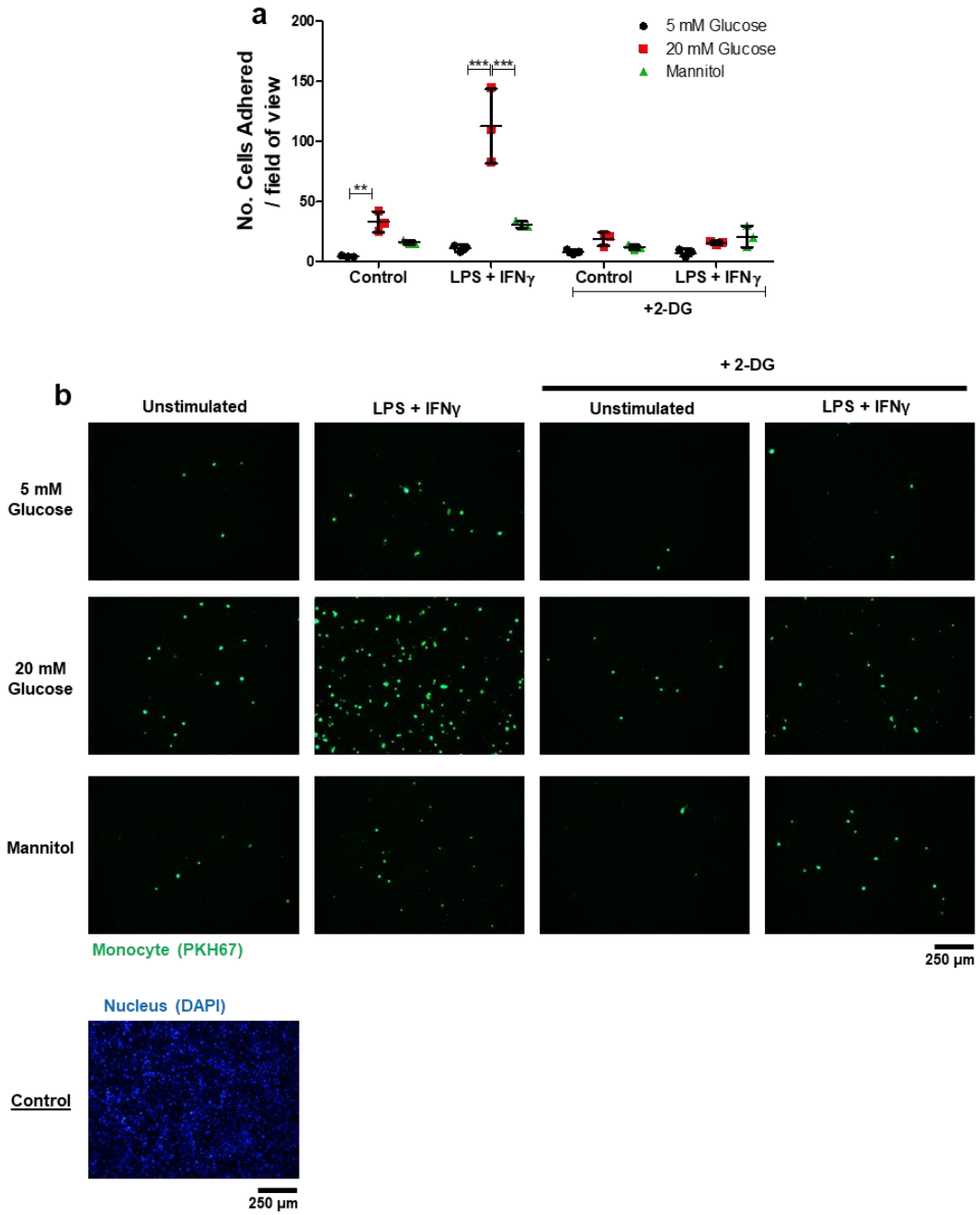


Figure 3.12 ***2-DG inhibits glucose altered monocyte adhesion to endothelial cells.***

*(a) Image quantification of PBMC adhesion to endothelial cells (sEND.1), with or without 2-deoxyglucose (2-DG) glycolytic inhibition. Representative (b) static adhesion images of fluorescently PKH67 labelled monocytes to endothelial cells or DAPI nuclear staining. All data (a) are shown as mean ± SD; 2-way ANOVA with Bonferonni Post-Hoc analysis; **p<0.01, ***p<0.001 and each point represents an individual animal (average of 4 images).*

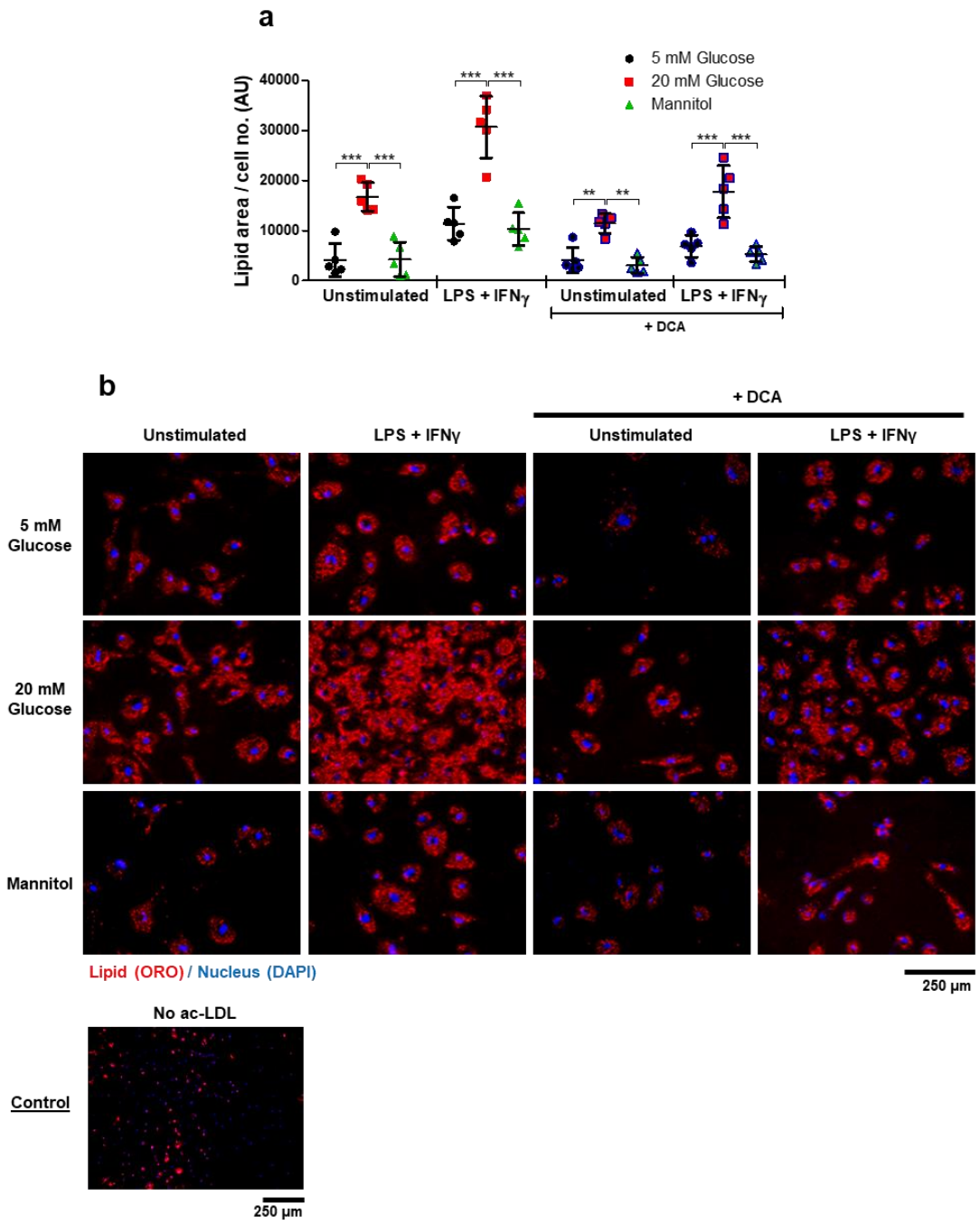


Figure 3.13 ***DCA reduces glucose enhanced BMDM foam cell formation.***

*(a) Image quantification of acetylated-LDL (ac-LDL) uptake by BMDM, normalised by cell number per image, with or without dichloroacetate (DCA) glycolytic inhibition. Representative (b) oil-red-o (ORO) and DAPI stained foam cell images. All data (a) are shown as mean ± SD; 2-way ANOVA with Bonferonni Post-Hoc analysis; **p<0.01, ***p<0.001 and each point represents an individual animal (average of 4 images).*

Summary

The main findings from this chapter demonstrate that:

1. High extracellular glucose alters human and mouse monocyte and macrophage metabolism, in particular increasing glycolytic flux.
2. High glucose altered metabolism simultaneously increases pro-inflammatory stimulated and decreases anti-inflammatory associated macrophage gene expression.
3. High glucose altered metabolism increases adhesion of monocytes to activated endothelium and macrophage foam cell formation.

Discussion

These findings illustrate how high extracellular glucose alters monocyte and macrophage metabolism, increasing glycolytic flux, dysregulating the TCA cycle and glutaminolysis. As previously described macrophage metabolism is altered in response to inflammatory stimuli, for example increasing glycolysis after LPS and IFNγ stimulation [79]. However, this is the first demonstration that increasing concentrations of glucose are sufficient of a stimulus to alter monocyte and macrophage cellular metabolism. Increased steady-state conditions of high glucose are known to increase glycolytic flux in cancerous cells and yeast, a phenomenon known as the Crabtree effect [174], but have yet to be described in myeloid cells.

Glucose uptake and utilisation appears to be affected by high extracellular glucose, and so to interrogate a potential mechanism controlling these metabolic alterations the surface expression of GLUT1, the primary glucose transporter in macrophages [84], was measured. Glycolytic rate has various rate limiting steps, one of the first is the surface expression of the glucose transporter. For all cell types and GLUT variants, a basal level of GLUTs are expressed at the surface with a reserve store held on intracellular vesicles [175]. Upon stimulation, these vesicles translocate to the cell surface to aid in rapidly modulating glucose uptake, avoiding delay which occurs by protein translation. The findings in this chapter show

that GLUT1 surface expression is not immediately increased under high glucose conditions, compared to physiological glucose conditions, but are significantly higher after 4-6 hours in unstimulated and M1 macrophages, suggesting high glucose may not affect GLUT1 translocation to the surface but rather be downregulating its removal through exocytosis.

Overexpression of GLUT1 in macrophages significantly increases glucose metabolism and PPP [84], displaying that changes in the ability to take up glucose is enough to alter metabolism in the absence of an inflammatory stimuli. This *in vitro* study also highlighted that an increase in GLUT1 and subsequent glucose metabolism caused an increase in pro-inflammatory gene expression. Although, *in vivo* myeloid-specific overexpression of the GLUT1 transporter does increase glycolysis and PPP flux, but is not sufficient in increasing pro-inflammatory cytokine production nor does it promote atherosclerosis [82]. This could suggest that the increases in GLUT1 expression are necessary to alter cellular metabolism but is not the mechanism driving associated downstream inflammation. Although this study is in direct contrast to the findings by Sarrazy V. *et al.*, who show bone marrow transplantation of GLUT1 knockout bone marrow into an $ApoE^{-/-}$ mouse did increase glucose uptake within the aortic arch and increased atherosclerotic burden [83]. GLUT1 knockout mice fed on a high fat diet were also shown to be resistant to obesity, with reduced liver and adipose tissue inflammation [176]. BMDM derived from these mice also displayed reduced glucose uptake and enhanced M1 inflammatory responses, again stressing its role in regulating macrophage inflammation [176]. These findings highlight the potential importance of GLUT1 in linking cellular metabolism, inflammation and subsequently atherosclerosis, however the lack of uniformity between all studies indicates a requirement for further investigation. The data in this chapter show that glucose positively regulates GLUT1 in macrophages and so this may be an important mechanism that underlies enhanced macrophage inflammation and atherosclerotic burden in diabetic hyperglycaemic conditions. The importance of GLUT1 in regulating high glucose induced metabolic changes,

downstream pro-inflammatory gene expression and functions and the mechanism underlying this control, as described in this chapter, also requires further investigation.

Another rate limiting step of glycolysis is the activity and cellular location of GAPDH. Increases in pro-inflammatory *Il*-6 and *Tnf*-α gene expression would suggest that GAPDH is no longer accumulated in the nucleus, exhibiting its inhibition over these gene promoter sites [86,87] and therefore potentially influencing glycolytic rate. GAPDH gene expression increased in M1 macrophages but appears to be unchanged by high glucose conditions, however further protein expression and protein activity studies would reveal a deeper insight into the potential regulatory role of GAPDH in high glucose conditions.

The studies in this chapter show that high glucose increases pro-inflammatory M1 and decreases anti-inflammatory associated M2 macrophage gene expression, which is consistent with data from Parathath et al. [19]. Multiple experimental and clinical data provide evidence for the role of inflammation in atherogenesis, disease progression and its complications [33,177]. Increased levels of pro-inflammatory cytokines, such as IL-6 [178], TNF-α [179] and IL-1β [180], are observed in patients with cardiovascular disease and have experimentally been shown to drive disease progression. These data provide an insight into how high glucose is affecting macrophage inflammation and potentially altering atherosclerosis. IL-1β has the added importance of being implicated in to diabetes [181] and metabolic memory [134].

Importantly, these bi-directional changes in gene expression were restored in the presence of DCA and 2-DG. All together indicating that the pro-inflammatory effects of high extracellular glucose were mediated through changes in glycolysis, and not merely due to non-specific changes to overall metabolic activity. This is with the exception of *Il-1β* expression, which was not lowered in the presence of DCA. As previously described, *Il-1β* gene expression is not only affected by altered glycolysis levels, as succinate, a TCA intermediate, induces *Il-1β* expression through the stabilisation of HIF-1α [182]. DCA's mechanism of action is to inhibit aerobic glycolysis and promote pyruvate oxidation through the inhibition of pyruvate

dehyrdrogenase kinase (PDHK), which increases pyruvate dehydrogenase (PDH) activity [183]. DCA therefore increases flux through the TCA cycle, increasing its intermediates such as succinate which could potentially explain the lack of normalisation of *Il-1β* gene expression.

Non-targeted metabolomics show that high glucose increases succinate levels, which is either derived from a broken TCA cycle but could also be due to altered glutaminolysis, both which are shown to be altered under conditions of high glucose. The metabolomics analysis performed in the chapter was non-quantitative and therefore all data shown can be considered as a screening experiment, hence confirmatory measurements of altered metabolites were required, as shown in Pentra data and through direct measurements of succinate and α-KG. High glucose appears to affect glutaminolysis. An increase in succinate : α-KG ratio, as described here, indicates decreased glutaminolysis and has been linked to enhancing M1 polarisation and decreasing or inhibiting M2 polarisation [99]. This may provide further insight into how high glucose is dysregulating these macrophage responses. Pentra data provided confirmation that glucose uptake and lactate production were changing, however from this it was inferred that glycolysis was therefore dysregulated. Metabolism is a complex system involving multiple pathways and isolating one specific pathway may lead to oversight of important changes in other pathways. Future experimentation using quantitative mass-spectrometry metabolomics analysis or radioactive labelled glucose tracer experiments would provide further quantitative metabolite information. Further investigation of BMDM metabolism using other techniques such as the Seahorse XF Bioanalyser assays, which allow live, real-time analysis of glycolytic or OXPHOS rate or energy profile characterisation to be determined, would also supply label-free, well characterised evidence on whether and how high extracellular glucose alters macrophage metabolism.

Given its effects on promoting inflammatory gene expression, the effect of high extracellular glucose on monocyte and macrophage functions relevant to atherogenesis, in particular monocyte adhesion to endothelium [184] and foam cell formation [185], was investigated.

The findings from this chapter illustrate how high glucose increases foam cell formation and monocyte adhesion to endothelial cells and are in line with previous studies that also demonstrate how high glucose increases THP-1 monocyte adhesion to endothelial monolayer [186] and uptake of modified LDL as well as increase production and storage of cholesteryl esters [173]. This is the first time the mechanism has been linked to changes in monocyte and macrophage glucose metabolism. Other studies have focused on how short term exposure to high glucose increases VCAM-1 and MCP-1 expression and hence subsequent adhesion [172], or increased expression of scavenger receptors for oxLDL [173]. DCA under high glucose conditions only partially restores the increased foam cell formation, suggesting that other pathways are involved and are important. Haq Khan et al. have previously described how DCA is able to inhibit cholesterol uptake through the downregulation of low density lipoprotein receptor (LDLR) expression by inhibition of the ERK5 / MEF2 pathway [187], and so could potentially be having the same effect on scavenger receptors. High glucose increases cholesteryl ester synthesis [173] and downregulates ABCG1 expression, which prevents cholesterol efflux. These remaining pathways may explain the residual heightened foam cell formation after DCA inhibition.

Although in agreeance with other studies, there are limitations to the experimentation performed in this chapter. There are caveats to the M1 and M2 macrophage model. They represent two very distinct, opposing and extreme phenotypes that occur after specific stimulation *in vitro* and so is questionable to whether this is representative of disease *in vivo*. Although M1 and M2 markers have been shown to be present in both human and mouse atherosclerotic plaques [19], it does not prove that lesional macrophages exist in these predetermined subsets. The M1 and M2 macrophage model is a useful tool for *in vitro* screening as is robust and well characterised, but it is always important to consider that other responses may be occurring. Unbiased methods of characterisation, such as RNA-

sequencing or non-targets proteomics provide a superior platform to characterise these cells and their responses.

Reported here are the effects of hyperglycaemia on LPS / IFNy or IL-4 stimulated macrophage gene expression, however it should be noted that hyperglycaemia did not alter *Il*-6, *iNos*, *Ym1* or *Fizz1* expression in unstimulated BMDM. This is likely to be due to the inducible nature of these genes which are specifically associated to the M1 or M2 macrophage phenotype. This displays the limitation of performing qPCR in that you are only able to characterise a small number of genes and may not accurately represent the transcriptional state of the cell. Thus, further unbiased transcriptome analysis would benefit these findings.

Acetylated LDL was used to induce foam cell formation. This differs from oxLDL in the type of modification and also in that ac-LDL produces cytoplasmic cholesteryl ester accumulation rather than being processed by cell-specific lysosomal pathways, as oxLDL [188,189]. Ac-LDL is also not a biological product nor has it been found *in vivo* [190]. Additional foam cell formation studies with oxLDL, or advanced glycosylation end products (AGEs) on LDL, which are also naturally increased *in vivo* under diabetic hyperglycaemia [191] and are linked to the promotion of atherosclerosis, could provide further mechanistic insight and understanding of the involvement of this process in driving diabetic atherosclerosis.

This is similar in principle to the method in which monocyte adhesion experiments were performed, in that during this study monocyte adhesion to endothelium was performed under static conditions. This is not as it occurs *in vivo*, where monocyte adhesion under flow would theoretically be more biologically relevant. As described in other studies, performing static adhesion under flow or static conditions can potentially alter the mechanism of adhesion as Chacko et al. [192] describe how a competitive inhibitor of N-glycans inhibits monocyte adhesion under flow but not static adhesion and Bradfield et al. [193] illustrate that LPS increases monocyte adhesion to endothelial cells under static condition but has no effect under flow.

In conclusion, this chapter clearly demonstrates that acute increases in extracellular glucose alter monocyte and macrophage metabolism. Through increases in glycolytic flux, high glucose increases pro-inflammatory gene expression, monocyte adhesion to endothelium and foam cell formation. Further investigation is required to identify if these metabolic changes are long-lasting and therefore provide novel therapeutic targets for treating diabetic CVD.

Chapter 4 : Diabetic Hyperglycaemic Memory in Macrophages Increases Atherosclerosis

Introduction

Diabetic hyperglycaemia *in vivo* increases systemic inflammation and therefore may contribute to atherogenesis [194]. However, clinical trials have consistently shown no effect [22-24] or a small beneficial effect [25,26] of glucose lowering therapies on reducing macrovascular complications. The increased risk of hyperglycaemia that fails to resolve on correction, suggests a "legacy effect" or hyperglycaemic memory driving disease progression. Hyperglycaemic memory has primarily been described in endothelial cells [141] following long periods of hyperglycaemia and / or oscillations [195] of normoglycaemia induce a long-lasting pro-inflammatory memory-like phenotype, which causes an increase in pro-inflammatory TNF-α secretion which continues post-glucose normalisation [148]. The role of hyperglycaemic memory in innate immune cells and its relevance to atherosclerosis are not fully understood.

Hypothesis

Diabetic hyperglycaemia induces long-lasting changes in monocyte and macrophage gene expression and functions, which persist post glucose normalisation. These changes will drive atherosclerosis disease progression.

Aims

To understand whether hyperglycaemic induced pro-inflammatory effects are long lasting and drive atherosclerosis *in vivo*, despite glucose normalisation, the influence of the following were investigated:

- Diabetic hyperglycaemia on macrophage inflammatory gene expression, post glucose normalisation
- Diabetic hyperglycaemia on macrophage functions relevant to atherosclerosis, after glucose normalisation
- Hyperglycaemic memory in BM cells on atherosclerosis *in vivo*

Methods

The methods description below is intended to provide an overview of experimental techniques used in this chapter. Full experimental details are described in *Materials and Methods* (Chapter 2).

BMDM gene expression, static adhesion and foam cell formation assays

BMDM from STZ diabetic or WT control mice were cultured, stimulated into M1 or M2 and assayed in a physiological concentration of glucose (5 mM), as illustrated in Figure 4.1. Stimulations for qPCR and gene expression analysis were performed for 18 hours.

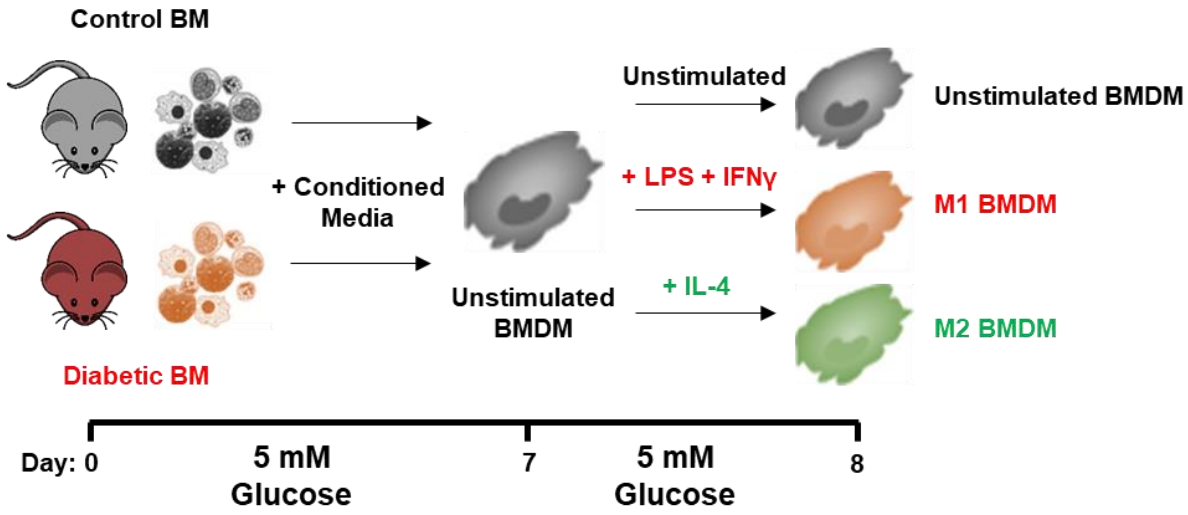


Figure 4.1 ***Schematic of diabetic BMDM protocol.***

BMDM from wild-type or diabetic mice were differentiated and stimulated in euglycaemic (5 mM glucose) conditions.

For static adhesion analysis, BMDM were stimulated for 18 hours, then fluorescently labelled green using PKH67 and added to TNF-α stimulated sEND.1 endothelial cell monolayers for 1 hour. Unadhered cells were then removed, cover slips washed, fixed with PFA and nuclear (DAPI) stained. Four images per cover slip were taken and the number of adhered macrophages quantified, per image, and averaged to provide the data points shown.

For foam cell formation analysis, BMDM were cultured with or without LPS plus DiI-ac-LDL for 48 hours. Cells were then washed, PFA fixed and lipid and nucleus stained with ORO and DAPI, respectively. Four images per cover slip were taken and the amount of lipid per image quantified and normalised to the number of cells. All four values were averaged to provide the individual data points shown.

Diabetic bone marrow transplant and atherosclerosis *in vivo*

STZ diabetic CD68-^{GFP} or non-diabetic control CD68-^{GFP} BM was transplanted into atherosclerosis-prone [normoglycaemic] *Ldlr*$^{-/-}$ recipient mice, as illustrated in Figure 4.2. Post engraftment chimeric mice were fed a “Western-type” diet for 12 weeks. Whole blood was collected to assess engraftment, by flow cytometry of peripheral blood mononuclear cells, and quantify cholesterol (LDL, HDL, triglycerides and NEFA) levels. Aortic roots were sectioned and stained to assess atherosclerotic burden, macrophage content (GAL3), smooth muscle cell content (α-actin) and images used to assess lipid. Plaque burden and necrotic area was quantified on five tri-Masson stained images and the averages reported. Three sections from each aortic root were immunofluorescence stained and quantified for GFP (for BM derived CD68 cells), GAL3 (macrophages), α-actin (smooth muscle cells) and the averages displayed.

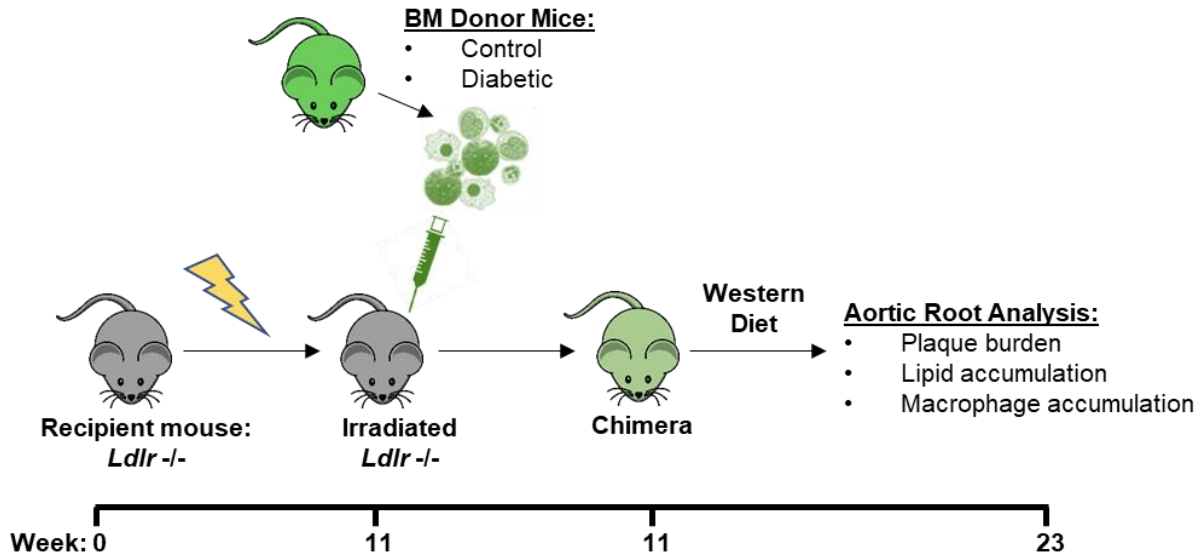


Figure 4.2 ***Schematic on bone marrow (BM) transplant experimental design.***

BM from non-diabetic or control CD68-^{GFP} mice were transplanted into an atherosclerotic prone Ldlr$^{-/-}$ recipient. Bone marrow transplant experimentation performed by The Jackson Laboratory, Bar Harbor, Maine, USA. Aortic root analysis performed by Laurienne Edgar.

Results

Bone marrow derived cells from diabetic mice exhibit enhanced pro-inflammatory responses

BM was obtained from non-diabetic, age matched control mice and syngeneic diabetic mice, in which hyperglycaemia had been induced by STZ and maintained for 6 weeks *in vivo*. STZ diabetic mice displayed decreased body weight (by 17 %; $p<0.0001$; Figure 4.3 A), increased blood glucose levels (2.5 fold; $p<0.0001$; Figure 4.3 B) with no change in absolute spleen weight (Figure 4.3 C), however when normalised to body weight diabetic mice displayed increased spleen weight to body weight ratio (SW / BW; 1.2 fold; $p=0.0068$; Figure 4.3 D).

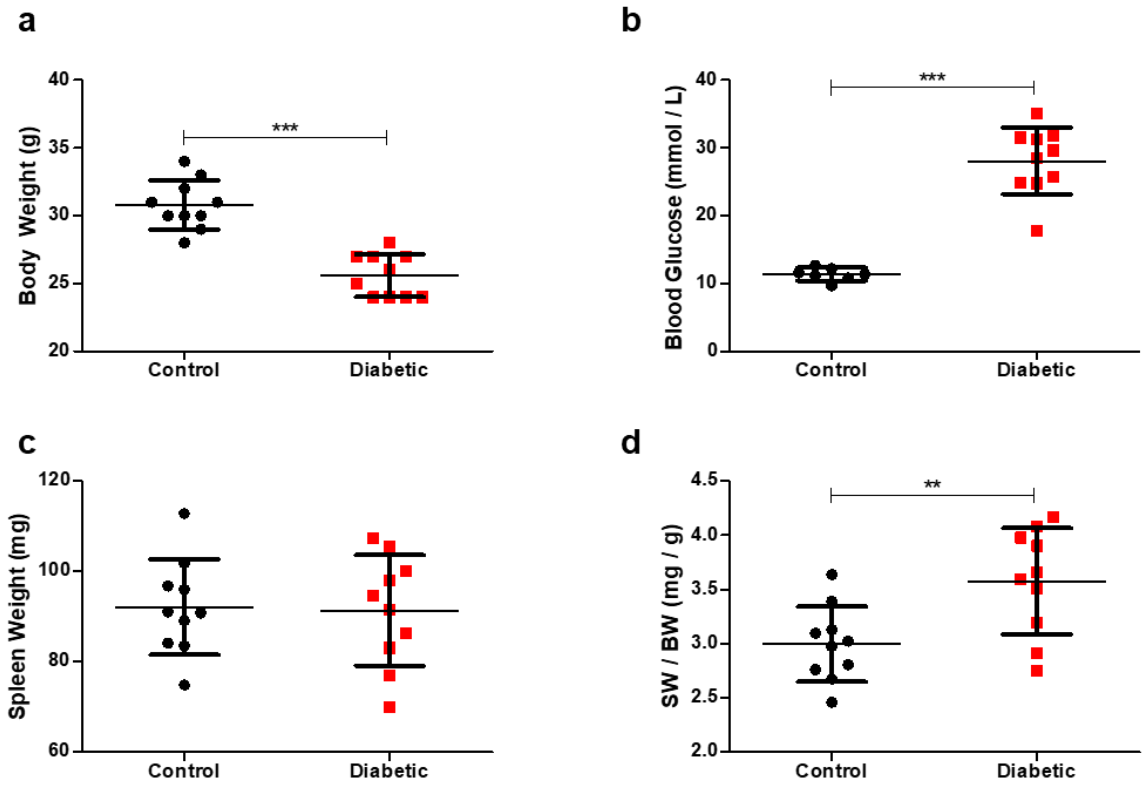


Figure 4.3 ***Streptozotocin-induced diabetic mouse model details.***

*At time of necropsy, after 6 weeks of maintained in vivo hyperglycaemia, measurements of (**a**) body weight ($p<0.0001$); (**b**) non-fasted blood glucose ($p<0.0001$); (**c**) whole spleen weight and (**d**) spleen weight (SW) normalised to body weight (BW) ($p=0.0068$). Data shown are mean ± SD (n=10); analysed by Student's unpaired t-test.*

BM cells were differentiated into BMDM under a physiological concentration of glucose (5 mM). Following LPS and IFNγ stimulation, BMDM of diabetic mouse origin displayed enhanced M1-associated *Il-6* (4.1 fold; p<0.0001; Figure 4.4 A), *Il-1β* (2 fold; p=0.0011; Figure 4.4 B), *Tnf-α* (1.9 fold; p=0.0002; Figure 4.4 C) and unchanged *iNos* (Figure 4.4 D) gene expression, and, upon IL-4 stimulation, diabetic BMDM displayed decreased M2-associated *Ym1* expression (by 75%; p=0.0003; Figure 4.4 E) and *Fizz1* (by 70%; p=0.0326; Figure 4.4 F).

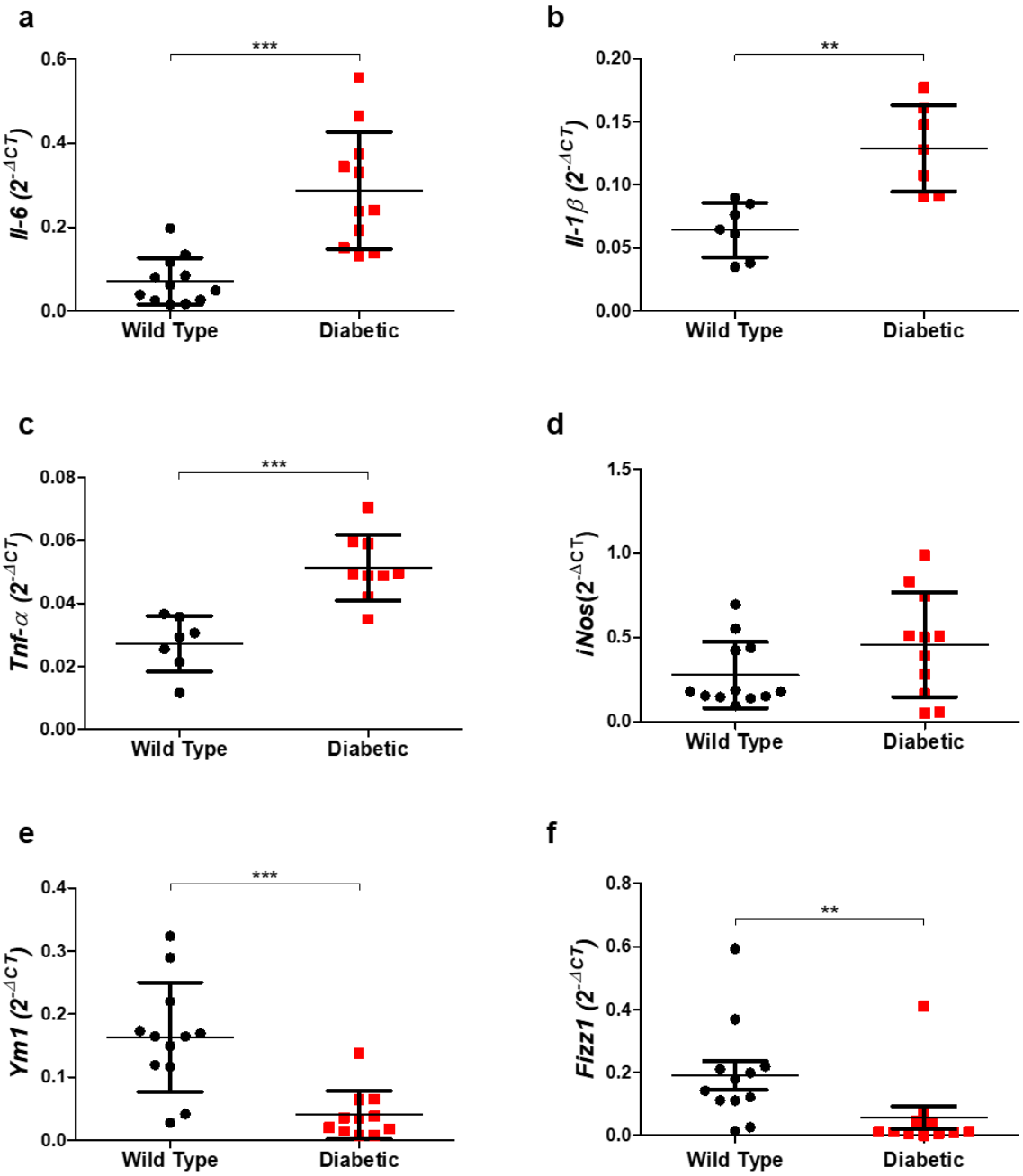


Figure 4.4 ***Diabetic bone marrow derived macrophages display hyperglycaemic memory gene expression responses***.

BMDM from non-diabetic control or diabetic mice were differentiated and stimulated in physiological glucose (5 mM glucose) conditions (n=10-12). M1 gene expression analysis of (a) Il-6 (p<0.0001), (b) Il-1β (p=0.0011), Tnf-α (p=0.0002) and (c) iNos. M2 (d) Ym1 (p=0.0003) and (e) Fizz1 (p=0.0326) gene expression. All qPCR data are normalised to B2m expression, analysed by unpaired t-test.

BMDM from a diabetic mouse origin displayed increased adhesion to activated endothelium (by 6.3 fold; $p<0.05$; and by 9.4 fold, when LPS-stimulated; $p<0.001$) (Figure 4.5 A, B) and enhanced modified-LDL uptake and foam cell formation (LPS stimulated 1.6 fold; $p<0.01$, no difference in unstimulated conditions) (Figure 4.5 C, D).

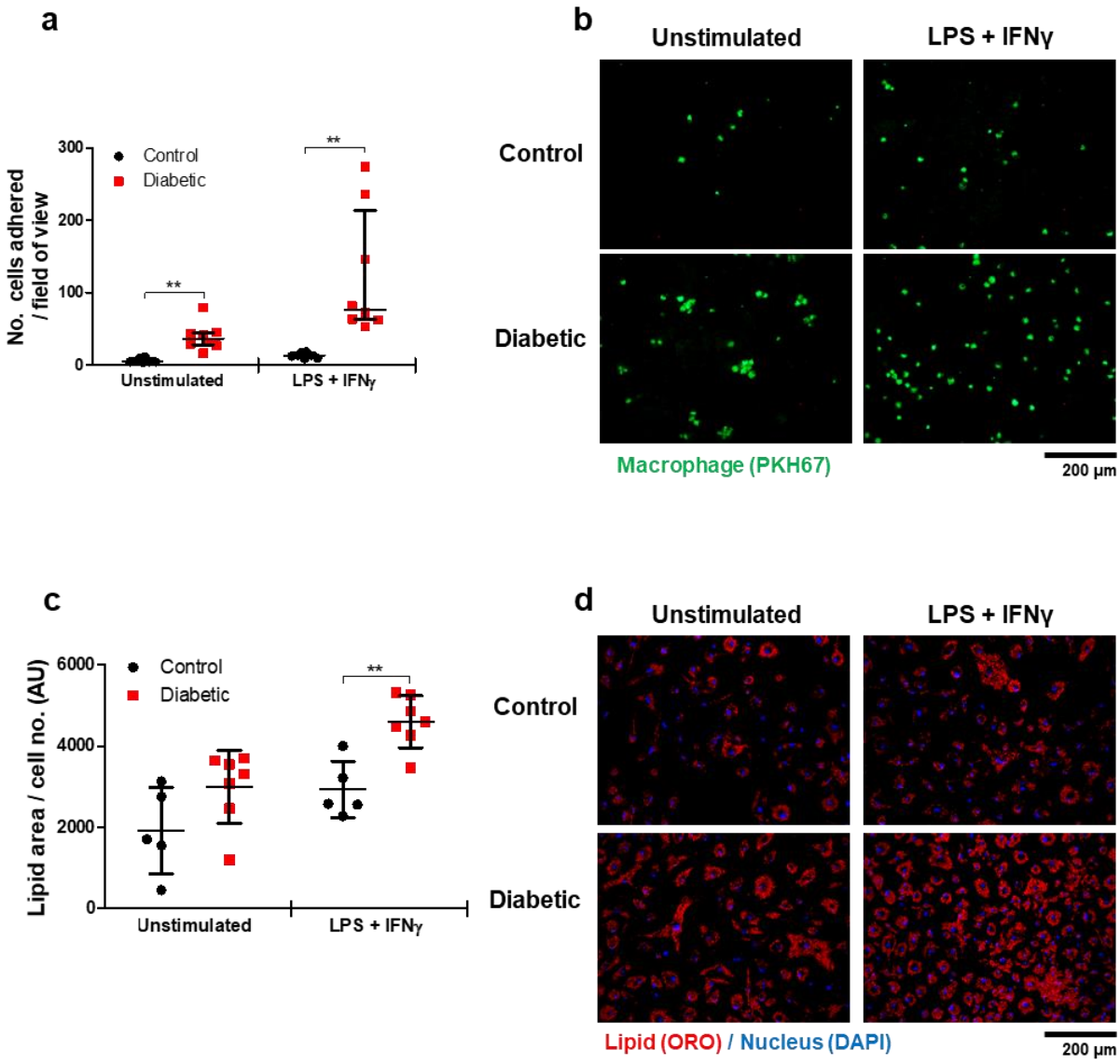


Figure 4.5 ***Bone marrow derived macrophages from diabetic mice manifest hyperglycaemic memory in functional responses.***

*(**a**) Image quantification of BMDM adhesion to endothelial cells (n=8) and (**b**) representative static adhesion images of fluorescently (PKH67) labelled BMDM to endothelial cells. (c) Image quantification of acetylated-LDL uptake by BMDM, normalised by cell number per image. Representative (**d**) oil-red-O (ORO) and DAPI stained foam cell images (n=5). All data are shown as mean ± SD and each point represents an individual animal (average 4 images for static adhesion and foam cell formation). Data analysed by two-way ANOVA with Bonferonni post-hoc test, **p<0.01.*

Hyperglycaemic memory drives atherosclerosis

To test the functional significance of hyperglycaemic memory in atherosclerosis we transplanted BM from normoglycaemic control or STZ-induced diabetic donor mice (blood glucose 33.9 ± 6.9 mmol/L) into atherosclerosis-prone [normoglycaemic] *Ldlr* $^{-/-}$ recipient mice, as illustrated in Figure 4.2. Effective and equivalent engraftment was shown by FACS of peripheral blood mononuclear cells, confirming the appearance of CD45+ GFP+ cells positive for Ly6C or CD11b (Figure 4.6 A or B, respectively).

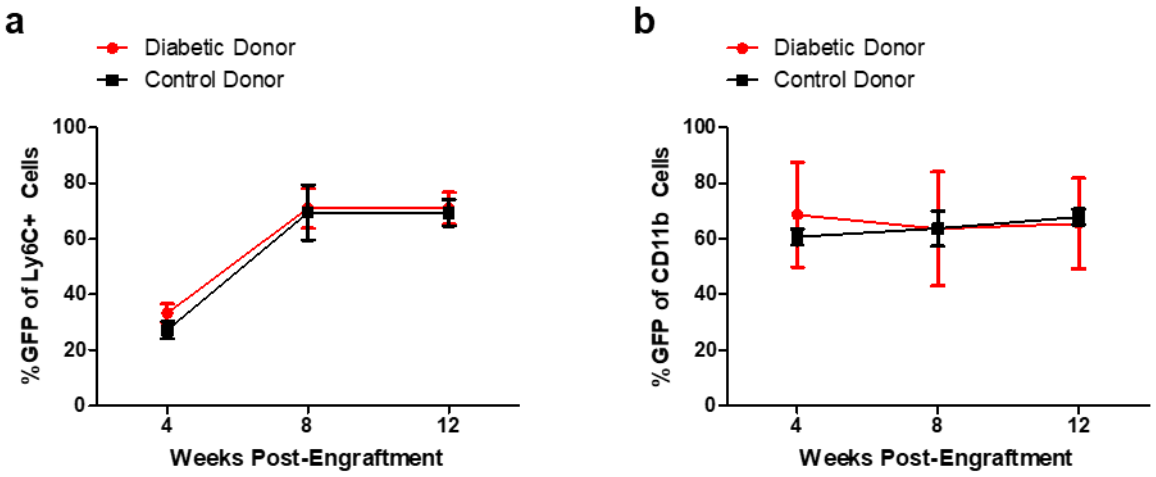


Figure 4.6 ***Bone marrow transplant engraftment.***

*Flow cytometric analysis of peripheral blood mononuclear cells to measure engraftment by proportion GFP+ cells positive for (**a**) Ly6C or (**b**) CD11b. Sample n=9-10. Data shown as mean ± SD. Flow analysis was performed by The Jackson Laboratory.*

After 12 weeks on a “Western-type” diet, there were no differences in blood lipid measurements, including LDL, HDL, triglycerides (TRIG) and non-esterified fatty acids (NEFA) (Figure 4.7).

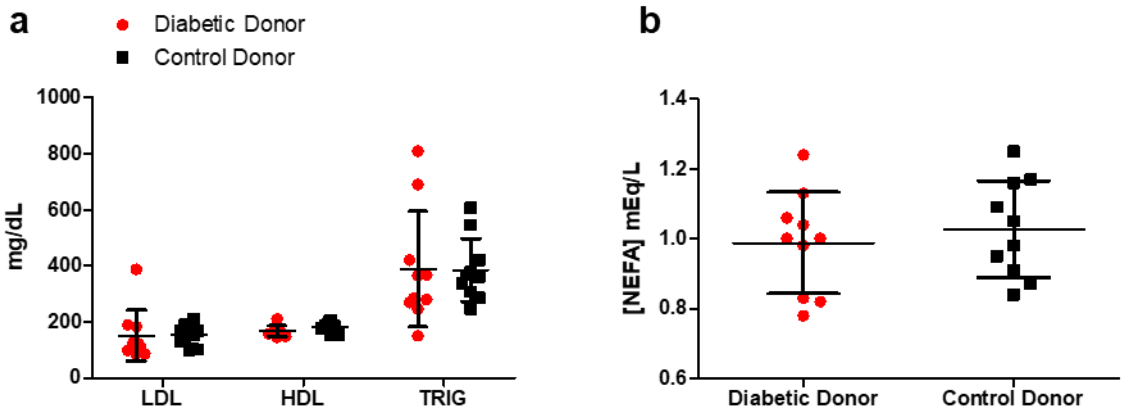


Figure 4.7 ***Bone marrow transplant lipid measurements.***

(a) Serum LDL-cholesterol, HDL-cholesterol, triglyceride (TRIG) and (b) non-esterified fatty acid (NEFA) measurements post-necropsy. Sample n=9-10. Data shown as mean ± SD. Lipid measurements were performed by The Jackson Laboratory Clinical Chemistry Core Facility.

Aortic roots were sectioned and Masson Trichrome stained and sections used to quantify plaque area (Figure 4.8 A), intraplaque collagen (Figure 4.8 B) and intraplaque lipid (Figure 4.8 C). Adjacent sections were immunofluorescently stained with α-actin to quantify smooth muscle actin (Figure 4.8 D) and GAL3 to quantify macrophage content (Figure 4.8 E).

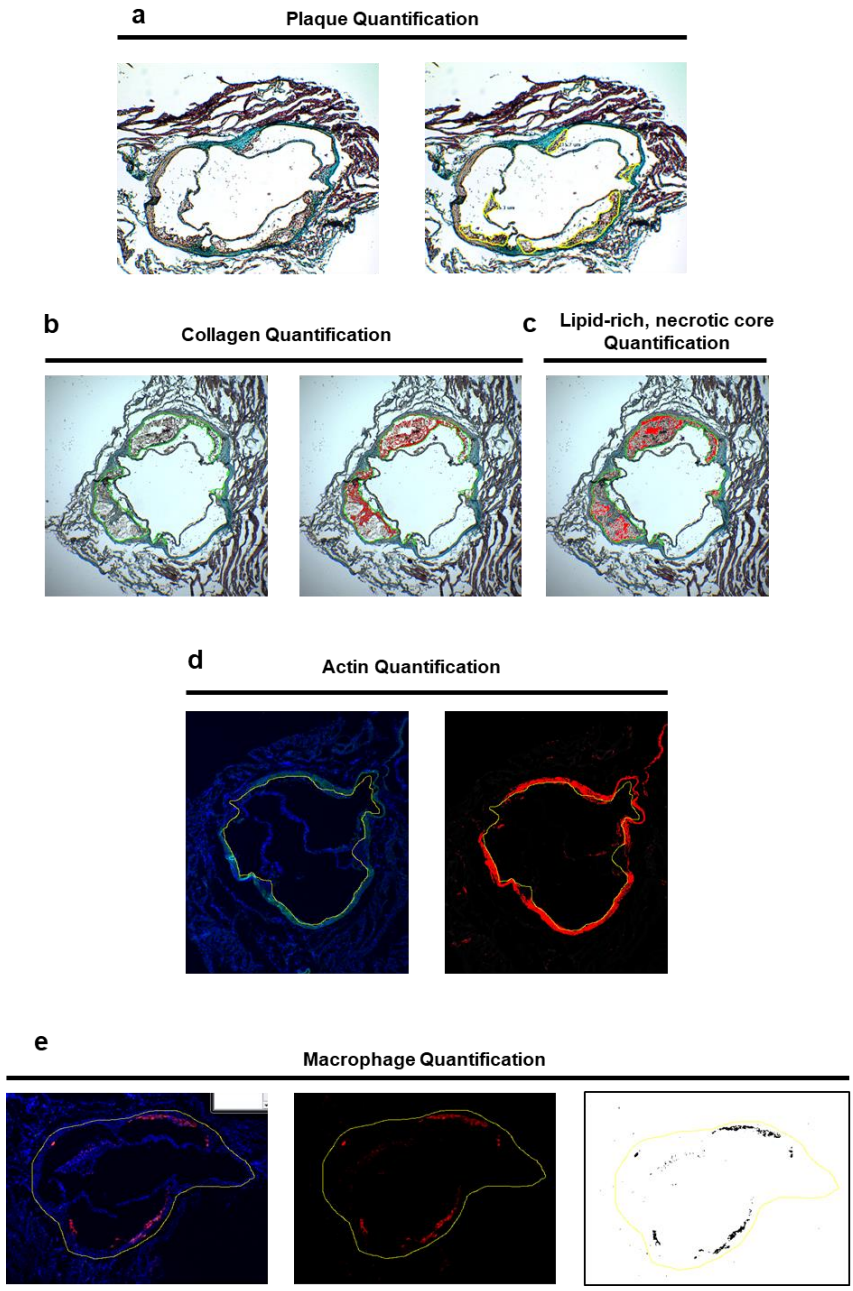


Figure 4.8 ***Aortic root image quantification methods.***

Masson trichrome stained aortic root sections were used to quantify (a) plaque area – by masking plaque area on ImagePro Plus software, (b) collagen – by masking green stained collagen within the plaque area on ImagePro Plus software and (c) lipid-rich, necrotic core area – by masking the white area within the plaque area on ImagePro Plus software. Nuclear stained (DAPI) and immunofluorescence stained (d) α-actin was masked on ImageJ to quantify intra-plaque actin content and (e) GAL3 was masked on ImageJ to quantify macrophage content.

Aortic root sections were stained with Masson Trichrome or immunofluorescently for GFP to identify cells originating from donor bone marrow and GAL3 to identify macrophages, example images shown in Figure 4.9.

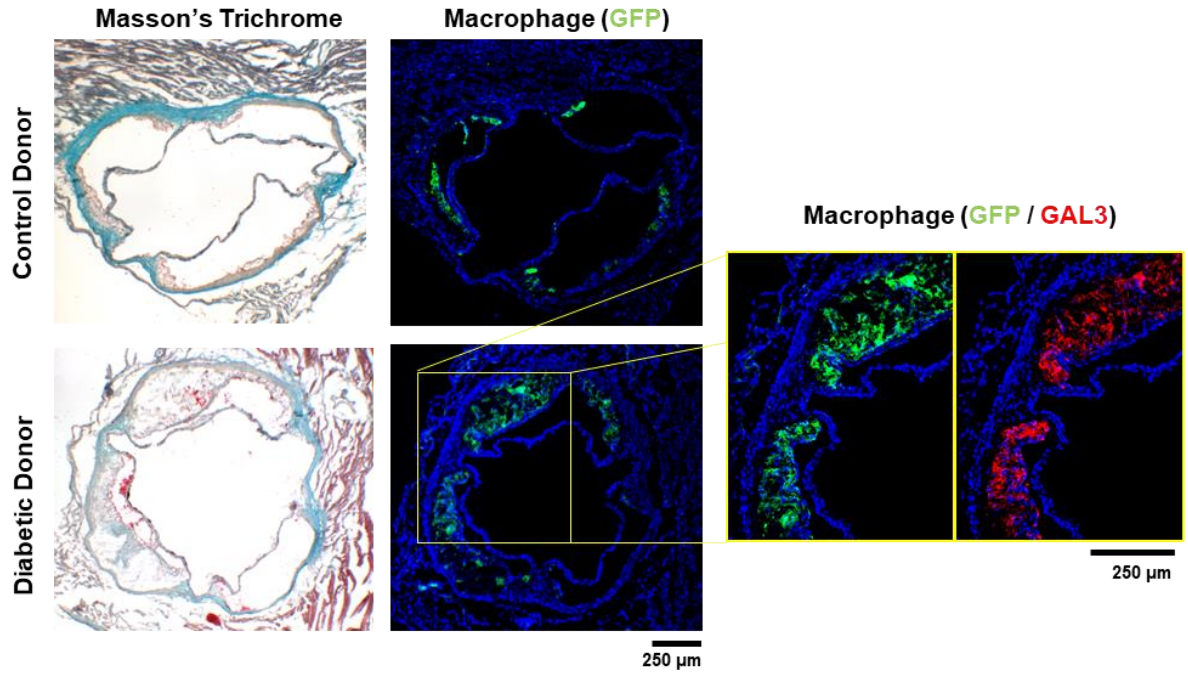


Figure 4.9 ***Example aortic root images.***

Example aortic root images from Ldlr$^{-/-}$ mice who have either received diabetic donor or control donor CD68-GFP BM. Masson Trichrome stained (left) and immunofluorescence stained for BM transplant-derived macrophages (green = GFP) or all macrophages (red=GAL3).

Mice who received diabetic BM showed marked increased aortic root atherosclerosis (2.85-fold; p=0.036; Figure 4.10 A), lipid-rich, necrotic core area (5-fold; p=0.0076; Figure 4.10 C), intra-plaque collagen (5.39-fold; p=0.036; Figure 4.10 E) and intraplaque smooth-muscle cell content (2-fold; p=0.033; Figure 4.10 G). However, when these measurements are normalised to plaque area (Figure 4.10 D, F and H), only lipid-rich, necrotic core area remains significantly upregulated in mice that received diabetic bone marrow (2.4 fold, p=0.046; Figure 4.10 D). Plaque macrophage content was not significantly different between groups (Figure 4.10 B).

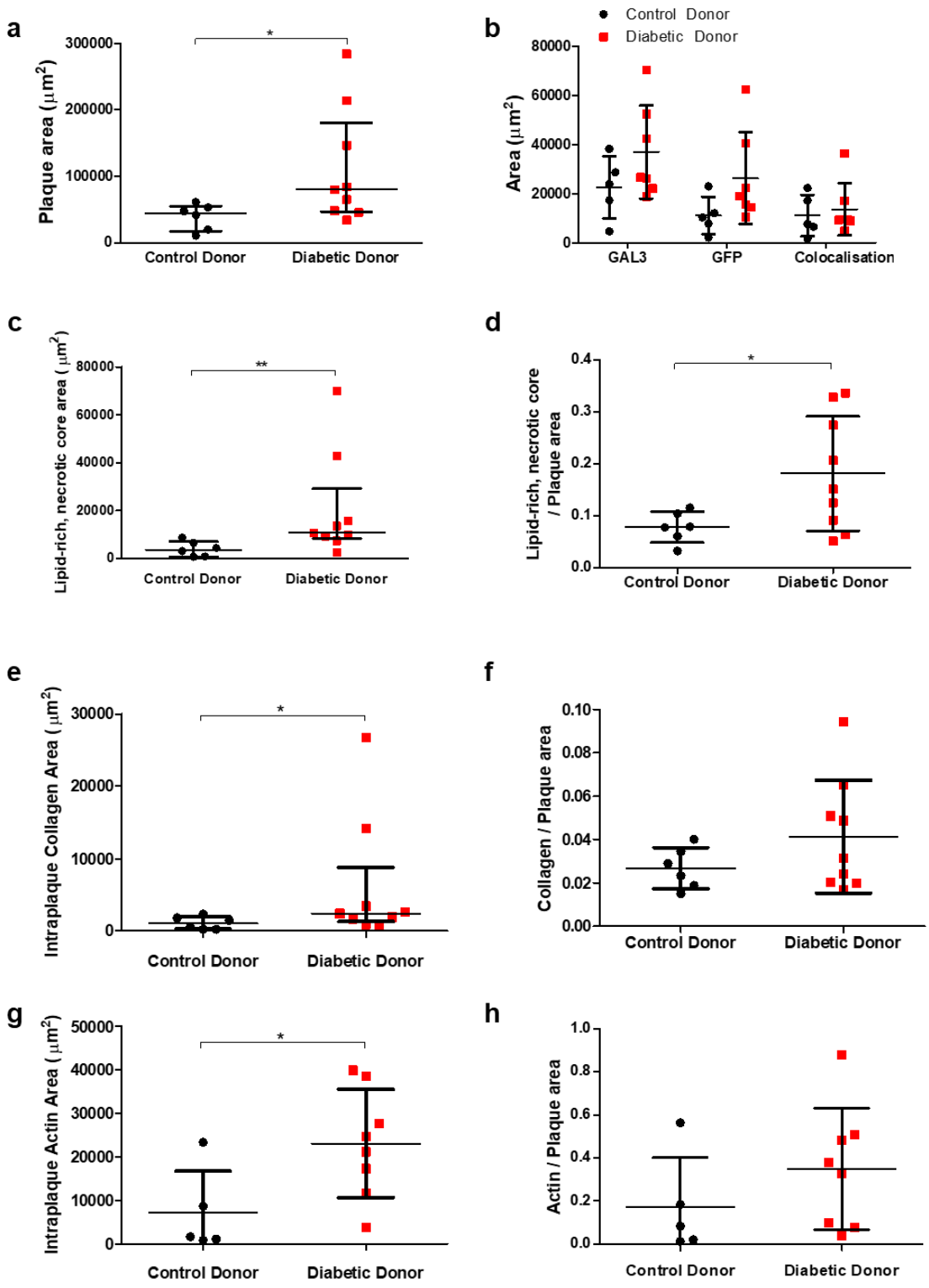


Figure 4.10 ***Diabetic bone marrow drives atherosclerosis, after glucose normalisation.***

Masson Trichrome image quantification of (a) plaque area (p=0.036) and immunofluorescence image quantification of (e) macrophage GAL3, GFP or colocalization of both staining. Masson Trichrome image quantification of lipid-rich necrotic core regions (c) before (p=0.0076) and (d) after normalisation to plaque area (p=0.046), and quantification of intra-plaque collagen (e) before (p=0.036) or (f) after normalisation to plaque area. Immunofluorescence image quantification of smooth muscle cell content (α-actin stained) (g) before and (h) after normalisation to plaque area. Data shown as (a, c, e) median ± interquartile range, analysed by Mann-Whitney U test or (b, d, e, f, g & h) mean ± SD and analysed by unpaired t-test; n=5-10.

Summary

The main findings from this chapter are that:

1. BMDM display persistent pro-inflammatory gene expression and functional responses, despite glucose normalisation, indicating hyperglycaemic memory.
2. Hyperglycaemic memory in BM cells increases atherosclerosis *in vivo*, regardless of normoglycemia restoration.

Discussion

A mouse model of diabetes was used to test whether diabetic hyperglycaemia induced persistent pro-inflammatory changes in macrophages, even after glucose normalisation. The model of diabetes used was a type 1 diabetic animal model as STZ leads to the destruction of the pancreatic β-cells [196]. This was the model of choice as the primary goal was to assess the long-lasting effects of hyperglycaemia, which this model provides. Type 2 diabetic models would provide the added complexity of hyperlipidaemia, obesity-induced inflammation and hyperinsulinemia. However, due to the destruction of the pancreatic β-cells by STZ, this model also leads to hypoinsulinemia which could have a role in the data presented. A recent study has described how insulin increased LPS stimulated TNF-α and IL-6 release from diabetic BMDM but reduced their secretion from diabetic peritoneal and alveolar macrophages, mirroring the reduction seen in non-diabetic macrophages [197]. This highlights the complex relationship between insulin signalling, inflammatory macrophage gene expression and cytokine secretion.

Even with the potential confounding results from the presence of hypoinsulinemia, the findings that diabetes induces heightened pro-inflammatory and dampened anti-inflammatory macrophage gene expression demonstrate a pro-inflammatory effect of diabetic hyperglycaemia and are consistent with the data previously presented by Parathath et al. [19]. They show that macrophages isolated using LCM from diabetic mouse atherosclerotic

plaques, even after lipid lowering, show heightened pro-inflammatory *iNos*, *Il-1* and *Vcam-1* expression and decreased anti-inflammatory associated *Fizz1* and *Arg1* expression. Peritoneal macrophages from mouse diabetic models have also been shown to have increased pro-inflammatory IL-6, IL-1β and TNF-α cytokine production [198], further emphasising the role for *in vivo* hyperglycaemia in augmenting pro-inflammatory cytokine expression. These mouse findings are representative of human disease, as monocytes from patients with type 1 [199] or type 2 [70] diabetes, too, show heightened release of pro-inflammatory cytokines such as IL-6, IL-1β and TNF-α, upon LPS stimulation.

Monocytes from patients with type 2 diabetes also show increased adhesion to endothelium [70] and those with poorly controlled hyperglycaemia also displayed an increased uptake of oxLDL [72], confirming the findings described here and translating them to a clinical setting. These persistent heightened responses were observed in BMDM that had been cultured in a physiological concentration of glucose for 9 days and are indicative of hyperglycaemia-induced memory, and present in altered gene expression as well as cellular functions pertinent to atherogenesis. It also importantly highlights the fact that the hyperglycaemic memory must have been induced in the BM progenitor cell niche itself, that persists through differentiation and manifests in BMDM.

The most interesting finding from this chapter is that hyperglycaemic memory in the BM niche increases atherosclerotic burden almost 2.8-fold, which mirrors the increased lesion size in STZ treated diabetic *Ldlr*$^{-/-}$ compared non diabetic *Ldlr*$^{-/-}$ [200] and the amplified atherosclerotic burden in humans with diabetes [201]. Masson Trichrome staining additionally revealed an increase in necrotic area, using a previously described method [161]. The expansion of the lipid-rich necrotic core is characteristic of diabetic atherosclerosis and suggest a more high-risk lesion [202]. Although oil-red-O staining of further sections to specifically quantify lipid area would provide reliable insight into how diabetic bone marrow is affecting lipid handling in the

atherosclerotic plaque. These findings clearly demonstrate the functional relevance of hyperglycaemic memory in the pathogenesis of atherosclerosis.

Effective and equivalent engraftment of both non-diabetic and diabetic BM was shown by flow cytometry of peripheral blood mononuclear cells, confirming the appearance of CD45+ GFP+ cells positive for CD11b or Ly6C in both. There were no differences in blood lipid measurements. Together this suggests that neither engraftment efficiency nor lipoprotein levels explain the difference observed in plaque characteristics.

Macrophage staining within the aortic root plaque samples allude at a trend for increased number, however it does not reach statistical significance and therefore suggests differential functional effects may be playing a role in driving disease rather than total numbers. To test this, further immunofluorescence staining of M1 and M2 macrophage markers, such as iNOS or ARGI respectively, would allow the interrogation of whether their inflammatory status is altered.

Aortic root staining also illustrated an increase in intraplaque collagen and smooth muscle cells content, suggesting more advanced lesions. Collagen contributes to plaque growth and could also further influence lesion progression by modulating macrophage functions [203]. However, increased collagen levels lend strength to a fibrous cap and potentially symbolizes a more stable plaque formation. Collagen content is the result of a balance between collagen synthesis, from smooth muscle cells [204] and macrophages [205,206], and its proteolytic degradation by MMPs or collagenases, also produced from lesional cells such as macrophages [207].

Many of the previous data, as well as the results described here, indicate an augmented pro-inflammatory monocyte and macrophage response caused by previous exposure to hyperglycaemia. However, it is important to note that often a secondary stimulus, for example LPS or IL-4, is required to see the altered response, suggesting that glucose itself may only

prime cells. Interrogating how glucose is potentially priming disease relevant monocytes, macrophages and their precursors could provide insight into the mechanism underlying hyperglycaemic memory.

In conclusion, this chapter demonstrates that diabetic hyperglycaemia induces long lasting, pro-inflammatory memory in BM progenitor cells that manifests in enhanced pro-inflammatory and dampened anti-inflammatory gene expression, heightened adhesion to endothelial cells and foam cell formation in BMDM that mirror high glucose responses. Importantly hyperglycaemic memory in the BM drives atherosclerosis *in vivo*, despite glucose normalisation, thereby demonstrating the relevance of hyperglycaemic memory in disease. Further interrogation of the mechanism underlying this memory could provide valuable novel therapeutic targets to prevent its role in driving diabetic vascular disease.

Chapter 5 : Hyperglycaemia Induces Long Lasting Memory through Alterations in Chromatin Accessibility and Transcription Factor Binding

Introduction

The experiments in the previous Chapter identify a new memory phenomenon as a results of hyperglycaemia bone marrow-derive innate immune cells. In this Chapter, its mechanism was investigated. With reference to hyperglycaemic memory in endothelial cells, both oxidative stress [208] and the activity of enzymes that alter chromatin accessibility have been implicated [141,146]. Recent reports have described a memory phenotype in innate immune cells, known as trained immunity [106,130,135]. For instance, a receptor mediated response induces changes in cellular metabolism, primarily increasing glycolysis and dysregulating the TCA cycle, leading to the build-up of metabolites such as lactate, succinate and pyruvate. These metabolites are then able to act as key regulating co-factors for histone modifying enzymes which provokes the induction of epigenetic modifications that affect chromatin accessibility, specifically H3K4me3 and H3K27ac [107]. The long-term persistence of circulating trained monocytes is driven by reprogramming of their BM progenitors [131,209]. Understanding how this process is regulated could provide mechanistic insight into hyperglycaemic memory with BM progenitors and their derived myeloid cells in diabetes. Previously described in Chapter 2, high glucose alters cellular metabolism, in particular glycolysis and increased levels of succinate and lactate, mirroring the metabolic changes relevant for trained immunity and further providing a hypothesis for applying the mechanism of trained immunity to hyperglycaemic memory.

As well as metabolic mediators, recent work has implicated the inflammatory cytokine interleukin-1β (IL-1β) in the development of trained immunity [134]. IL-1β has been implicated in diabetes [181] and acts as an important driver of atherosclerosis, and in obesity where adipose tissue macrophage released IL-1β induces proliferation of BM progenitors [210,211]. Therefore, it was hypothesised that IL-1β and hyperglycaemia may work synergistically to induce atherosclerosis-relevant epigenetic changes that alter chromatin structure in HSC.

Hypothesis

Hyperglycaemic memory is induced in BM progenitors through long-lasting metabolically driven epigenetic modifications that alter chromatin accessibility and transcription factor binding, similar to the mechanism underlying trained immunity. Further, that these changes are relevant to human disease and can be pharmacologically altered.

Aims

To interrogate the mechanism underlying hyperglycaemic memory, the following was investigated:

- The influence of hyperglycaemia altered metabolism on epigenetic marks that have previously been associated with trained immunity.
- Changes in the epigenome on chromatin accessibility and transcription factor binding in HSC.
- Whether hyperglycaemic memory is relevant to human atherosclerosis.
- Whether hyperglycaemic memory can be modelled *in vitro* and used to investigate clinically relevant pharmacological inhibitors.

Methods

The methods description below is intended to provide an overview of experimental techniques used in this chapter. Full experimental details are described in *Materials and Methods* (Chapter 2).

Western Blot

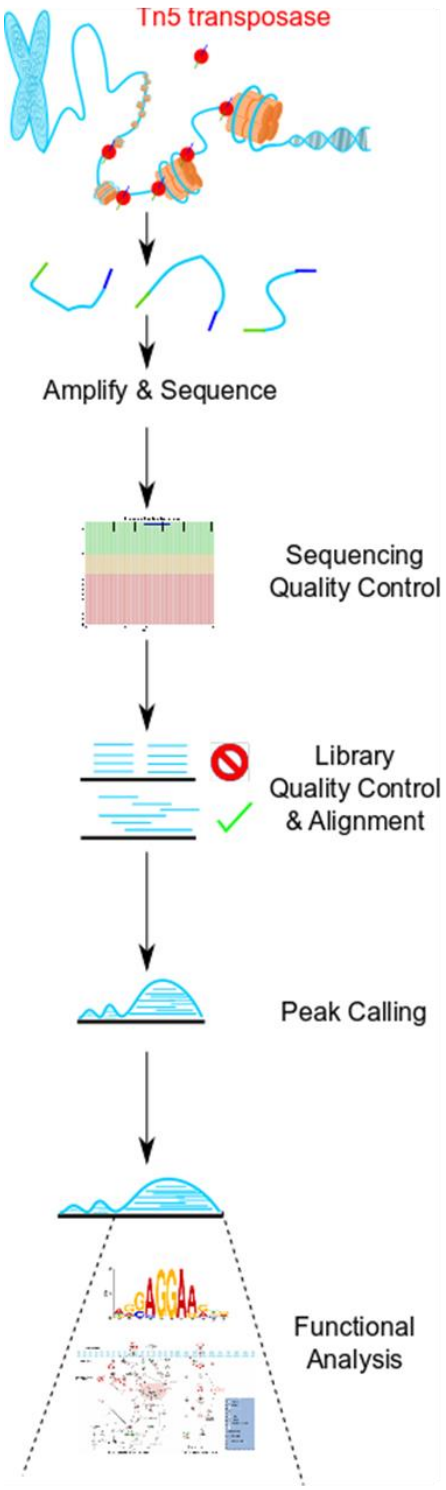
HSC and BMDM from WT C57/Bl6 mice cultured in various glycaemic conditions ± DCA and STZ mice were interrogated for the presence of H3K4me3 and H3K27ac. Equal concentration of 20 µg protein from HSC or BMDM lysates were loaded and run on an SDS-PAGE gel (4-12% Bis-Tris), transferred onto a nitrocellulose membrane and probed with antibodies against

the epigenetic marks H3K4me3, H3K27ac and the protein β-actin, which was used as a loading control. Band densities were quantified, and the data displayed was normalised to β-actin band density.

ATAC-seq

ATAC-seq was performed on WT control and diabetic HSCs as previously described [167]. Tagmentation was performed using the Tn5 transposase, followed by amplification of the DNA and a size selection to exclude fragments larger than 1,200 bp. Libraries were prepared using custom Nextera primers and sequenced by the Biomedical Sequencing Facility (BSF) at CeMM.

Sequencing data reads were aligned to the mouse genome and low-quality matches, reads mapping to mitochondrial sequences and non-uniquely mapped reads were removed. Differential regions between diabetic and control cells were identified and peaks enriched in the diabetic samples (FDR≤0.1) were put through pathway analysis [168] and analysed for enriched transcription factor binding motifs [169]. An overview of the ATAC-seq protocol and analysis pipeline is illustrated in Figure 5.1.



Description
• Cells are lysed and nuclei isolated • Tn5 transposase simultaneously fragments open regions of chromatin and tags DNA with sequencing adapters
• Fragmented and tagged DNA isolated
• DNA fragments were sequenced by the Biomedical Sequencing Facility at CeMM by Dr Thomas Krausgruber using the Illumina HiSeq 3000/4000 platform and the 50-bp single-read configuration

Description	Results
Raq sequencing files are run through FastQC software to assess quality by assessing for expected number of reads and sequence lengths.	All sequencing files passed sufficient quality control.
Reads were aligned to the mouse genome and low quality matches or reads mapping to the mitochondria were removed. Important to consider the percentage of uniquely mapped reads as a low percentage <50% often due to excessive amplification or sequencing problems.	On average, 16 million uniquely mapped reads (13.4-24.6 million representing 60% of total) were retained per sample.
Used to predict the regions of the genome that are open by finding regions with significant numbers of mapped reads. Peak calling algorithms use user-defined parameters to identify enriched (by FDR) regions.	Peak calling was performed using MACS2 and differentially bound regions identified using DiffBind and edgeR. Results summarised in Table 5.2
To gain insight into whether regions of the genome differentially open between experimental conditions have biological relevance and whether transcription factor (TF) binding sites are enriched and therefore more available for TF binding, pathway analysis and motif analysis are performed, respectively.	Pathway analysis (using GREAT) and motif analysis (using MEME-ChIP) was performed on peaks enriched in diabetic samples (FDR<0.1). The top 9 pathways (lowest FDR) are reported. The top 3 most enriched motifs were taken forward for further analysis.

Figure 5.1 ***ATAC-seq protocol and analysis pipeline.***

Tagmentation and library preparation performed by Laurienne Edgar. Sequencing performed by Dr Thomas Krausgruber. Sequencing data analysis was performed by Dr Madeleine Lemieux. Functional analysis performed by Laurienne Edgar.

Laser Capture Microdissection (LCM) and Transcriptome Analysis of Human Carotid Plaque Macrophages

LCM was used to specifically isolate macrophages from excised human carotid plaques. Carotid plaque samples were sectioned at 15 µm, cresyl-violet stained and macrophage rich clusters were excised, as guided by CD68 positively stained regions on the guide slide [159]. Cells were lysed, RNA isolated using the RNEasy micro kit (Qiagen) and gene expression assessed through microarray analysis, performed at Cambridge Genomic Services. Sequencing data were analysed by Dr Madeleine Lemieux.

Transcription factors identified to be enriched in diabetic HSC from ATAC-seq analysis were assessed for their relevance in human plaque macrophages. Transcription factor motifs were used to scan gene promoters and those conserved in both mouse and human ($p<0.05$ or $p<0.01$) were taken forward as target genes. Identified target genes were compared to genes differentially expressed (FDR<0.02) between diabetic and non-diabetic plaque macrophages to assess the presence.

BMDM Memory Model

BMDM from WT control mice were cultured under various glycaemic conditions in the presence or absence of 1, 5, 10 or 20 mM DCA (glycolytic inhibition) or 0.25, 0.5, 1, 5 or 10 µM Ro5-3335 (RUNX1 inhibition), as summarised in Figure 2.2 and the exact set up illustrated below in Figure 5.8 A, Figure 5.9 A and Figure 5.10 A. Ro5-3335 has previously been shown to specifically inhibit the heterodimer formation RUNX1-CBFβ, therefore preventing their ability to bind to DNA and regulate gene expression [212]. After positive selection cells were rested in 5 mM glucose DMEM for 48 hours and then stimulated with LPS + IFNγ for 18 hours in the presence or absence of matching concentrations of DCA or Ro5-3335. RNA was isolated and gene expression was assessed by qPCR. Data shown is normalised to *B2m* gene expression.

Results

Diabetic hyperglycaemic memory is induced in HSC and driven by changes in metabolism leading to epigenetic reprogramming

HSC cultured in conditions of high extracellular glucose display increased glucose uptake (17.4 fold, $p<0.001$), which remains elevated with DCA (7.9 fold, $p<0.001$; Figure 5.2 A) and increased lactate production (1.5 fold, $p<0.05$; Figure 5.2 B). DCA reduces lactate production for all glycaemic (5 mM: by 39 %; 20 mM: by 63 %, $p<0.001$) and control conditions (Mannitol: by 28 %; Figure 5.2 B).

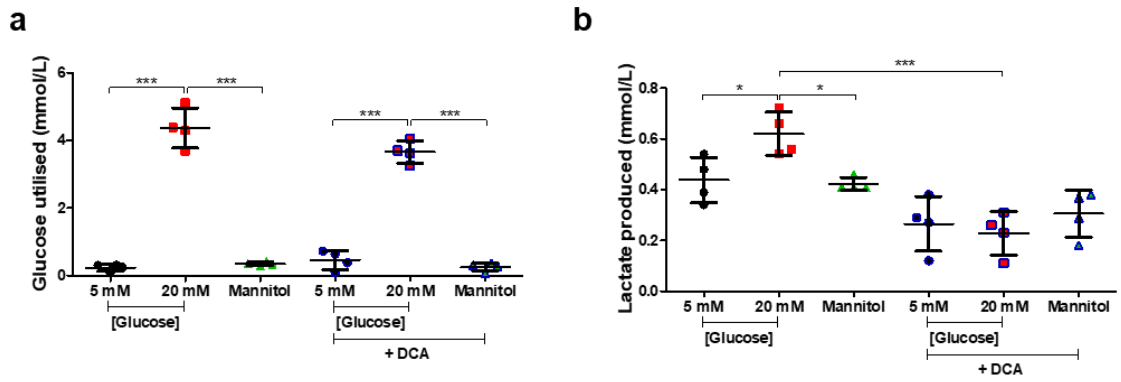


Figure 5.2 ***HSC display increased glucose uptake and lactate production***.

*Pentra measurements of (a) amount of glucose taken up and (b) lactate produced in the supernatants obtained from mouse HSC cultured in various glucose conditions (5 mM or 20 mM) or an osmotic control (mannitol), in the absence or presence of the glycolytic inhibitor dichloroacetate (DCA). Data shown n = 5 per condition; two-way ANOVA with Bonferroni post-hoc analysis; *p<0.05, ***p<0.001. All data shown are mean ± SD.*

HSC cultured in high glucose display increased H3K4me3 (1.5-fold, $p<0.05$, unstimulated; 1.5-fold, $p<0.01$, stimulated) and H3K27ac (1.6-fold, $p<0.05$, unstimulated; 1.8-fold, $p<0.01$, stimulated) modifications (Figure 5.3 A - D). In the case of H3K4me3, this effect was negated with DCA inhibition (Figure 5.3 C). In the presence of DCA, H3K27ac increased and was higher in unstimulated under 20 mM glucose conditions compared to 5 mM glucose (1.5-fold, $p<0.05$, Figure 5.3 D). These chromatin marks were also consistently increased in HSC from diabetic mice compared with WT HSC (H3K4me3: 2.5-fold, $p<0.05$, unstimulated; 1.9-fold, $p<0.01$, stimulated. H3K27ac: 3-fold, $p<0.05$, unstimulated; 2.1-fold, $p<0.05$, stimulated) and H3K4me3 remained heightened after differentiation into BMDM in physiological glucose (5 mM) (H3K4me3: 2.5-fold, $p<0.05$, unstimulated; 1.9-fold, $p<0.01$, stimulated) (Figure 5.3 E), with H3K27ac showing no difference in unstimulated BMDM, but was increased in diabetic BMDM after LPS + IFNγ stimulation (1.6-fold, $p<0.05$; Figure 5.3 F).

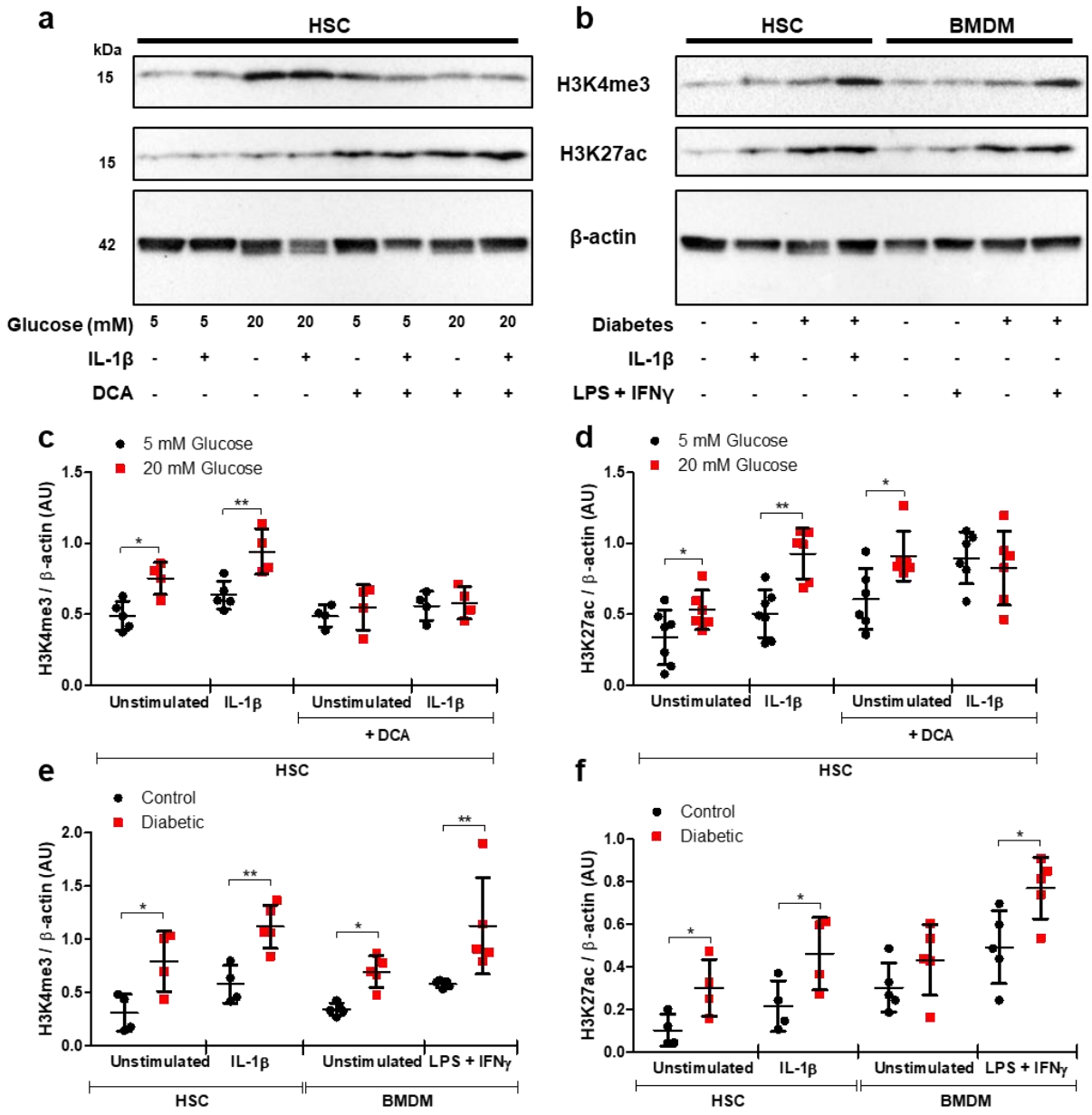


Figure 5.3 ***Epigenetic changes induced by high glucose or diabetes.***

Example H3K4me3, H3K27ac and β-actin western blots of (a) haematopoietic stem cells (HSC) in varying glycaemic conditions in the absence or presence of dichloroacetate (DCA) and (b) HSC or BMDM derived from control or diabetic mice, in unstimulated or pro-inflammatory stimulated conditions. Quantification of western blot band intensity (AU = arbitrary units) for (c) H3K4me3 or (d) H3K27ac (normalised to loading control β-actin) in control HSC in varying glycaemic conditions or for (e) H3K4me3 or (f) H3K27ac (normalised to loading control β-actin) for control or diabetic derived HSC or

*BMDM. All data are shown as mean ± SD; two-way ANOVA analysis; *p<0.05, **p<0.01, ***p<0.001 and each point represents an individual animal (average 2 blots per data point; n=5; samples derive from the same experiment and blots were processed in parallel).*

To interrogate chromatin openness, ATAC-seq was performed on HSC from diabetic or control mice, both with and without IL-1β stimulation, the samples and sequencing quality are summarised in Table 5.1.

Sample ID	raw reads	trimmed reads	net reads	uniquely aligned reads	% uniquely aligned reads	non-chrM uniquely aligned reads	% non-chrM reads	Biological Replicate	Mouse Phenotype	Stimulation
STZ1	28951008	554	28,950,454	17,050,368	0.589	16,313,923	0.957	Replicate 1	Diabetic	Unstimulated
STZ1_IL1	34088226	605	34,087,621	19,319,212	0.567	18,242,133	0.944	Replicate 1	Diabetic	IL-1β
STZ2	27816329	554	27,815,775	16,533,598	0.594	15,591,663	0.943	Replicate 2	Diabetic	Unstimulated
STZ2_IL1	29689791	564	29,689,227	17,262,100	0.581	16,284,237	0.943	Replicate 2	Diabetic	IL-1β
STZ3	31316977	641	31,316,336	19,042,973	0.608	17,959,807	0.943	Replicate 3	Diabetic	Unstimulated
STZ3_IL1	27947622	538	27,947,084	15,829,444	0.566	14,872,114	0.940	Replicate 3	Diabetic	IL-1β
STZ4	24062031	423	24,061,608	12,384,407	0.515	10,214,824	0.825	Replicate 4	Diabetic	Unstimulated
STZ4_IL1	25188380	464	25,187,916	14,312,781	0.568	13,420,003	0.938	Replicate 4	Diabetic	IL-1β
WT1	26428446	548	26,427,898	16,525,726	0.625	15,665,684	0.948	Replicate 1	Wild-type	Unstimulated
WT1_IL1	28859888	566	28,859,322	17,740,133	0.615	16,696,358	0.941	Replicate 1	Wild-type	IL-1β
WT2	28575687	560	28,575,127	17,155,676	0.600	15,721,524	0.916	Replicate 2	Wild-type	Unstimulated
WT2_IL1	27055401	498	27,054,903	15,372,902	0.568	14,795,046	0.962	Replicate 2	Wild-type	IL-1β
WT3	42946519	883	42,945,636	25,978,966	0.605	24,591,923	0.947	Replicate 3	Wild-type	Unstimulated
WT3_IL1	25446898	470	25,446,428	14,497,677	0.570	13,864,746	0.956	Replicate 3	Wild-type	IL-1β
WT4	29751486	561	29,750,925	17,400,611	0.585	16,591,770	0.954	Replicate 4	Wild-type	Unstimulated
WT4_IL1	24273566	433	24,273,133	14,389,613	0.593	13,465,987	0.936	Replicate 4	Wild-type	IL-1β

Table 5.1 ***ATAC-seq peak processing.***

Summary of sample conditions used for ATAC-seq experimentation and of the read number during peak processing. ChrM = chromosome M. Data analysis performed by Dr Madeleine Lemieux.

HSC from a diabetic origin showed differential chromatin openness (Table 5.2) in response to IL-1β exposure, with 530 differential peaks (FDR<0.1) of which 50 % of these regions exhibited increased accessibility in diabetic cells. Examples of differential peak regions are shown in Figure 5.4.

Experimental Condition	Comparison (sample number)	FRiP	
Basal Conditions	Diabetic (n=3)	0.29	
		0.34	
		0.37	
	Control (n=4)	0.42	
		0.42	
		0.37	
		0.31	**No. Peaks**
	No. differential peaks (FDR < 0.05)		**14**
	No. differential peaks (FDR < 0.10)		**39**
IL-1β stimulation	Diabetic (n=4)	0.26	
		0.33	
		0.24	
		0.26	
	Control (n=4)	0.39	
		0.22	
		0.3	
		0.34	**No. Peaks**
	No. differential peaks (FDR < 0.05)		**166**
	No. differential peaks (FDR < 0.10)		**525**

Table 5.2 ***Differential ATAC-seq peak analysis.***

Table highlights the comparisons made, each sample's corresponding FRiP score (fraction of reads in called peak) and a summary of the number of differential peaks identified. Analysis performed by Dr Madeleine Lemieux.

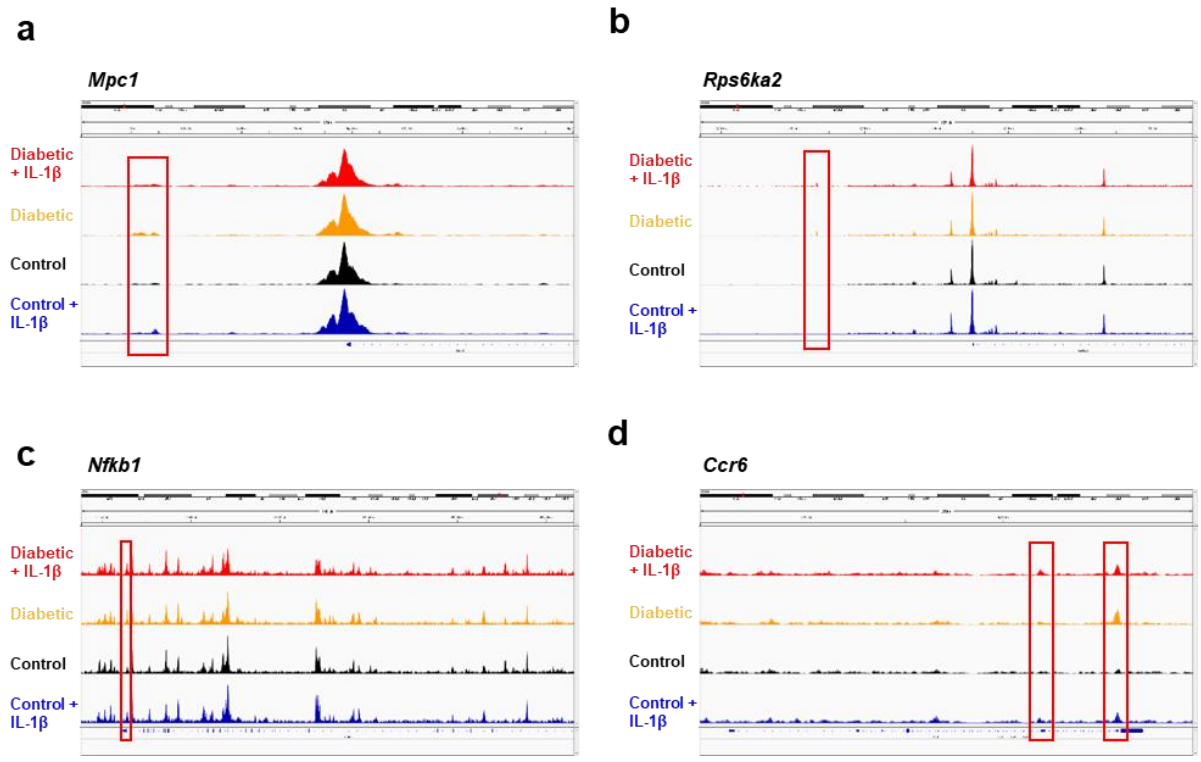


Figure 5.4 ***ATAC-seq Differential Peak Examples.***

Example integrative genome browser track plots for (a) mitochondrial pyruvate carrier 1 (Mpc1) (b) Ribosomal Protein S6 Kinase A2 (Rps6ka2) (c) Nuclear Factor Kappa B Subunit 1 (Nfkb1) and (d) Chemokine receptor 6 (Ccr6), with differential peaks highlighted by red boxes (FDR<0.2).

To explore the biological relevance of the non-coding genomic regions differentially open in diabetic cells under IL-1β stimulation, (with emphasis on putative cis regulatory function), the regions of chromatin with increased accessibility were assigned names of the two nearest genes (within 1000 kb) and analysed using Genomic Regions Enrichment of Annotations Tool (GREAT) [168]. GREAT pathway analysis revealed augmentation of several inflammation-related pathways, including 'leukocyte activation' (3.3 fold; FDR=0.0005), and genes associated with LPS tolerization in macrophages (2.7 fold, FDR=0.0009) (Table 5.3).

GREAT© Pathway Description	Database	Database ID	P-Value	FDR	Fold Enrichment
Cardiovascular System Disease	Disease Ontology	DOID:1287	1.16E-09	2.57E-06	1.80
T cell receptor signalling pathway	MSigDB Pathway	hsa04660	1.02E-08	6.74E-06	6.27
Genes involved in Adaptive Immune System	MSigDB Pathway	R-HSA-1280218	3.75E-08	1.65E-05	3.24
Leukocyte Activation	GO Biological Process	GO:0045321	5.75E-08	5.79E-04	3.36
Class NT (non-tolerizeable) genes: induced during the first LPS stimulation and induced at equal or greater degree in tolerant macrophages.	MSigDB Perturbation	FOSTER M12676	1.67E-06	9.34E-04	2.69
Genes involved in Cytokine Signalling in Immune system	MSigDB Pathway	R-HSA-1280215	2.85E-06	9.39E-04	3.87
Hematopoietic System Disease	Disease Ontology	DOID:74	2.25E-06	9.96E-04	1.80
Cell Activation	GO Biological Process	GO:0001775	2.80E-07	1.41E-03	3.02
Genes forming the macrophage-enriched metabolic network (MEMN) claimed to have a causal relationship with the metabolic syndrome traits	MSigDB Perturbation	CHEN METABOLIC M1920	3.39E-06	1.42E-03	2.07

Table 5.3 ***Differential ATAC-seq peak pathway analysis.***

Genes associated with peak regions differentially present between IL-1β stimulated diabetic HSC, compared to IL-1β stimulated control HSC were put through GREAT pathway analysis. Table displays top 9 pathways predicted to be upregulated in diabetic HSC.

In diabetic cells, upon IL-1β stimulation (261 peaks; FDR<0.1 and $\log_2$ fold change > 0), several transcription factor motifs were significantly enriched, of which the top 3 are summarised in Figure 5.5 A and include ETS-related gene (ERG; FDR=0.002), zinc finger protein 263 (ZNF263; FDR=0.00117) and, notably, included Runt-related transcription factor 1 (RUNX1; FDR=0.01). The E-value is a measure of significance and is an estimate of the number of motifs with an equal or higher likelihood ratio of being generated randomly [169].

a

HSC IL-1β Stimulated Diabetic Peak Analysis				
Motif Found	**Known or Similar Motifs**	**No. Sites**	**E-value**	**Motif FDR**
	ERG	76	4.7E-25	2.41E-03
	ZNF263	37	4.9E-17	1.17E-03
	**RUNX1**	**72**	**2.9E-08**	**1.58E-02**

b

HSC Unstimulated Diabetic Peak Analysis				
Motif Found	**Known or Similar Motifs**	**No. Sites**	**E-value**	**Motif FDR**
	PU.1	57	5.3E-06	4.9E-02
	CTCF	19	2.6E-05	1.8E-07
	**RUNX1**	**66**	**1.5E-03**	**1.42E-04**

Figure 5.5 ***Top 3 transcription factor motifs identified in ATAC-seq HSC analysis****.*

Tables summarise top 3 transcription factor motifs identified from peaks differentially enriched in (a) IL-1β stimulated diabetic HSC compared to IL-1β stimulated control HSC or (b) unstimulated diabetic HSC compared to unstimulated control HSC. Motifs identified using MEME-ChIP platform.

Unstimulated HSC displayed 357 differential peaks (FDR≤0.2), of which 51 % of these regions had increased accessibility in cells from a diabetic origin compared to a control origin, and the majority in intronic (48 %) or intergenic (21 %) regions (Table 5.2 and example differential peaks shown in Figure 5.4). Upon examination of over-represented transcription factor binding motifs, RUNX1 was significantly enriched (FDR=0.0001), as well as PU.1 (FDR=0.04) and CCCTC-binding factor (CTCF) (FDR=1.8×10^{-7}) (Figure 5.5 B).

LCM was used to isolate macrophages from human carotid atherosclerosis plaques in patients undergoing clinically-driven endarterectomy [213], as shown in Figure 5.6. Patient characteristics are summarised in Table 5.4.

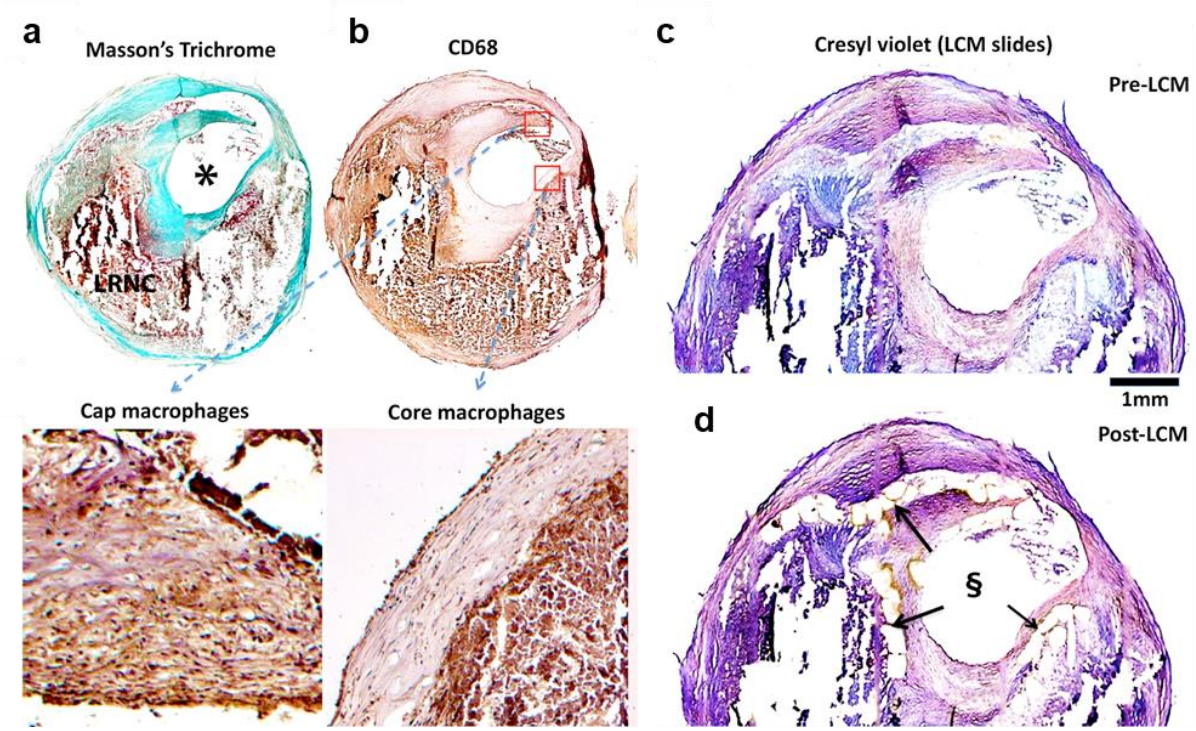


Figure 5.6 ***LCM example carotid plaque sections.***

Carotid plaque guide sections were (a) Masson Trichrome stained or (b) CD68 stained to identify macrophage rich regions within the cap or lipid core. Sections used for LCM were (c) cresyl violet stained and macrophage rich regions (d) specifically excised using LCM. Images provided by Dr Joshua Chai.

Characteristic	Diabetic	Control
Patient Number	8	16
No. Symptomatic (TIA / CVA)	2 (2 / 0)	10 (7 / 3)
Percentage Male	94%	88%
Average Age (± SD)	64 ± 9.5	66 ± 11.6
Percentage Smokers	35%	25%

Table 5.4 ***Patient characteristics.***

Summary of the carotid endarterectomy patients whose plaque macrophages were used for array analysis. Patients were characterised on whether they had type 2 diabetes of not, or whether they were asymptomatic or symptomatic (TIA = transient ischemic attack or CVA = cerebrovascular accident). Patient samples collected by Dr Joshua Chai.

Figure 5.7 shows the genes differentially expressed (DE) between diabetic and non-diabetic plaque macrophages (FDR<0.2) and highlights in green the RUNX1-associated genes (further detailed in Figure 5.7 B, C). RUNX1 target genes were significantly over-represented among differentially expressed genes, even more so when target binding sites were more stringently restricted: at a binding site p-value < 0.05, 12/106 DE genes were among the 1,251 RUNX1 targets (p-value = 0.03, odds ratio = 2.0) while at the more stringent cut off of 0.01, 6/347 RUNX1 targets were still DE (p-value = 0.008, odds ratio = 3.6).

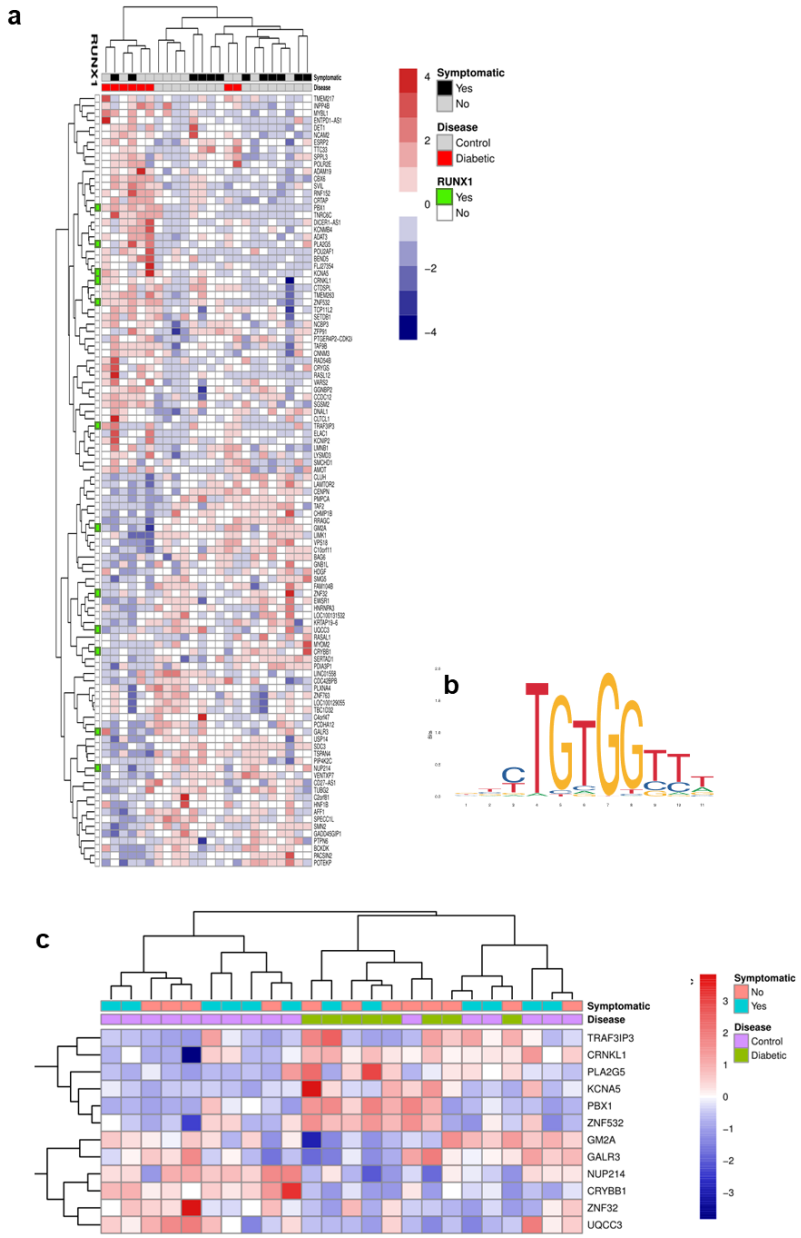


Figure 5.7 ***RUNX1 target genes are over represented in diabetic plaque macrophages.***

(a) Unsupervised hierarchical clustering of differentially expressed genes from diabetic (red, n=8) or control (grey, n=16) laser capture microdissected human carotid plaque macrophage samples. RUNX1 target genes (p<0.05 stringency) are highlighted in green in the indicator column to the left of the heat map, as discovered using the consensus RUNX1 binding matrix M0002.2 as depicted in the (b) the logo. RUNX1 target genes discovered at a p-value of (c) p<0.05. Row-normalized log_2 values are shown for genes differentially expressed in diabetic (green, n=8) and control (purple, n=16) samples. Analysis performed by Dr Madeleine Lemieux.

An *in vitro* model of hyperglycaemic memory was generated by differentiating WT BM into BMDM in high glucose (20 mM), followed by a 48-hour rest and M1 stimulation in a physiological concentration of glucose (5 mM) (depicted in Figure 5.8 A). After 4 days of high extracellular glucose (20 mM) during differentiation and LPS + IFNγ stimulation, cells exhibited exaggerated *Il-6* gene expression (2.7-fold, $p<0.01$; Figure 5.8 B), and after 7 days *Il-1β* expression was heightened (2-fold, $p<0.01$; Figure 5.8 C), despite restoration of 5 mM glucose.

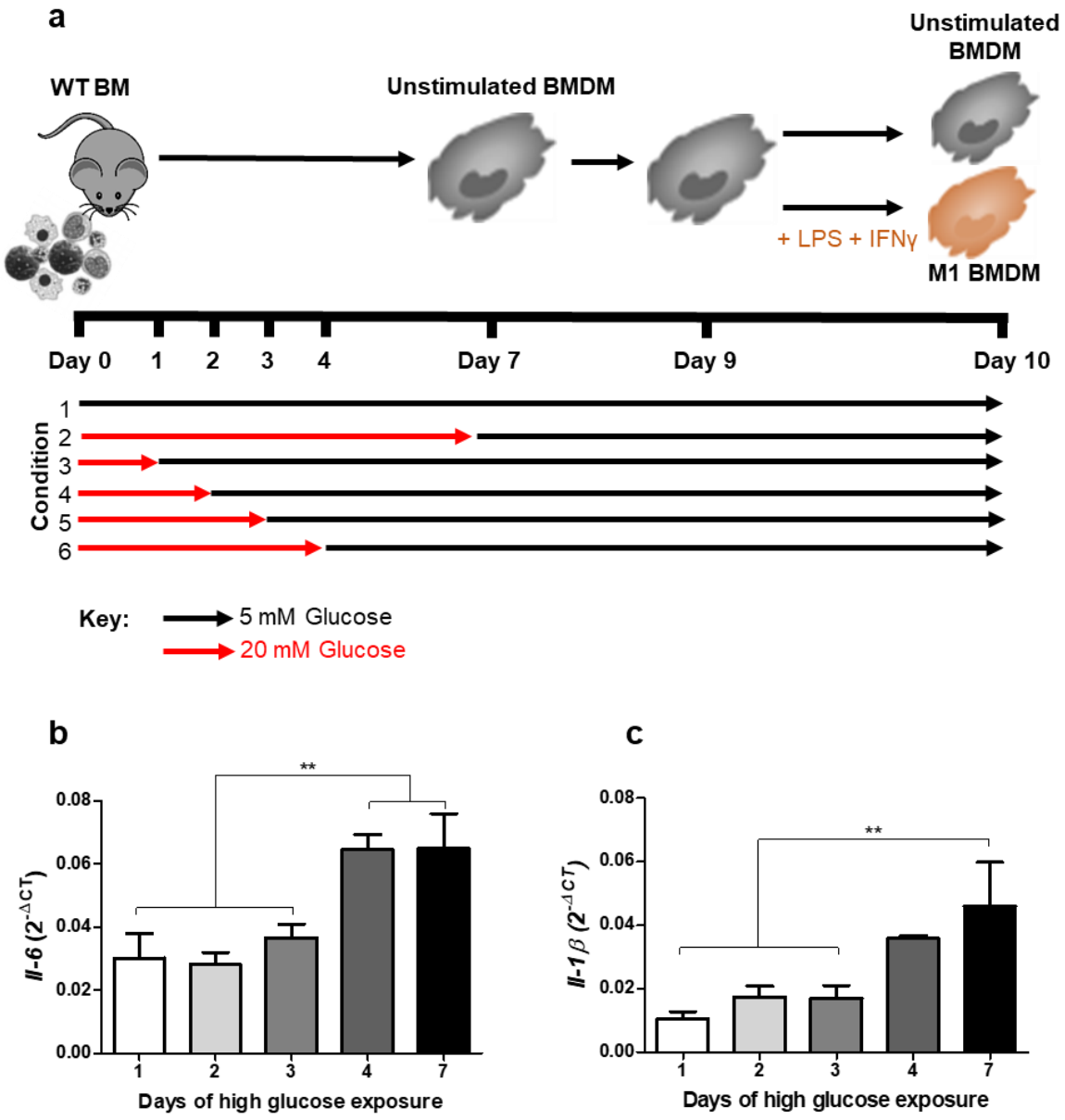


Figure 5.8 ***In vitro hyperglycaemic memory model.***

*Wild-type (WT) bone marrow (BM) was differentiated into bone marrow derived macrophages (BMDM) for varying periods of physiological (5 mM) or high glucose (20 mM), (a) as illustrated. After LPS + IFNγ stimulation, M1 BMDM (a) Il-6 and (b) Il-1β were assessed by qPCR. Sample n=3-5. Data displayed as mean ± SD, 1-way ANOVA with Bonferroni Post-Hoc, **p<0.01.*

To interrogate the involvement of RUNX1 and glycolysis in the development hyperglycaemic memory, WT BM was differentiated into BMDM and stimulated into an M1 phenotype with varying concentrations of glucose ± DCA (glycolysis inhibitor) or Ro5-3335 (RUNX1 inhibitor), as depicted in Figure 5.9 A. Both *Il-6* (Figure 5.9 B) and *Il-1β (*Figure 5.9 *C)* gene expression were assessed. Heightened *Il*-6 gene expression in high glucose grown M1 BMDM was significantly reduced by DCA at a concentration of 10 mM (by 90 %, $p<0.01$) and Ro5-3335 at a concentration of 1 µM (by 77 %, $p<0.05$) and 10 µM (by 79.5 %, $p<0.01$).

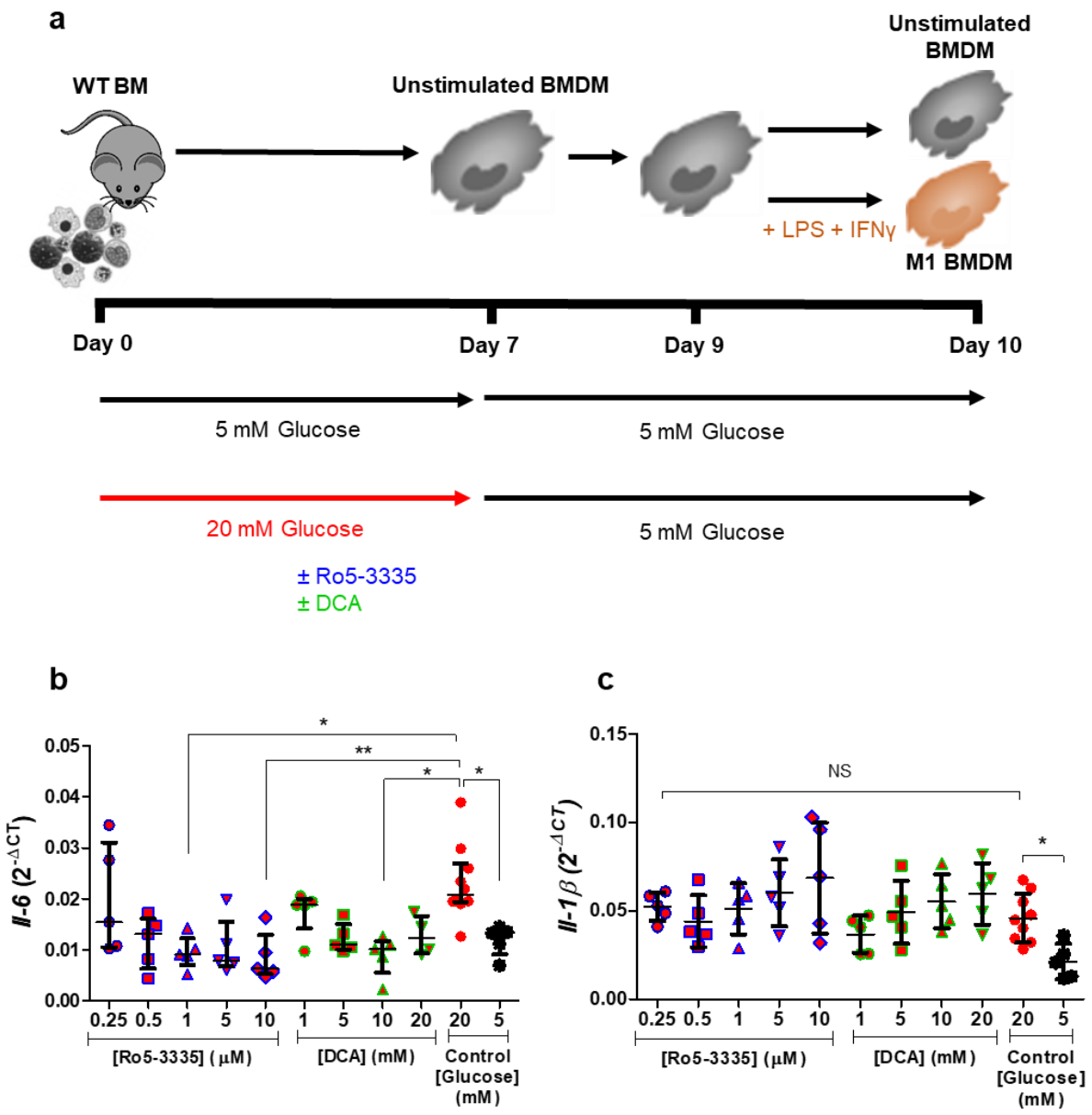


Figure 5.9 ***RUNX1 and Glycolysis inhibition prevents generation of hyperglycaemic memory, in vitro****.*

*Wild-type (WT) bone marrow (BM) was differentiated into bone marrow derived macrophages (BMDM) in physiological (5 mM) or high glucose (20 mM) ± varying concentrations of DCA or Ro5-3335, (a) as illustrated. After LPS + IFNγ stimulation, M1 BMDM (a) Il-6, data shown as median ± IQR, analysed by Kruskal-Wallis with Dunn's multiple comparison test; *p<0.05, **p<0.01 and (b) Il-1β; data displayed as mean ± SD, 1-way ANOVA with Bonferroni Post-Hoc, *p<0.05. Sample n=5.*

To assess the contribution of RUNX1 in the downstream hyperglycaemic memory gene expression responses, WT BM differentiated into BMDM in high extracellular glucose (20 mM) was stimulated into an M1 phenotype in the presence of varying concentrations of Ro5-3335, as depicted in Figure 5.10 A. Differentiation in 20 mM glucose increased *Il*-6 expression (2-fold, $p<0.001$), which remains elevated in the presence of 0.25 µM Ro5-3335 (1.8-fold, $p<0.05$). However, Ro5-3335 at a concentration of 0.5, 1, 5 and 10 µM reduced high glucose induced heightened *Il-6* gene expression (Figure 5.10 B). Differentiation in 20 mM glucose exaggerated *Il-1β* expression, despite glucose restoration (2-fold, $p<0.001$). Expression remained elevated in the presence of 0.25 µM Ro5-3335 (1.6-fold, $p<0.05$) and 0.5 µM Ro5-3335 (1.9-fold, $p<0.05$). Ro5-3335 at a concentration of 1, 5 and 10 µM normalised heightened *Il-1β* gene expression (Figure 5.10 C).

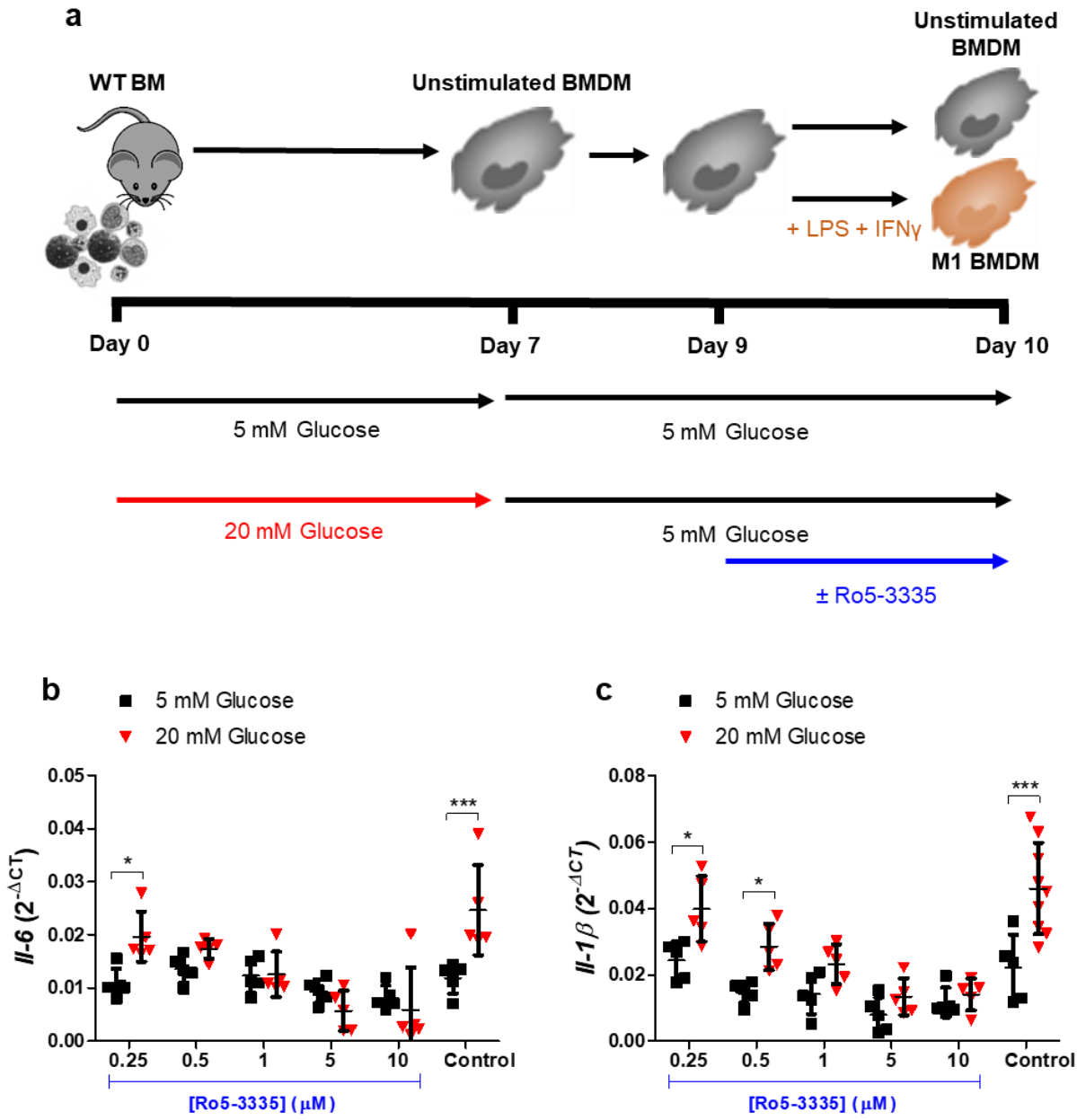


Figure 5.10 ***RUNX1 inhibition normalises hyperglycaemic memory gene expression, in vitro.***

*Wild-type (WT) bone marrow (BM) was differentiated into bone marrow derived macrophages (BMDM) in physiological (5 mM) or high glucose (20 mM) and then stimulated with LPS + IFNγ in 5 mM glucose ± varying concentrations of Ro5-3335, (a) as illustrated. After LPS + IFNγ stimulation, M1 BMDM (a) Il-6 and (b) Il-1β gene expression was assessed by qPCR. Data displayed as mean ± SD, 2-way ANOVA with Bonferroni Post-Hoc, *p<0.05, ***p<0.001. Sample n=5.*

Summary

The main findings from this chapter demonstrate:

1. Hyperglycaemic driven metabolic changes lead to the induction of epigenetic marks, in particular H3K4me3 and H3K27ac, and induce hyperglycaemic memory
2. Diabetic hyperglycaemia alters chromatin accessibility and increases transcription factor binding, in particular RUNX1, CTCF and PU.1
3. Human atherosclerotic plaque macrophages displayed differential expression of RUNX1 regulated genes
4. RUNX1 inhibition decreases the altered gene expression associated with *in vitro* "hyperglycaemic memory"

Discussion

Given the demonstration that BM from hyperglycaemic mice promoted atherosclerosis, along with the persistent pro-inflammatory gene expression and functional responses found in BMDM *in vitro*, it was reasoned that this 'hyperglycaemic memory' was a manifestation of trained immunity in BM-derived cells. Trained immunity has been associated with alterations in cellular metabolism that consequently induce long-lasting, chromatin-altering epigenetic marks, such as H3K4me3 and H3K27ac [130] [108,214]. Firstly, in line with this, HSC cultured in conditions of high extracellular glucose display increased glucose uptake and lactate production, indicating dysregulated glycolysis.

Alterations to HSC metabolism can have drastic downstream effects, as HSC metabolic profile and the intermediates generated by glycolysis, the TCA cycle and FAO are directly linked to their fate, lineage commitment, proliferative and differentiation status [215]. HSC are maintained in a quiescent state in the BM niche through upregulated HIF1 which, as previously described, increases glycolysis [216]. This is in direct opposition to when OXPHOS is upregulated in HSC, which drives their division, proliferation and differentiation [217,218]. This continues to provide

evidence for the link between metabolism, cellular gene expression and function. Effects of diabetes and diabetic hyperglycaemia on HSC metabolism have not previously been characterised or defined. However, previous studies have revealed that STZ diabetic BM supernatants display increased proinflammatory cytokine release, in particular TNF-α and IL-1β [219], indicating increased activation and potential metabolic changes. Mangialardi *et al*. demonstrate that markers of oxidative stress are increased in STZ BM endothelial cells compared to controls. This is caused by increased ROS production from the mitochondria and glycolysis, indicating diabetes alters BM endothelial cell metabolic profile [220] and could be representative of other BM cells.

Secondly, with relevance to trained immunity, both H3K4me3 and H3K27ac modifications were increased in HSC incubated in high extracellular glucose. Both these marks were also increased in diabetic HSC and, interestingly, H3K4me3 appears to persistently remain elevated through differentiation into diabetic BMDM. The combination of H3K4me3 and H3K27ac are known to be associated with active transcription [221]. Histone H3K4me3 primes enhancers and then the recruitment of transcription factors to these primed sites leads to H3K27ac which results in enhancer activation [222]. As histone acetylation is associated with rapid activation, and not long-term priming or programming, it is unsurprising that H3K27ac does not remain elevated in diabetic BMDM. H3K27ac is also shown to be highly dynamic with regards to monocyte trained immunity as is evidenced by response to β-glucan its levels increase as early as 1 hour post stimulation but decreases after 6 hours only to increase significantly upon restimulation [223]. This is in contrast to H3K4me3 which is a more long-term histone modification [125].

In the case of H3K4me3 (but not H3K27Ac), heightened levels in HSC caused by high extracellular glucose were negated with DCA inhibition. This indicates a direct link between glucose driven metabolic changes and histone modifications in HSC. The fact that H3K27ac is unaltered, if not increased, by DCA is anticipated, as the mechanism underlying DCA

involves the redirection of pyruvate into the TCA cycle and its conversion into acetyl-CoA [224]. Acetyl-CoA is the essential co-factor for histone acetylation and therefore DCA has previously been described to increase overall histone acetylation in stem cells [225]. The data showing that DCA inhibits the generation of *in vitro* hyperglycaemic memory combined with the changes in epigenetic marks, suggests that H3K4me3 is more relevant than H3K27ac to the initiation and generation of hyperglycaemic memory.

DCA inhibited the generation of hyperglycaemic memory *in vitro* and decreased H3K4me3 in BMDM. This indicates a direct causal link between increased glycolytic rate and the development of trained immunity in hyperglycaemia. Diabetes was also shown to have an effect on chromatin structure and transcription factor binding motif accessibility. While diabetes alone showed effects on chromatin accessibility, the effects of IL-1β, in the context of cells that were primed by diabetes, were even more pronounced. This is particularly relevant as IL-1β has been implicated in diabetes [181] and as an important driver of atherosclerosis, and in obesity where adipose tissue macrophage produced IL-1β induces proliferation of BM progenitors [210,211]. The enhanced effect also suggests a hierarchical relationship in which macrophages primed by hyperglycaemia, but manifest more florid changes in response to a second stimulus [134]. Indeed, it is well-recognised that changes in chromatin states at promoters can underlie complex functional interactions between different macrophage-activating stimuli. For instance, while IFNγ is unable to activate many LPS-inducible genes, it can induce histone acetylation and chromatin remodelling at their promoters, thereby priming the cell for future activation in response to LPS [129].

Pathway analysis of the genes in close proximity to the regions of chromatin more open in diabetic HSC upon IL-1β stimulation, reveal that several inflammation-related pathways, including LPS tolerization in macrophages, are upregulated. This provides confidence that the open regions are relevant to the altered immune responses seen in other assays, however

RNA-seq of HSCs would provide experimental confirmation of the bioinformatically identified pathways.

Chromatin accessibility with diabetes alone implicated PU.1, RUNX1 and CTCF, whilst upon IL-1β ERG, ZNF263 and RUNX1 were inferred. RUNX1 is the only transcription factor to be inferred by both data sets, underlining its potential relevance to hyperglycaemic memory. RUNX1 is a well-defined regulator of HSC maintenance and differentiation into diverse lineages [226], but only recently its role in innate immunity and inflammation is being identified and understood. In macrophages, overexpression of RUNX1 was shown to directly interact with the NF-κB subunit p50 to enhance its activity and promote IL-1β and IL-6 production [227,228], suggesting a synergising role for RUNX1 as a NF-κB transcriptional co-activator. Further *in vivo* evidence of this interaction, and of RUNX1 involvement in TLR4-associated inflammation, was provided with data demonstrating that Ro5-3335 treatment protected mice from LPS-induced endotoxic shock, also significantly reducing IL-6 levels [227]. These data also support the findings that Ro5-3335 inhibits hyperglycaemic induced long-lasting *Il-6* and *Il-1β* expression, as shown in the hyperglycaemic memory *in vitro* model.

The pro-inflammatory role of RUNX1 was further described by Navarro-Montero *et al.*, as RUNX1 overexpression in hematoendothelial progenitors during differentiation saw an increase in pro-inflammatory signalling, including increased expression of *Tnf-α*, *Ifn-a2* and *Nf-κB1* [229]. And importantly, in NK cells, IL-12 stimulation with shown to increase H3K4me3 marks at RUNX gene loci, through STAT4 activations, which in turn increased RUNX target gene expression [230]. This provides evidence that the increase in H3K4me3 identified in diabetic HSC and BMDM may be affecting RUNX1 binding site availability and, therefore potentially affect downstream gene expression. RNA-seq analysis of diabetic HSC could confirm these findings and provide further insight into the chromatin sites affected and transcription factor activity.

The CCCTC-binding factor (CTCF) was also identified in motif analysis. This protein is important in the regulation of higher order chromatin structure [231], acting as an insulator. By affecting DNA accessibility in the vicinity of transcription factor binding sites, CTCF, has the potential to act synergistically with RUNX1 and other transcription factors [232] and has been shown to affect the rate of differentiation of myeloid precursor cells [233]. PU.1 is another transcription factor identified. PU.1 is a lineage determining transcription factor, and previously described to be important in monocyte to macrophage differentiation [234,235]. Interestingly though, RUNX1 is known to cooperate with PU.1 to regulate expression of the macrophage colony-stimulating factor receptor (M-CSFR) [235], hence also playing a vital role in macrophage growth and survival and further confirming its relevance.

Taken altogether, there is evidence for strong convergence of RUNX1 function in macrophages towards regulating processes that are important in atherogenesis. We therefore cross-referenced genes under putative control of RUNX1 with the transcriptional profiles of cells derived from a relevant, human *in vivo* setting. Human atherosclerotic plaque macrophages in the presence of diabetes showed differential expression of RUNX1 regulated genes. These dysregulated target genes include the expression of atherosclerotic relevant genes such as TRAF3 Interacting Protein 3 [236], Crooked Neck Pre-MRNA Splicing Factor 1 (Crnkl1) [237] and phospholipase A2, group V (Pla2g5) which of particular note, promoted atherosclerosis in *Ldlr*$^{-/-}$ mice after receiving an adoptive transfer of bone marrow from transgenic mice expressing human Pla2g5 [238]. This provides strong supportive evidence for the relevance of hyperglycaemic memory and RUNX1 in human disease.

An interesting observation is that some of these RUNX1 target genes display increased expression in diabetic plaque macrophages, namely CRNKl1 and PLA2G5, and others displayed lower expression in diabetic plaque macrophages compared to non-diabetic plaque macrophages, like zinc finger protein 32 (ZNF32) and nucleoporin 214 (NUP214). Although this initially looks like confounding results, RUNX1 has been previously demonstrated to both

promote gene expression and act as a transcriptional repressor [239]. This primarily occurs through the recruitment of histone deacetylases, such as HDAC1 and 6 [240] and histone methyltransferases [239]. This may also hint that RUNX1 is not only contributing to downstream altered inflammatory gene expression in diabetes but may play a role in generating the epigenetic hyperglycaemic memory. This may be the mechanism underlying how Ro5-3335 was able to inhibit the generation of hyperglycaemic memory, *in vitro*. Further investigation, for example by performing ChIP-seq for RUNX1 or associated epigenetic marks, would enable further understanding of the mechanisms underlying hyperglycaemic memory and the involvement of RUNX1.

In conclusion, this chapter provides mechanistic insight into hyperglycaemic memory in HSC and macrophages and importantly describes the relevance of this mechanism in human atherosclerosis. Through a similar mechanism to trained immunity, hyperglycaemia leads to altered cellular metabolism which increases the epigenetic marks H3K4me3 and H3K27ac. Diabetes alters chromatin openness, of particular relevance to human disease, increasing accessibility of RUNX1 binding sites. Inhibiting glycolysis and RUNX1 prevents the generation of hyperglycaemic memory. Inhibiting RUNX1 after induction of hyperglycaemic memory decreases pro-inflammatory gene expression.

Chapter 6 : Discussion

The data presented in this thesis (summarised in Figure 6.1) shows that diabetic hyperglycaemia induces a long lasting, pro-inflammatory memory in HSC and macrophages through a mechanism that mirrors trained immunity. High glucose provokes alterations in cellular metabolism, in particular increasing glycolysis, dysregulating the TCA cycle and decreasing glutaminolysis, which induces epigenetic modifications and subsequent alterations in chromatin structure leading to increased accessibility at specific transcription factor binding sites, notably RUNX1. Hyperglycaemic memory, in macrophages, led to heightened pro-inflammatory gene expression, enhanced adhesion to endothelial cells and increased foam cell formation in diabetic cells, despite glucose normalisation. Pharmacological inhibition of glycolysis or RUNX1 prevented the generation of hyperglycaemic memory *in vitro*, and RUNX1 inhibition normalised persistent heightened pro-inflammatory gene expression. Of particular importance, hyperglycaemic memory, in HSC, markedly exacerbated atherosclerosis *in vivo* and RUNX1 associated genes displayed dysregulated expression in human plaque macrophages, clearly demonstrating the relevance of RUNX1 and hyperglycaemic memory in the pathogenesis of atherosclerosis and in human disease.

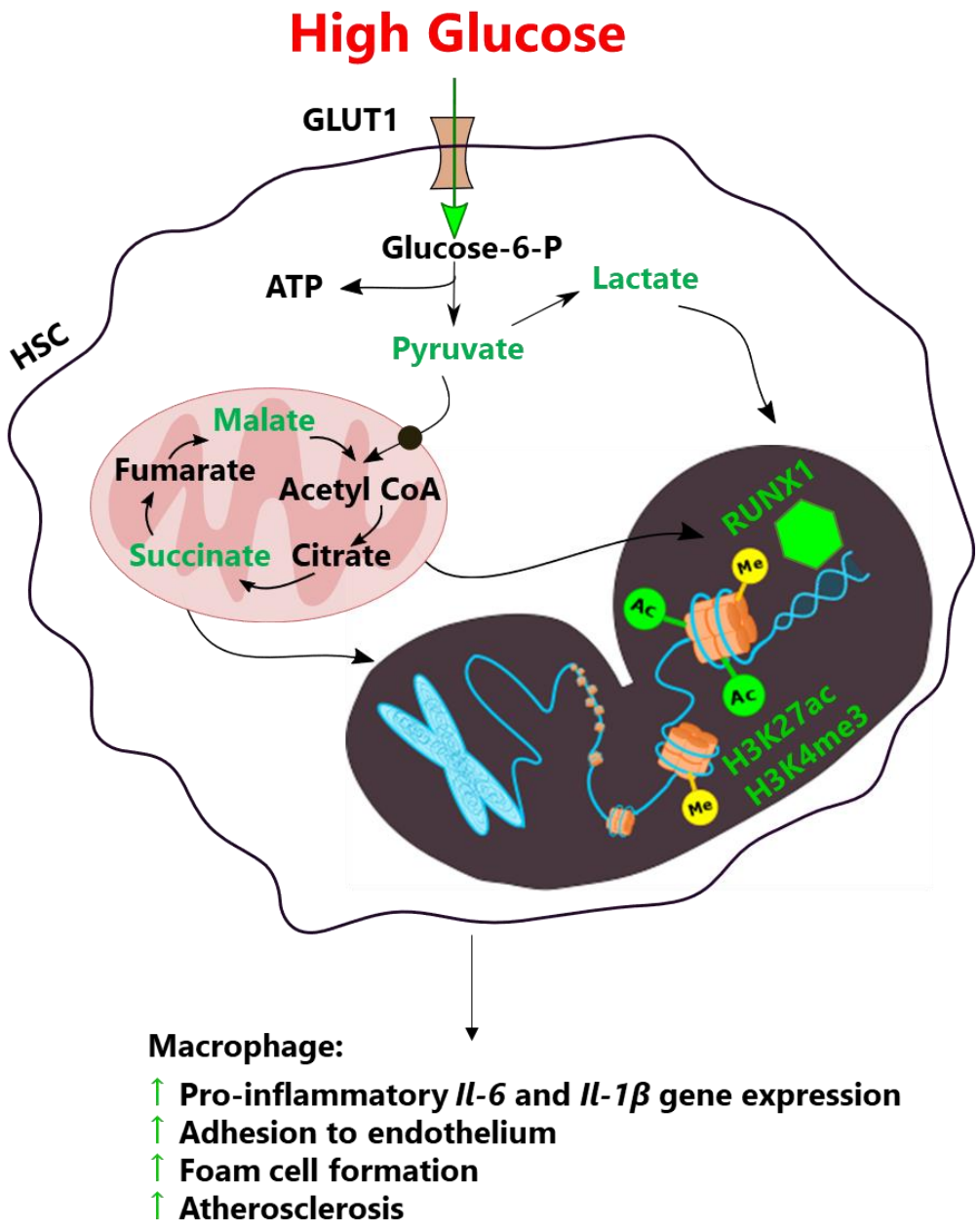


Figure 6.1 ***Proposed mechanism underlying hyperglycaemic memory in haematopoietic stem cells (HSC) and macrophages.***

Diabetic hyperglycaemia alters HSC metabolism increasing pyruvate, lactate, succinate and malate. Metabolic changes lead to increases in long-lasting H3K4me3 and H3K27ac epigenetic marks which alter chromatin structure allowing increased access to transcription factor binding sites, of particular relevance is RUNX1. Epigenetic marks persist in differentiated macrophages, causing increases in pro-inflammatory stimulated gene expression, functional responses and hence drive atherosclerosis in vivo.

Patients with diabetes suffer from exacerbated atherosclerosis and hence have an increased risk of cardiovascular diseases such as myocardial infarction and stroke. The primary treatment goal in diabetes is to lower and normalise blood glucose levels, however these have previously show to have no [22-24] or little [25,26] beneficial effects on reducing cardiovascular outcomes. The persistence of cardiovascular complications, even after glucose lowering therapies, indicates hyperglycaemic memory in cells driving disease. These findings may help to explain the resistance of diabetic cardiovascular complications to treatments that reduce blood glucose. As such, these data have the potential to fundamentally alter the approach to the management of diabetes, expanding treatments beyond the current focus on glycaemic control towards targeting disordered innate immune cell function.

Targeting the immune system is not a novel concept in treating cardiovascular diseases, especially where macrophages and inflammation are a primary therapeutic target in treating atherosclerosis [33,241]. The association between inflammation, diabetes and vascular complications is also well established, and previously identified as a potential therapeutic target [242]. However, the primary therapeutic goal is still to lower blood glucose and any anti-inflammatory effects identified are an additional benefit.

Metformin improves glycaemic control by decreasing hepatic glucose production and enhancing insulin sensitivity, but also activated AMPK, which is thought to lead to its anti-inflammatory and antioxidant effects. Its activation of AMPK has already been shown to prevent monocyte to macrophage differentiation [243] and decreases mitochondrial ROS to decrease IL-1β secretion from M1 macrophages [244]. Although these point to a potential ability to decrease atherosclerosis and therefore cardiovascular risk, currently no cardiovascular endpoint trial exists to provide evidence. Sulfonylureas, which directly stimulate the release of insulin from pancreatic β-cells and reduce insulin clearance by the level to overall improve glycaemic levels [245], are also known to have anti-inflammatory effects. Glyburide, for example, is known to decrease IL-1β secretion through inflammasome inhibition [246]. However, it is

interesting to note that when assessed for their effect on diabetic cardiovascular outcomes, sulfonylurea treatment in combination with metformin was associated with an increased risk of myocardial infarction and sever hypoglycaemia [247], hence highlighting the dangers of continually aiming to lower blood glucose levels and the potential risk of off target effects. Having a therapeutic that targets a specific mechanism underlying hyperglycaemic memory and diabetic complications, without lowering blood glucose levels further, would have the potential to stop these outcomes.

Sodium-glucose cotransporter 2 (SGLT2) inhibitors improve glycaemia through the inhibition of glucose reabsorption through the kidney. The EMPA-REG OUTCOME Cardiovascular Outcome trial revealed Empagliflozin, as stated previously, decreased hyperglycaemic levels were associated with a reduce in death from cardiovascular causes in patients with Type 2 diabetes by 38 % reduction in relative risk [24]. However, the causal link is not specifically shown, and recent reports have shown that Empaglifozin is able to reduce M1 and increase M2 macrophage polarisation within adipose tissue, with a reduction in TNF-α [248]. Overall, suggesting that a dampening effect on inflammation may also have a part to play in reducing CVD risk and again emphasising the need for a therapy that specifically targets mechanisms of increased atherosclerosis.

One of the major findings from this study shows that inhibiting RUNX1 with the pharmacological inhibitor Ro5-3335 reduces persistent *Il-6* and *Il-1β* macrophage gene expression. Of relevance to the functional memory effects that we observed in diabetic macrophage adhesion, RUNX1 is also an important controller of monocyte-endothelial interactions through regulation of (LFA-1) / CD11a [249]. Taken altogether, there is evidence for strong convergence of RUNX1 function in macrophages towards regulating processes that are important in atherogenesis. These both illustrate RUNX1 inhibition as a potential new therapeutic option for reversing persistent macrophage inflammation associated with hyperglycaemic memory. Performing further *in vivo* studies, whereby Ro5-3335 is

administered to STZ mice during exposure to diabetic hyperglycaemia and interrogating its effect on hyperglycaemic memory associated *Il-6* and *Il-1β* BMDM gene expression, could provide a clear demonstration of the involvement of RUNX1 in hyperglycaemic memory and its therapeutic potential.

Induction of trained immunity in peripheral macrophages alone could have driven disease progression, but given the long-term effects of trained immunity and the relatively short life span of peripheral myeloid cells, we reasoned that trained immunity could be induced at the level of haematopoietic stem and progenitors cells, as has recently been demonstrated for β-glucan and for Western diet [209]. BM progenitors, especially HSC, have previously been described to be key to many microvascular diseases, in particular retinopathy [250]. Experimental models of diabetes show a decrease in circulating BM progenitor cells [251], primarily put down to an impaired mobilisation from the BM niche [252]. Diabetes was also shown to impair HSC vascular repair potential and heighten their differentiation into inflammatory monocytes [219], although the mechanism was not previously understood and therefore could be a manifestation of hyperglycaemic memory, as described here.

While previous studies have typically related epigenetic changes in trained immunity to an *in vitro* phenotype (e.g. cytokine production), we show how trained immunity directly drives the progression of atherosclerosis, an important pathology with an integral inflammatory component. Trained immunity is relevant to atherosclerosis, as monocytes from patients with severe symptomatic coronary atherosclerosis display a trained immunity phenotype with increased pro-inflammatory TNF-α production and glycolytic enzyme gene expression, upon LPS stimulation, and increased H3K4me3 at pro-inflammatory gene promoters [253]. The data described here were able to provide further insight into immune cell memory in atherosclerosis, as RUNX1 associated genes were over represented in the list of genes dysregulated in diabetic plaque macrophages. Further immunohistological staining for

epigenetic marks H3K4me3 and H3K27ac in human plaque macrophages would continue to demonstrate relevance of trained immunity in human atherosclerosis.

The identification of metabolic drivers and of particular epigenetic modifications also recommends potential new therapeutic targets. There are multiple small molecules that modulate the epigenome in clinical trials. For example recently the pan-HDAC inhibitor Panobinostat has been approved for treatment in multiple myeloma [254] and ORY-1001, a lysine-specific demethylase KDM1A inhibitor, is currently in clinical trials for leukaemia [255]. For this to be a potential therapeutic method in hyperglycaemic memory, further investigation of the abundance of all epigenetic marks and identification of epigenetic modifying enzymes would need to be defined. A non-target proteomics analysis of diabetic HSC and BMDM histones under basal and stimulated conditions would help to reveal differences in epigenome patterning under disease conditions.

One of the limitations of this study is the assumption that the mechanism by which diabetic bone marrow is exacerbating atherosclerosis *in vivo* after transplantation into a normoglycaemic environment is through the mechanism described in the *in vitro* studies. Immunofluorescence staining for RUNX1, PLA2G5, macrophage M1 marker iNOS and M2 marker ARGI in aortic root sections were all attempted but failed due to PFA fixation methods. Repeating the bone marrow transplant protocol without this method of fixation or altering it to allow for better staining post necropsy would amend this issue. An even more effective method of confirming the mechanism and involvement of glycolysis and RUNX1 would be to repeat the transplant experiment with the addition of extra experimental groups. One in which donor mice will receive oral DCA or Ro5-3335 inhibitors during the period of diabetes, prior to bone marrow transplantation, to identify if they prevent the generation of hyperglycaemic memory and reduce atherosclerosis in the recipient mice. Another additional group that receive Ro5-3335 inhibitor post diabetic bone marrow transplantation would reveal if the effects of

hyperglycaemic memory on atherosclerotic burden has the potential for pharmacological reversal.

Another limitation is that hyperglycaemic memory was only shown in a type 1 model of diabetes. Repeating BMDM gene expression and function assays in a model of type 2 diabetes would provide additional confirmation of the relevance of these findings to type 2 diabetes. This is similar to the fact that the data shown was performed only in male mice, therefore disregarding possible contradictory effects of gender. In a statement released by the AHA, women with diabetes have an amplified coronary heart disease risk of up to 2-fold, compared to men as well as an earlier occurrence of and higher mortality after myocardial infarction [256]. Overall suggesting more adverse effects on cardiovascular complications in woman. Thus, future investigation of hyperglycaemic memory in female mice should be carried out.

All the data presented provides evidence that extracellular high glucose or diabetic hyperglycaemia is altering cellular metabolism, chromatin structure and transcription factor binding accessibility. However, to see an effect on gene expression and function requires further stimulation by LPS, modified lipid or cytokines, like IL-1β. This would suggest that glucose is having a priming effect, and just like trained immunity responses, requires the secondary stimulus to see an augmented effect. Macrophages are highly sensitive to their surroundings and changes in the local microenvironment, including cytokine concentrations and metabolic environment, can therefore have dramatic effects on macrophage polarisation and plasticity [257]. The atherosclerotic plaque milieu is full of various stimuli - including lipid, cytokines, ROS - and if the infiltrating monocytes and macrophages are already primed, this could noticeably alter their responses to such stimuli and therefore alter the atherogenesis. Although the bone marrow transplant experiment shown here provides initial experimental evidence for this phenomenon, further experimentation using an inhibitor that prevents the priming of progenitor cells by hyperglycaemia would provide further insight.

It is important to point out that a high fat western diet causes a trained immunity response in bone marrow myeloid progenitor cells and monocytes as well [133]. This is notable as obesity is a common type 2 diabetes co-morbidity and therefore may be playing a role in inducing pro-inflammatory memory within these cells as well as hyperglycaemia. It is therefore important, in future studies, to interrogate whether other diabetic features, such as hyperinsulinemia and hyperlipidaemia, are also driving a memory phenotype or contributing to the development of hyperglycaemic memory in bone marrow, monocytes and macrophages. This is similar to the need to understand the duration of hyperglycaemia needed to induce hyperglycaemic memory or the effect of oscillating blood glucose levels compared to constant hyperglycaemia on its generation.

Conclusion

To conclude, these findings have important implications for the management of the atherosclerotic complications of diabetes. Most importantly, pro-atherogenic characteristics of myeloid cells and bone marrow precursors persist after normalisation of blood glucose. This may help to explain the lack of efficacy of conventional treatments and fundamentally challenges the approach to the management of the vascular risk and complications of diabetes. The identification of metabolic drivers and of particular epigenetic modifications also recommends potential new therapeutic targets.

References

1. Foundation, B.H. BHF CVD Statistics Factsheet - UK (2018).
2. Ogurtsova, K.*, et al.* IDF Diabetes Atlas: Global estimates for the prevalence of diabetes for 2015 and 2040. *Diabetes Res Clin Pract* **128**, 40-50 (2017).
3. Q&A: Key points for IDF Diabetes Atlas 2017. *Diabetes Res Clin Pract* **135**, 235-236 (2018).
4. Leon, B.M. & Maddox, T.M. Diabetes and cardiovascular disease: Epidemiology, biological mechanisms, treatment recommendations and future research. *World J Diabetes* **6**, 1246-1258 (2015).
5. Huo, L.*, et al.* Impact of age at diagnosis and duration of type 2 diabetes on mortality in Australia 1997-2011. *Diabetologia* **61**, 1055-1063 (2018).
6. Dinesh Shah, A.*, et al.* Type 2 diabetes and incidence of a wide range of cardiovascular diseases: a cohort study in 1·9 million people. *Lancet* **385 Suppl 1**, S86 (2015).
7. de Ferranti, S.D.*, et al.* Type 1 diabetes mellitus and cardiovascular disease: a scientific statement from the American Heart Association and American Diabetes Association. *Circulation* **130**, 1110-1130 (2014).
8. Association, A.D. Diagnosis and classification of diabetes mellitus. *Diabetes Care* **33 Suppl 1**, S62-69 (2010).
9. Laing, S.P.*, et al.* Mortality from heart disease in a cohort of 23,000 patients with insulin-treated diabetes. *Diabetologia* **46**, 760-765 (2003).
10. Norhammar, A. & Schenck-Gustafsson, K. Type 2 diabetes and cardiovascular disease in women. *Diabetologia* **56**, 1-9 (2013).
11. Burke, A.P.*, et al.* Morphologic findings of coronary atherosclerotic plaques in diabetics: a postmortem study. *Arterioscler Thromb Vasc Biol* **24**, 1266-1271 (2004).
12. England, P.H. CVD Profiles - Diabetes (February 2018 Update). (2018).
13. Chamberlain, J.J.*, et al.* Cardiovascular Disease and Risk Management: Review of the American Diabetes Association Standards of Medical Care in Diabetes 2018. *Ann Intern Med* **168**, 640-650 (2018).
14. Stone, N.J.*, et al.* 2013 ACC/AHA guideline on the treatment of blood cholesterol to reduce atherosclerotic cardiovascular risk in adults: a report of the American College of Cardiology/American Heart Association Task Force on Practice Guidelines. *Circulation* **129**, S1-45 (2014).
15. Colhoun, H.M.*, et al.* Primary prevention of cardiovascular disease with atorvastatin in type 2 diabetes in the Collaborative Atorvastatin Diabetes Study (CARDS): multicentre randomised placebo-controlled trial. *Lancet* **364**, 685-696 (2004).
16. Collins, R.*, et al.* MRC/BHF Heart Protection Study of cholesterol-lowering with simvastatin in 5963 people with diabetes: a randomised placebo-controlled trial. *Lancet* **361**, 2005-2016 (2003).
17. Ridker, P.M., Pradhan, A., MacFadyen, J.G., Libby, P. & Glynn, R.J. Cardiovascular benefits and diabetes risks of statin therapy in primary prevention: an analysis from the JUPITER trial. *Lancet* **380**, 565-571 (2012).
18. Crandall, J.P.*, et al.* Statin use and risk of developing diabetes: results from the Diabetes Prevention Program. *BMJ Open Diabetes Res Care* **5**, e000438 (2017).

19. Parathath, S., *et al.* Diabetes adversely affects macrophages during atherosclerotic plaque regression in mice. *Diabetes* **60**, 1759-1769 (2011).

20. Nathan, D.M., *et al.* Intensive diabetes treatment and cardiovascular disease in patients with type 1 diabetes. *N Engl J Med* **353**, 2643-2653 (2005).

21. Nathan, D.M., *et al.* The effect of intensive treatment of diabetes on the development and progression of long-term complications in insulin-dependent diabetes mellitus. *N Engl J Med* **329**, 977-986 (1993).

22. Group, A.S. Nine-Year Effects of 3.7 Years of Intensive Glycemic Control on Cardiovascular Outcomes. *Diabetes Care* **39**, 701-708 (2016).

23. Patel, A., *et al.* Intensive blood glucose control and vascular outcomes in patients with type 2 diabetes. *N Engl J Med* **358**, 2560-2572 (2008).

24. Zinman, B., *et al.* Empagliflozin, Cardiovascular Outcomes, and Mortality in Type 2 Diabetes. *N Engl J Med* **373**, 2117-2128 (2015).

25. Marso, S.P., *et al.* Semaglutide and Cardiovascular Outcomes in Patients with Type 2 Diabetes. *N Engl J Med* **375**, 1834-1844 (2016).

26. Neal, B., Perkovic, V. & Matthews, D.R. Canagliflozin and Cardiovascular and Renal Events in Type 2 Diabetes. *N Engl J Med* **377**, 2099 (2017).

27. Holman, R.R., Paul, S.K., Bethel, M.A., Matthews, D.R. & Neil, H.A. 10-year follow-up of intensive glucose control in type 2 diabetes. *N Engl J Med* **359**, 1577-1589 (2008).

28. Tabas, I., Williams, K.J. & Borén, J. Subendothelial lipoprotein retention as the initiating process in atherosclerosis: update and therapeutic implications. *Circulation* **116**, 1832-1844 (2007).

29. Borén, J. & Williams, K.J. The central role of arterial retention of cholesterol-rich apolipoprotein-B-containing lipoproteins in the pathogenesis of atherosclerosis: a triumph of simplicity. *Curr Opin Lipidol* **27**, 473-483 (2016).

30. Edwards, I.J., Wagner, J.D., Vogl-Willis, C.A., Litwak, K.N. & Cefalu, W.T. Arterial heparan sulfate is negatively associated with hyperglycemia and atherosclerosis in diabetic monkeys. *Cardiovasc Diabetol* **3**, 6 (2004).

31. Packard, R.R. & Libby, P. Inflammation in atherosclerosis: from vascular biology to biomarker discovery and risk prediction. *Clin Chem* **54**, 24-38 (2008).

32. Szmitko, P.E., *et al.* New markers of inflammation and endothelial cell activation: Part I. *Circulation* **108**, 1917-1923 (2003).

33. Libby, P. Interleukin-1 Beta as a Target for Atherosclerosis Therapy: Biological Basis of CANTOS and Beyond. *J Am Coll Cardiol* **70**, 2278-2289 (2017).

34. Brånén, L., *et al.* Inhibition of tumor necrosis factor-alpha reduces atherosclerosis in apolipoprotein E knockout mice. *Arterioscler Thromb Vasc Biol* **24**, 2137-2142 (2004).

35. Mestas, J. & Ley, K. Monocyte-endothelial cell interactions in the development of atherosclerosis. *Trends Cardiovasc Med* **18**, 228-232 (2008).

36. Esposito, C., *et al.* Long-term exposure to high glucose up-regulates VCAM-induced endothelial cell adhesiveness to PBMC. *Kidney Int* **59**, 1842-1849 (2001).

37. Gustavsson, C., *et al.* Vascular cellular adhesion molecule-1 (VCAM-1) expression in mice retinal vessels is affected by both hyperglycemia and hyperlipidemia. *PLoS One* **5**, e12699 (2010).

38. Muller, W.A. How endothelial cells regulate transmigration of leukocytes in the inflammatory response. *Am J Pathol* **184**, 886-896 (2014).

39. Stöger, J.L.*, et al.* Distribution of macrophage polarization markers in human atherosclerosis. *Atherosclerosis* **225**, 461-468 (2012).

40. de Gaetano, M., Crean, D., Barry, M. & Belton, O. M1- and M2-Type Macrophage Responses Are Predictive of Adverse Outcomes in Human Atherosclerosis. *Front Immunol* **7**, 275 (2016).

41. Kzhyshkowska, J., Neyen, C. & Gordon, S. Role of macrophage scavenger receptors in atherosclerosis. *Immunobiology* **217**, 492-502 (2012).

42. Jones, N.L., Reagan, J.W. & Willingham, M.C. The pathogenesis of foam cell formation: modified LDL stimulates uptake of co-incubated LDL via macropinocytosis. *Arterioscler Thromb Vasc Biol* **20**, 773-781 (2000).

43. Rader, D.J. & Puré, E. Lipoproteins, macrophage function, and atherosclerosis: beyond the foam cell? *Cell Metab* **1**, 223-230 (2005).

44. Moore, K.J., Sheedy, F.J. & Fisher, E.A. Macrophages in atherosclerosis: a dynamic balance. *Nat Rev Immunol* **13**, 709-721 (2013).

45. Levitan, I., Volkov, S. & Subbaiah, P.V. Oxidized LDL: diversity, patterns of recognition, and pathophysiology. *Antioxid Redox Signal* **13**, 39-75 (2010).

46. Kojima, Y., Weissman, I.L. & Leeper, N.J. The Role of Efferocytosis in Atherosclerosis. *Circulation* **135**, 476-489 (2017).

47. Tabas, I. Consequences and therapeutic implications of macrophage apoptosis in atherosclerosis: the importance of lesion stage and phagocytic efficiency. *Arterioscler Thromb Vasc Biol* **25**, 2255-2264 (2005).

48. Seimon, T. & Tabas, I. Mechanisms and consequences of macrophage apoptosis in atherosclerosis. *J Lipid Res* **50 Suppl**, S382-387 (2009).

49. Kolodgie, F.D.*, et al.* Pathologic assessment of the vulnerable human coronary plaque. *Heart* **90**, 1385-1391 (2004).

50. Yonetsu, T.*, et al.* Features of coronary plaque in patients with metabolic syndrome and diabetes mellitus assessed by 3-vessel optical coherence tomography. *Circ Cardiovasc Imaging* **6**, 665-673 (2013).

51. Wynn, T.A., Chawla, A. & Pollard, J.W. Macrophage biology in development, homeostasis and disease. *Nature* **496**, 445-455 (2013).

52. Martinez, F.O., Gordon, S., Locati, M. & Mantovani, A. Transcriptional profiling of the human monocyte-to-macrophage differentiation and polarization: new molecules and patterns of gene expression. *J Immunol* **177**, 7303-7311 (2006).

53. Jablonski, K.A.*, et al.* Novel Markers to Delineate Murine M1 and M2 Macrophages. *PLoS One* **10**, e0145342 (2015).

54. Martinez, F.O. & Gordon, S. The M1 and M2 paradigm of macrophage activation: time for reassessment. *F1000Prime Rep* **6**, 13 (2014).

55. Nizet, V. Antimicrobial peptide resistance mechanisms of human bacterial pathogens. *Curr Issues Mol Biol* **8**, 11-26 (2006).

56. Zhu, J.*, et al.* Parasitic antigens alter macrophage polarization during Schistosoma japonicum infection in mice. *Parasit Vectors* **7**, 122 (2014).

57. Gordon, S. & Martinez, F.O. Alternative activation of macrophages: mechanism and functions. *Immunity* **32**, 593-604 (2010).

58. Chinetti-Gbaguidi, G., Colin, S. & Staels, B. Macrophage subsets in atherosclerosis. *Nat Rev Cardiol* **12**, 10-17 (2015).

59. Kratz, M., *et al.* Metabolic dysfunction drives a mechanistically distinct proinflammatory phenotype in adipose tissue macrophages. *Cell Metab* **20**, 614-625 (2014).

60. Coats, B.R., *et al.* Metabolically Activated Adipose Tissue Macrophages Perform Detrimental and Beneficial Functions during Diet-Induced Obesity. *Cell Rep* **20**, 3149-3161 (2017).

61. Kzhyshkowska, J., Gudima, A., Moganti, K., Gratchev, A. & Orekhov, A. Perspectives for Monocyte/Macrophage-Based Diagnostics of Chronic Inflammation. *Transfus Med Hemother* **43**, 66-77 (2016).

62. van Diepen, J.A., *et al.* Diabetes propels the risk for cardiovascular disease: sweet monocytes becoming aggressive? *Cell Mol Life Sci* **73**, 4675-4684 (2016).

63. Menart-Houtermans, B., *et al.* Leukocyte profiles differ between type 1 and type 2 diabetes and are associated with metabolic phenotypes: results from the German Diabetes Study (GDS). *Diabetes Care* **37**, 2326-2333 (2014).

64. Tanaka, M., *et al.* Hyperglycemia and Inflammatory Property of Circulating Monocytes are Associated with Inflammatory Property of Carotid Plaques in Patients Undergoing Carotid Endarterectomy. *J Atheroscler Thromb* **23**, 1212-1221 (2016).

65. Nagareddy, P.R., *et al.* Hyperglycemia promotes myelopoiesis and impairs the resolution of atherosclerosis. *Cell Metab* **17**, 695-708 (2013).

66. Lee, H.M., *et al.* Upregulated NLRP3 inflammasome activation in patients with type 2 diabetes. *Diabetes* **62**, 194-204 (2013).

67. Kitahara, M., Eyre, H.J., Lynch, R.E., Rallison, M.L. & Hill, H.R. Metabolic activity of diabetic monocytes. *Diabetes* **29**, 251-256 (1980).

68. Distel, E., *et al.* miR33 inhibition overcomes deleterious effects of diabetes mellitus on atherosclerosis plaque regression in mice. *Circ Res* **115**, 759-769 (2014).

69. Kanter, J.E., *et al.* Diabetes promotes an inflammatory macrophage phenotype and atherosclerosis through acyl-CoA synthetase 1. *Proc Natl Acad Sci U S A* **109**, E715-724 (2012).

70. Devaraj, S. & Jialal, I. Low-density lipoprotein postsecretory modification, monocyte function, and circulating adhesion molecules in type 2 diabetic patients with and without macrovascular complications: the effect of alpha-tocopherol supplementation. *Circulation* **102**, 191-196 (2000).

71. Kunt, T., *et al.* Binding of monocytes from normolipidemic hyperglycemic patients with type 1 diabetes to endothelial cells is increased in vitro. *Exp Clin Endocrinol Diabetes* **107**, 252-256 (1999).

72. Cipolletta, C., Ryan, K.E., Hanna, E.V. & Trimble, E.R. Activation of peripheral blood CD14+ monocytes occurs in diabetes. *Diabetes* **54**, 2779-2786 (2005).

73. Kimball, A., *et al.* Ly6C. *Arterioscler Thromb Vasc Biol* **38**, 1102-1114 (2018).

74. Shanmugam, N., Gaw Gonzalo, I.T. & Natarajan, R. Molecular mechanisms of high glucose-induced cyclooxygenase-2 expression in monocytes. *Diabetes* **53**, 795-802 (2004).

75. Li, M.F., *et al.* High Glucose Increases the Expression of Inflammatory Cytokine Genes in Macrophages Through H3K9 Methyltransferase Mechanism. *J Interferon Cytokine Res* **36**, 48-61 (2016).

76. Dasu, M.R., Devaraj, S. & Jialal, I. High glucose induces IL-1beta expression in human monocytes: mechanistic insights. *Am J Physiol Endocrinol Metab* **293**, E337-346 (2007).

77. Shanmugam, N., Reddy, M.A., Guha, M. & Natarajan, R. High glucose-induced expression of proinflammatory cytokine and chemokine genes in monocytic cells. *Diabetes* **52**, 1256-1264 (2003).

78. Li, L., Sawamura, T. & Renier, G. Glucose enhances human macrophage LOX-1 expression: role for LOX-1 in glucose-induced macrophage foam cell formation. *Circ Res* **94**, 892-901 (2004).

79. O'Neill, L.A. & Pearce, E.J. Immunometabolism governs dendritic cell and macrophage function. *J Exp Med* **213**, 15-23 (2016).

80. Kelly, B. & O'Neill, L.A. Metabolic reprogramming in macrophages and dendritic cells in innate immunity. *Cell Res* **25**, 771-784 (2015).

81. Geeraerts, X., Bolli, E., Fendt, S.M. & Van Ginderachter, J.A. Macrophage Metabolism As Therapeutic Target for Cancer, Atherosclerosis, and Obesity. *Front Immunol* **8**, 289 (2017).

82. Nishizawa, T.*, et al.* Testing the role of myeloid cell glucose flux in inflammation and atherosclerosis. *Cell Rep* **7**, 356-365 (2014).

83. Sarrazy, V.*, et al.* Disruption of Glut1 in Hematopoietic Stem Cells Prevents Myelopoiesis and Enhanced Glucose Flux in Atheromatous Plaques of ApoE(-/-) Mice. *Circ Res* **118**, 1062-1077 (2016).

84. Freemerman, A.J.*, et al.* Metabolic reprogramming of macrophages: glucose transporter 1 (GLUT1)-mediated glucose metabolism drives a proinflammatory phenotype. *J Biol Chem* **289**, 7884-7896 (2014).

85. Haschemi, A.*, et al.* The sedoheptulose kinase CARKL directs macrophage polarization through control of glucose metabolism. *Cell Metab* **15**, 813-826 (2012).

86. Millet, P., Vachharajani, V., McPhail, L., Yoza, B. & McCall, C.E. GAPDH Binding to TNF-α mRNA Contributes to Posttranscriptional Repression in Monocytes: A Novel Mechanism of Communication between Inflammation and Metabolism. *J Immunol* **196**, 2541-2551 (2016).

87. Takaoka, Y.*, et al.* Glyceraldehyde-3-phosphate dehydrogenase (GAPDH) prevents lipopolysaccharide (LPS)-induced, sepsis-related severe acute lung injury in mice. *Sci Rep* **4**, 5204 (2014).

88. Williams, N.C. & O'Neill, L.A.J. A Role for the Krebs Cycle Intermediate Citrate in Metabolic Reprogramming in Innate Immunity and Inflammation. *Front Immunol* **9**, 141 (2018).

89. Koivunen, P.*, et al.* Inhibition of hypoxia-inducible factor (HIF) hydroxylases by citric acid cycle intermediates: possible links between cell metabolism and stabilization of HIF. *J Biol Chem* **282**, 4524-4532 (2007).

90. Everts, B.*, et al.* Commitment to glycolysis sustains survival of NO-producing inflammatory dendritic cells. *Blood* **120**, 1422-1431 (2012).

91. Clementi, E., Brown, G.C., Feelisch, M. & Moncada, S. Persistent inhibition of cell respiration by nitric oxide: crucial role of S-nitrosylation of mitochondrial complex I and protective action of glutathione. *Proc Natl Acad Sci U S A* **95**, 7631-7636 (1998).

92. Zasłona, Z.*, et al.* The Induction of Pro-IL-1β by Lipopolysaccharide Requires Endogenous Prostaglandin E. *J Immunol* **198**, 3558-3564 (2017).

93. Hu, L.*, et al.* Epigenetic Regulation of Interleukin 6 by Histone Acetylation in Macrophages and Its Role in Paraquat-Induced Pulmonary Fibrosis. *Front Immunol* **7**, 696 (2016).

94. Mills, E.L.*, et al.* Itaconate is an anti-inflammatory metabolite that activates Nrf2 via alkylation of KEAP1. *Nature* **556**, 113-117 (2018).

95. Lampropoulou, V.*, et al.* Itaconate Links Inhibition of Succinate Dehydrogenase with Macrophage Metabolic Remodeling and Regulation of Inflammation. *Cell Metab* **24**, 158-166 (2016).

96. Serena, C.*, et al.* Elevated circulating levels of succinate in human obesity are linked to specific gut microbiota. *ISME J* (2018).

97. Nagao, H.*, et al.* Increased Dynamics of Tricarboxylic Acid Cycle and Glutamate Synthesis in Obese Adipose Tissue: IN VIVO METABOLIC TURNOVER ANALYSIS. *J Biol Chem* **292**, 4469-4483 (2017).

98. Mills, E. & O'Neill, L.A. Succinate: a metabolic signal in inflammation. *Trends Cell Biol* **24**, 313-320 (2014).

99. Liu, P.S.*, et al.* α-ketoglutarate orchestrates macrophage activation through metabolic and epigenetic reprogramming. *Nat Immunol* **18**, 985-994 (2017).

100. Wang, F.*, et al.* SIRT5 Desuccinylates and Activates Pyruvate Kinase M2 to Block Macrophage IL-1β Production and to Prevent DSS-Induced Colitis in Mice. *Cell Rep* **19**, 2331-2344 (2017).

101. Yang, P., Li, Z., Li, H., Lu, Y. & Wu, H. Pyruvate kinase M2 accelerates pro-inflammatory cytokine secretion and cell proliferation induced by lipopolysaccharide in colorectal cancer. *Cell Signal* **27**, 1525-1532 (2015).

102. Palsson-McDermott, E.M.*, et al.* Pyruvate Kinase M2 Regulates Hif-1α Activity and IL-1β Induction and Is a Critical Determinant of the Warburg Effect in LPS-Activated Macrophages. *Cell Metab* **21**, 347 (2015).

103. Shirai, T.*, et al.* The glycolytic enzyme PKM2 bridges metabolic and inflammatory dysfunction in coronary artery disease. *J Exp Med* **213**, 337-354 (2016).

104. Donohoe, D.R. & Bultman, S.J. Metaboloepigenetics: interrelationships between energy metabolism and epigenetic control of gene expression. *J Cell Physiol* **227**, 3169-3177 (2012).

105. Garcia-Valtanen, P., Guzman-Genuino, R.M., Williams, D.L., Hayball, J.D. & Diener, K.R. Evaluation of trained immunity by β-1, 3 (d)-glucan on murine monocytes in vitro and duration of response in vivo. *Immunol Cell Biol* **95**, 601-610 (2017).

106. Quintin, J.*, et al.* Candida albicans infection affords protection against reinfection via functional reprogramming of monocytes. *Cell Host Microbe* **12**, 223-232 (2012).

107. Netea, M.G., Quintin, J. & van der Meer, J.W. Trained immunity: a memory for innate host defense. *Cell Host Microbe* **9**, 355-361 (2011).

108. Arts, R.J.W.*, et al.* Immunometabolic Pathways in BCG-Induced Trained Immunity. *Cell Rep* **17**, 2562-2571 (2016).

109. Eccleston, A., DeWitt, N., Gunter, C., Marte, B. & Nath, D. Epigenetics. *Nature* **447**, 395-395 (2007).

110. Luger, K., Mäder, A.W., Richmond, R.K., Sargent, D.F. & Richmond, T.J. Crystal structure of the nucleosome core particle at 2.8 A resolution. *Nature* **389**, 251-260 (1997).

111. Misteli, T., Gunjan, A., Hock, R., Bustin, M. & Brown, D.T. Dynamic binding of histone H1 to chromatin in living cells. *Nature* **408**, 877-881 (2000).

112. Alberts, B.*, et al. Molecular Biology of the Cell*, (Garland Science, New York, 2002).

113. Bowman, G.D. & Poirier, M.G. Post-translational modifications of histones that influence nucleosome dynamics. *Chem Rev* **115**, 2274-2295 (2015).

114. Kinnaird, A.*, et al.* Metabolic Modulation of Clear-cell Renal Cell Carcinoma with Dichloroacetate, an Inhibitor of Pyruvate Dehydrogenase Kinase. *Eur Urol* **69**, 734-744 (2016).

115. Zhang, P., Torres, K., Liu, X., Liu, C.G. & Pollock, R.E. An Overview of Chromatin-Regulating Proteins in Cells. *Curr Protein Pept Sci* **17**, 401-410 (2016).

116. Eberharter, A. & Becker, P.B. Histone acetylation: a switch between repressive and permissive chromatin. Second in review series on chromatin dynamics. *EMBO Rep* **3**, 224-229 (2002).

117. Zhao, S.*, et al.* ATP-Citrate Lyase Controls a Glucose-to-Acetate Metabolic Switch. *Cell Rep* **17**, 1037-1052 (2016).

118. Wellen, K.E.*, et al.* ATP-citrate lyase links cellular metabolism to histone acetylation. *Science* **324**, 1076-1080 (2009).

119. Grummt, I. & Ladurner, A.G. A metabolic throttle regulates the epigenetic state of rDNA. *Cell* **133**, 577-580 (2008).

120. Latham, T.*, et al.* Lactate, a product of glycolytic metabolism, inhibits histone deacetylase activity and promotes changes in gene expression. *Nucleic Acids Res* **40**, 4794-4803 (2012).

121. Ahmed, M., de Winther, M.P.J. & Van den Bossche, J. Epigenetic mechanisms of macrophage activation in type 2 diabetes. *Immunobiology* **222**, 937-943 (2017).

122. Xiao, M.*, et al.* Inhibition of α-KG-dependent histone and DNA demethylases by fumarate and succinate that are accumulated in mutations of FH and SDH tumor suppressors. *Genes Dev* **26**, 1326-1338 (2012).

123. Jha, A.K.*, et al.* Network integration of parallel metabolic and transcriptional data reveals metabolic modules that regulate macrophage polarization. *Immunity* **42**, 419-430 (2015).

124. Lau, C.M.*, et al.* Epigenetic control of innate and adaptive immune memory. *Nat Immunol* **19**, 963-972 (2018).

125. Saeed, S.*, et al.* Epigenetic programming of monocyte-to-macrophage differentiation and trained innate immunity. *Science* **345**, 1251086 (2014).

126. O'Connell, R.M., Chaudhuri, A.A., Rao, D.S. & Baltimore, D. Inositol phosphatase SHIP1 is a primary target of miR-155. *Proc Natl Acad Sci U S A* **106**, 7113-7118 (2009).

127. Monticelli, S. & Natoli, G. Short-term memory of danger signals and environmental stimuli in immune cells. *Nat Immunol* **14**, 777-784 (2013).

128. Netea, M.G.*, et al.* Trained immunity: A program of innate immune memory in health and disease. *Science* **352**, aaf1098 (2016).

129. Arts, R.J.*, et al.* Glutaminolysis and Fumarate Accumulation Integrate Immunometabolic and Epigenetic Programs in Trained Immunity. *Cell Metab* **24**, 807-819 (2016).

130. Bekkering, S.*, et al.* Metabolic Induction of Trained Immunity through the Mevalonate Pathway. *Cell* **172**, 135-146.e139 (2018).

131. Kaufmann, E.*, et al.* BCG Educates Hematopoietic Stem Cells to Generate Protective Innate Immunity against Tuberculosis. *Cell* **172**, 176-190.e119 (2018).

132. Leentjens, J.*, et al.* Trained Innate Immunity as a Novel Mechanism Linking Infection and the Development of Atherosclerosis. *Circ Res* **122**, 664-669 (2018).

133. Christ, A.*, et al.* Western Diet Triggers NLRP3-Dependent Innate Immune Reprogramming. *Cell* **172**, 162-175.e114 (2018).

134. Moorlag, S.J.C.F., Röring, R.J., Joosten, L.A.B. & Netea, M.G. The role of the interleukin-1 family in trained immunity. *Immunol Rev* **281**, 28-39 (2018).

135. Arts, R.J.W.*, et al.* BCG Vaccination Protects against Experimental Viral Infection in Humans through the Induction of Cytokines Associated with Trained Immunity. *Cell Host Microbe* **23**, 89-100.e105 (2018).

136. Engerman, R.L. & Kern, T.S. Progression of incipient diabetic retinopathy during good glycemic control. *Diabetes* **36**, 808-812 (1987).

137. Roy, S., Sala, R., Cagliero, E. & Lorenzi, M. Overexpression of fibronectin induced by diabetes or high glucose: phenomenon with a memory. *Proc Natl Acad Sci U S A* **87**, 404-408 (1990).

138. El-Osta, A.*, et al.* Transient high glucose causes persistent epigenetic changes and altered gene expression during subsequent normoglycemia. *J Exp Med* **205**, 2409-2417 (2008).

139. Brasacchio, D.*, et al.* Hyperglycemia induces a dynamic cooperativity of histone methylase and demethylase enzymes associated with gene-activating epigenetic marks that coexist on the lysine tail. *Diabetes* **58**, 1229-1236 (2009).

140. Pirola, L.*, et al.* Genome-wide analysis distinguishes hyperglycemia regulated epigenetic signatures of primary vascular cells. *Genome Res* **21**, 1601-1615 (2011).

141. Paneni, F., Volpe, M., Lüscher, T.F. & Cosentino, F. SIRT1, p66(Shc), and Set7/9 in vascular hyperglycemic memory: bringing all the strands together. *Diabetes* **62**, 1800-1807 (2013).

142. Prattichizzo, F.*, et al.* Extracellular microRNAs and endothelial hyperglycaemic memory: a therapeutic opportunity? *Diabetes Obes Metab* **18**, 855-867 (2016).

143. Okabe, J.*, et al.* Distinguishing hyperglycemic changes by Set7 in vascular endothelial cells. *Circ Res* **110**, 1067-1076 (2012).

144. Li, Y.*, et al.* Role of the histone H3 lysine 4 methyltransferase, SET7/9, in the regulation of NF-kappaB-dependent inflammatory genes. Relevance to diabetes and inflammation. *J Biol Chem* **283**, 26771-26781 (2008).

145. Deering, T.G., Ogihara, T., Trace, A.P., Maier, B. & Mirmira, R.G. Methyltransferase Set7/9 maintains transcription and euchromatin structure at islet-enriched genes. *Diabetes* **58**, 185-193 (2009).

146. Paneni, F.*, et al.* Adverse epigenetic signatures by histone methyltransferase Set7 contribute to vascular dysfunction in patients with type 2 diabetes mellitus. *Circ Cardiovasc Genet* **8**, 150-158 (2015).

147. Miao, F., Gonzalo, I.G., Lanting, L. & Natarajan, R. In vivo chromatin remodeling events leading to inflammatory gene transcription under diabetic conditions. *J Biol Chem* **279**, 18091-18097 (2004).

148. Paneni, F.*, et al.* Gene silencing of the mitochondrial adaptor p66(Shc) suppresses vascular hyperglycemic memory in diabetes. *Circ Res* **111**, 278-289 (2012).

149. Cosentino, F.*, et al.* Final common molecular pathways of aging and cardiovascular disease: role of the p66Shc protein. *Arterioscler Thromb Vasc Biol* **28**, 622-628 (2008).

150. Zhou, S.*, et al.* Repression of P66Shc expression by SIRT1 contributes to the prevention of hyperglycemia-induced endothelial dysfunction. *Circ Res* **109**, 639-648 (2011).

151. Kumar, S.*, et al.* Sirtuin1-regulated lysine acetylation of p66Shc governs diabetes-induced vascular oxidative stress and endothelial dysfunction. *Proc Natl Acad Sci U S A* **114**, 1714-1719 (2017).

152. Zheng, Z.*, et al.* Sirtuin 1-mediated cellular metabolic memory of high glucose via the LKB1/AMPK/ROS pathway and therapeutic effects of metformin. *Diabetes* **61**, 217-228 (2012).

153. Pagnin, E.*, et al.* Diabetes induces p66shc gene expression in human peripheral blood mononuclear cells: relationship to oxidative stress. *J Clin Endocrinol Metab* **90**, 1130-1136 (2005).

154. Kim, C.S.*, et al.* Homocysteine promotes human endothelial cell dysfunction via site-specific epigenetic regulation of p66shc. *Cardiovasc Res* **92**, 466-475 (2011).

155. Wei, D. & Loeken, M.R. Increased DNA methyltransferase 3b (Dnmt3b)-mediated CpG island methylation stimulated by oxidative stress inhibits expression of a gene required for neural tube and neural crest development in diabetic pregnancy. *Diabetes* **63**, 3512-3522 (2014).

156. Yang, X.*, et al.* Epigenetic regulation of macrophage polarization by DNA methyltransferase 3b. *Mol Endocrinol* **28**, 565-574 (2014).

157. Iqbal, A.J.*, et al.* Human CD68 promoter GFP transgenic mice allow analysis of monocyte to macrophage differentiation in vivo. *Blood* **124**, e33-44 (2014).

158. Williams, R.L.*, et al.* Endothelioma cells expressing the polyoma middle T oncogene induce hemangiomas by host cell recruitment. *Cell* **57**, 1053-1063 (1989).

159. Feig, J.E.*, et al.* Regression of atherosclerosis is characterized by broad changes in the plaque macrophage transcriptome. *PLoS One* **7**, e39790 (2012).

160. Chai, J.T.*, et al.* Nicotinic acid receptor GPR109A is down-regulated in human macrophage-derived foam cells. *PLoS One* **8**, e62934 (2013).

161. Choudhury, R.P.*, et al.* High-density lipoproteins retard the progression of atherosclerosis and favorably remodel lesions without suppressing indices of inflammation or oxidation. *Arterioscler Thromb Vasc Biol* **24**, 1904-1909 (2004).

162. Kamleh, M.A.*, et al.* LC-MS metabolomics of psoriasis patients reveals disease severity-dependent increases in circulating amino acids that are ameliorated by anti-TNFα treatment. *J Proteome Res* **14**, 557-566 (2015).

163. Chong, J.*, et al.* MetaboAnalyst 4.0: towards more transparent and integrative metabolomics analysis. *Nucleic Acids Res* (2018).

164. Huber, W.*, et al.* Orchestrating high-throughput genomic analysis with Bioconductor. *Nat Methods* **12**, 115-121 (2015).

165. Dunning, M.J., Smith, M.L., Ritchie, M.E. & Tavaré, S. beadarray: R classes and methods for Illumina bead-based data. *Bioinformatics* **23**, 2183-2184 (2007).

166. Ritchie, M.E.*, et al.* limma powers differential expression analyses for RNA-sequencing and microarray studies. *Nucleic Acids Res* **43**, e47 (2015).

167. Buenrostro, J.D., Wu, B., Chang, H.Y. & Greenleaf, W.J. ATAC-seq: A Method for Assaying Chromatin Accessibility Genome-Wide. *Curr Protoc Mol Biol* **109**, 21.29.21-29 (2015).

168. McLean, C.Y.*, et al.* GREAT improves functional interpretation of cis-regulatory regions. *Nat Biotechnol* **28**, 495-501 (2010).

169. Machanick, P. & Bailey, T.L. MEME-ChIP: motif analysis of large DNA datasets. *Bioinformatics* **27**, 1696-1697 (2011).

170. Bailey, T.L.*, et al.* MEME SUITE: tools for motif discovery and searching. *Nucleic Acids Res* **37**, W202-208 (2009).

171. Buske, F.A., Bodén, M., Bauer, D.C. & Bailey, T.L. Assigning roles to DNA regulatory motifs using comparative genomics. *Bioinformatics* **26**, 860-866 (2010).

172. Piga, R., Naito, Y., Kokura, S., Handa, O. & Yoshikawa, T. Short-term high glucose exposure induces monocyte-endothelial cells adhesion and transmigration by increasing VCAM-1 and MCP-1 expression in human aortic endothelial cells. *Atherosclerosis* **193**, 328-334 (2007).

173. Naito, T., Oikawa, S., Kotake, H., Hayasaka, K. & Toyota, T. Effect of glucose concentration on foam cell formation in THP-1 cells. *J Atheroscler Thromb* **8**, 55-62 (2001).

174. de Alteriis, E., Cartenì, F., Parascandola, P., Serpa, J. & Mazzoleni, S. Revisiting the Crabtree/Warburg effect in a dynamic perspective: a fitness advantage against sugar-induced cell death. *Cell Cycle* **17**, 688-701 (2018).

175. Malide, D., Davies-Hill, T.M., Levine, M. & Simpson, I.A. Distinct localization of GLUT-1, -3, and -5 in human monocyte-derived macrophages: effects of cell activation. *Am J Physiol* **274**, E516-526 (1998).

176. Johnson, A.R., Freemerman, A.J., Abel, D.E., Rathmell, J. & Makowski, L. Glucose metabolism is linked to the inflammatory status of macrophages. Vol. 6 62 (BMC Proc., 2012).

177. Libby, P. Inflammation in atherosclerosis. *Arterioscler Thromb Vasc Biol* **32**, 2045-2051 (2012).

178. Huber, S.A., Sakkinen, P., Conze, D., Hardin, N. & Tracy, R. Interleukin-6 exacerbates early atherosclerosis in mice. *Arterioscler Thromb Vasc Biol* **19**, 2364-2367 (1999).

179. Ohta, H.*, et al.* Disruption of tumor necrosis factor-alpha gene diminishes the development of atherosclerosis in ApoE-deficient mice. *Atherosclerosis* **180**, 11-17 (2005).

180. Merhi-Soussi, F.*, et al.* Interleukin-1 plays a major role in vascular inflammation and atherosclerosis in male apolipoprotein E-knockout mice. *Cardiovasc Res* **66**, 583-593 (2005).

181. Herder, C., Dalmas, E., Böni-Schnetzler, M. & Donath, M.Y. The IL-1 Pathway in Type 2 Diabetes and Cardiovascular Complications. *Trends Endocrinol Metab* **26**, 551-563 (2015).

182. Tannahill, G.M.*, et al.* Succinate is an inflammatory signal that induces IL-1β through HIF-1α. *Nature* **496**, 238-242 (2013).

183. Sanchez, W.Y.*, et al.* Dichloroacetate inhibits aerobic glycolysis in multiple myeloma cells and increases sensitivity to bortezomib. *Br J Cancer* **108**, 1624-1633 (2013).

184. Herbin, O.*, et al.* Monocyte Adhesion and Plaque Recruitment During Atherosclerosis Development Is Regulated by the Adapter Protein Chat-H/SHEP1. *Arterioscler Thromb Vasc Biol* **36**, 1791-1801 (2016).

185. Luo, Y.*, et al.* Macrophagic CD146 promotes foam cell formation and retention during atherosclerosis. *Cell Res* **27**, 352-372 (2017).

186. Nandy, D., Janardhanan, R., Mukhopadhyay, D. & Basu, A. Effect of hyperglycemia on human monocyte activation. *J Investig Med* **59**, 661-667 (2011).

187. Khan, A.U.H.*, et al.* The PDK1 Inhibitor Dichloroacetate Controls Cholesterol Homeostasis Through the ERK5/MEF2 Pathway. *Sci Rep* **7**, 10654 (2017).

188. Yancey, P.G., Miles, S., Schwegel, J. & Jerome, W.G. Uptake and trafficking of mildly oxidized LDL and acetylated LDL in THP-1 cells does not explain the differences in lysosomal metabolism of these two lipoproteins. *Microsc Microanal* **8**, 81-93 (2002).

189. Wang, M.D.*, et al.* Different cellular traffic of LDL-cholesterol and acetylated LDL-cholesterol leads to distinct reverse cholesterol transport pathways. *J Lipid Res* **48**, 633-645 (2007).

190. Steinberg, D. The LDL modification hypothesis of atherogenesis: an update. *J Lipid Res* **50 Suppl**, S376-381 (2009).

191. Klein, R.L., Laimins, M. & Lopes-Virella, M.F. Isolation, characterization, and metabolism of the glycated and nonglycated subfractions of low-density lipoproteins isolated from type I diabetic patients and nondiabetic subjects. *Diabetes* **44**, 1093-1098 (1995).

192. Chacko, B.K., Scott, D.W., Chandler, R.T. & Patel, R.P. Endothelial surface N-glycans mediate monocyte adhesion and are targets for anti-inflammatory effects of peroxisome proliferator-activated receptor γ ligands. *J Biol Chem* **286**, 38738-38747 (2011).

193. Bradfield, P.F., Johnson-Léger, C.A., Zimmerli, C. & Imhof, B.A. LPS differentially regulates adhesion and transendothelial migration of human monocytes under static and flow conditions. *Int Immunol* **20**, 247-257 (2008).

194. Kanter, J.E. & Bornfeldt, K.E. Inflammation and diabetes-accelerated atherosclerosis: myeloid cell mediators. *Trends Endocrinol Metab* **24**, 137-144 (2013).

195. Schisano, B., Tripathi, G., McGee, K., McTernan, P.G. & Ceriello, A. Glucose oscillations, more than constant high glucose, induce p53 activation and a metabolic memory in human endothelial cells. *Diabetologia* **54**, 1219-1226 (2011).

196. Lenzen, S. The mechanisms of alloxan- and streptozotocin-induced diabetes. *Diabetologia* **51**, 216-226 (2008).

197. Tessaro, F.H.G., Ayala, T.S., Nolasco, E.L., Bella, L.M. & Martins, J.O. Insulin Influences LPS-Induced TNF-α and IL-6 Release Through Distinct Pathways in Mouse Macrophages from Different Compartments. *Cell Physiol Biochem* **42**, 2093-2104 (2017).

198. Wen, Y.*, et al.* Elevated glucose and diabetes promote interleukin-12 cytokine gene expression in mouse macrophages. *Endocrinology* **147**, 2518-2525 (2006).

199. Devaraj, S.*, et al.* Increased monocytic activity and biomarkers of inflammation in patients with type 1 diabetes. *Diabetes* **55**, 774-779 (2006).

200. Vikramadithyan, R.K.*, et al.* Human aldose reductase expression accelerates diabetic atherosclerosis in transgenic mice. *J Clin Invest* **115**, 2434-2443 (2005).

201. Moreno, P.R.*, et al.* Coronary composition and macrophage infiltration in atherectomy specimens from patients with diabetes mellitus. *Circulation* **102**, 2180-2184 (2000).

202. Kolodgie, F.D.*, et al.* Intraplaque hemorrhage and progression of coronary atheroma. *N Engl J Med* **349**, 2316-2325 (2003).

203. Wesley, R.B., Meng, X., Godin, D. & Galis, Z.S. Extracellular matrix modulates macrophage functions characteristic to atheroma: collagen type I enhances acquisition of resident macrophage traits by human peripheral blood monocytes in vitro. *Arterioscler Thromb Vasc Biol* **18**, 432-440 (1998).

204. Doran, A.C., Meller, N. & McNamara, C.A. Role of smooth muscle cells in the initiation and early progression of atherosclerosis. *Arterioscler Thromb Vasc Biol* **28**, 812-819 (2008).

205. Schnoor, M.*, et al.* Production of type VI collagen by human macrophages: a new dimension in macrophage functional heterogeneity. *J Immunol* **180**, 5707-5719 (2008).

206. Weitkamp, B., Cullen, P., Plenz, G., Robenek, H. & Rauterberg, J. Human macrophages synthesize type VIII collagen in vitro and in the atherosclerotic plaque. *FASEB J* **13**, 1445-1457 (1999).

207. Newby, A.C. Metalloproteinase production from macrophages - a perfect storm leading to atherosclerotic plaque rupture and myocardial infarction. *Exp Physiol* **101**, 1327-1337 (2016).

208. Voronova, V., Zhudenkov, K., Helmlinger, G. & Peskov, K. Interpretation of metabolic memory phenomenon using a physiological systems model: What drives oxidative stress following glucose normalization? *PLoS One* **12**, e0171781 (2017).

209. Mitroulis, I.*, et al.* Modulation of Myelopoiesis Progenitors Is an Integral Component of Trained Immunity. *Cell* **172**, 147-161.e112 (2018).

210. Engelbertsen, D.*, et al.* IL-1R and MyD88 signalling in CD4+ T cells promote Th17 immunity and atherosclerosis. *Cardiovasc Res* **114**, 180-187 (2018).

211. Nagareddy, P.R.*, et al.* Adipose tissue macrophages promote myelopoiesis and monocytosis in obesity. *Cell Metab* **19**, 821-835 (2014).

212. Cunningham, L.*, et al.* Identification of benzodiazepine Ro5-3335 as an inhibitor of CBF leukemia through quantitative high throughput screen against RUNX1-CBFβ interaction. *Proc Natl Acad Sci U S A* **109**, 14592-14597 (2012).

213. Trogan, E.*, et al.* Laser capture microdissection analysis of gene expression in macrophages from atherosclerotic lesions of apolipoprotein E-deficient mice. *Proc Natl Acad Sci U S A* **99**, 2234-2239 (2002).

214. Cheng, S.C.*, et al.* mTOR- and HIF-1α-mediated aerobic glycolysis as metabolic basis for trained immunity. *Science* **345**, 1250684 (2014).

215. Kohli, L. & Passegué, E. Surviving change: the metabolic journey of hematopoietic stem cells. *Trends Cell Biol* **24**, 479-487 (2014).

216. Takubo, K.*, et al.* Regulation of glycolysis by Pdk functions as a metabolic checkpoint for cell cycle quiescence in hematopoietic stem cells. *Cell Stem Cell* **12**, 49-61 (2013).

217. Maryanovich, M.*, et al.* An MTCH2 pathway repressing mitochondria metabolism regulates haematopoietic stem cell fate. *Nat Commun* **6**, 7901 (2015).

218. Vannini, N.*, et al.* Specification of haematopoietic stem cell fate via modulation of mitochondrial activity. *Nat Commun* **7**, 13125 (2016).

219. Hazra, S.*, et al.* Long-term type 1 diabetes influences haematopoietic stem cells by reducing vascular repair potential and increasing inflammatory monocyte generation in a murine model. *Diabetologia* **56**, 644-653 (2013).

220. Mangialardi, G.*, et al.* Diabetes causes bone marrow endothelial barrier dysfunction by activation of the RhoA-Rho-associated kinase signaling pathway. *Arterioscler Thromb Vasc Biol* **33**, 555-564 (2013).

221. Song, M.J.*, et al.* Epigenome mapping highlights chromatin-mediated gene regulation in the protozoan parasite Trichomonas vaginalis. *Sci Rep* **7**, 45365 (2017).

222. Heinz, S.*, et al.* Simple combinations of lineage-determining transcription factors prime cis-regulatory elements required for macrophage and B cell identities. *Mol Cell* **38**, 576-589 (2010).

223. Novakovic, B.*, et al.* β-Glucan Reverses the Epigenetic State of LPS-Induced Immunological Tolerance. *Cell* **167**, 1354-1368.e1314 (2016).

224. Matsuhashi, T.*, et al.* Activation of pyruvate dehydrogenase by dichloroacetate has the potential to induce epigenetic remodeling in the heart. *J Mol Cell Cardiol* **82**, 116-124 (2015).

225. Moussaieff, A.*, et al.* Glycolysis-mediated changes in acetyl-CoA and histone acetylation control the early differentiation of embryonic stem cells. *Cell Metab* **21**, 392-402 (2015).

226. Voon, D.C., Hor, Y.T. & Ito, Y. The RUNX complex: reaching beyond haematopoiesis into immunity. *Immunology* **146**, 523-536 (2015).

227. Luo, M.C.*, et al.* Runt-related Transcription Factor 1 (RUNX1) Binds to p50 in Macrophages and Enhances TLR4-triggered Inflammation and Septic Shock. *J Biol Chem* **291**, 22011-22020 (2016).

228. Zhang, S.*, et al.* Annexin A2 binds to endosomes and negatively regulates TLR4-triggered inflammatory responses via the TRAM-TRIF pathway. *Sci Rep* **5**, 15859 (2015).

229. Navarro-Montero, O.*, et al.* RUNX1c Regulates Hematopoietic Differentiation of Human Pluripotent Stem Cells Possibly in Cooperation with Proinflammatory Signaling. *Stem Cells* **35**, 2253-2266 (2017).

230. Rapp, M.*, et al.* Core-binding factor β and Runx transcription factors promote adaptive natural killer cell responses. *Sci Immunol* **2**(2017).

231. Hnisz, D., Day, D.S. & Young, R.A. Insulated Neighborhoods: Structural and Functional Units of Mammalian Gene Control. *Cell* **167**, 1188-1200 (2016).

232. Bevington, S.L.*, et al.* Inducible chromatin priming is associated with the establishment of immunological memory in T cells. *EMBO J* **35**, 515-535 (2016).

233. Ouboussad, L., Kreuz, S. & Lefevre, P.F. CTCF depletion alters chromatin structure and transcription of myeloid-specific factors. *J Mol Cell Biol* **5**, 308-322 (2013).

234. Jego, G.*, et al.* Dual regulation of SPI1/PU.1 transcription factor by heat shock factor 1 (HSF1) during macrophage differentiation of monocytes. *Leukemia* **28**, 1676-1686 (2014).

235. Zhang, D.E.*, et al.* Identification of a region which directs the monocytic activity of the colony-stimulating factor 1 (macrophage colony-stimulating factor) receptor promoter and binds PEBP2/CBF (AML1). *Mol Cell Biol* **14**, 8085-8095 (1994).

236. Puig, O.*, et al.* A gene expression signature that classifies human atherosclerotic plaque by relative inflammation status. *Circ Cardiovasc Genet* **4**, 595-604 (2011).

237. Turner, R.J., Bushnell, C.D., Register, T.C. & Sharp, F.R. Gender-dependent correlations of carotid intima-media thickness with gene expression in blood. *Transl Stroke Res* **2**, 171-178 (2011).

238. Webb, N.R.*, et al.* Macrophage-expressed group IIA secretory phospholipase A2 increases atherosclerotic lesion formation in LDL receptor-deficient mice. *Arterioscler Thromb Vasc Biol* **23**, 263-268 (2003).

239. Durst, K.L. & Hiebert, S.W. Role of RUNX family members in transcriptional repression and gene silencing. *Oncogene* **23**, 4220-4224 (2004).

240. Amann, J.M.*, et al.* ETO, a target of t(8;21) in acute leukemia, makes distinct contacts with multiple histone deacetylases and binds mSin3A through its oligomerization domain. *Mol Cell Biol* **21**, 6470-6483 (2001).

241. Fredman, G. & Tabas, I. Boosting Inflammation Resolution in Atherosclerosis: The Next Frontier for Therapy. *Am J Pathol* **187**, 1211-1221 (2017).

242. Pollack, R.M., Donath, M.Y., LeRoith, D. & Leibowitz, G. Anti-inflammatory Agents in the Treatment of Diabetes and Its Vascular Complications. *Diabetes Care* **39 Suppl 2**, S244-252 (2016).

243. Vasamsetti, S.B.*, et al.* Metformin inhibits monocyte-to-macrophage differentiation via AMPK-mediated inhibition of STAT3 activation: potential role in atherosclerosis. *Diabetes* **64**, 2028-2041 (2015).

244. Kelly, B., Tannahill, G.M., Murphy, M.P. & O'Neill, L.A. Metformin Inhibits the Production of Reactive Oxygen Species from NADH:Ubiquinone Oxidoreductase to Limit Induction of Interleukin-1β (IL-1β) and Boosts Interleukin-10 (IL-10) in Lipopolysaccharide (LPS)-activated Macrophages. *J Biol Chem* **290**, 20348-20359 (2015).

245. Sola, D.*, et al.* Sulfonylureas and their use in clinical practice. *Arch Med Sci* **11**, 840-848 (2015).

246. Lamkanfi, M.*, et al.* Glyburide inhibits the Cryopyrin/Nalp3 inflammasome. *J Cell Biol* **187**, 61-70 (2009).

247. Douros, A.*, et al.* Sulfonylureas as second line drugs in type 2 diabetes and the risk of cardiovascular and hypoglycaemic events: population based cohort study. *BMJ* **362**, k2693 (2018).

248. Xu, L.*, et al.* SGLT2 Inhibition by Empagliflozin Promotes Fat Utilization and Browning and Attenuates Inflammation and Insulin Resistance by Polarizing M2 Macrophages in Diet-induced Obese Mice. *EBioMedicine* **20**, 137-149 (2017).

249. Puig-Kröger, A.*, et al.* RUNX/AML and C/EBP factors regulate CD11a integrin expression in myeloid cells through overlapping regulatory elements. *Blood* **102**, 3252-3261 (2003).

250. Fadini, G.P. & Avogaro, A. It is all in the blood: the multifaceted contribution of circulating progenitor cells in diabetic complications. *Exp Diabetes Res* **2012**, 742976 (2012).

251. Asahara, T., *et al.* Isolation of putative progenitor endothelial cells for angiogenesis. *Science* **275**, 964-967 (1997).

252. Ferraro, F., *et al.* Diabetes impairs hematopoietic stem cell mobilization by altering niche function. *Sci Transl Med* **3**, 104ra101 (2011).

253. Bekkering, S., *et al.* Innate immune cell activation and epigenetic remodeling in symptomatic and asymptomatic atherosclerosis in humans in vivo. *Atherosclerosis* **254**, 228-236 (2016).

254. Tzogani, K., *et al.* EMA Review of Panobinostat (Farydak) for the Treatment of Adult Patients with Relapsed and/or Refractory Multiple Myeloma. *Oncologist* **23**, 870 (2018).

255. Maes, T., *et al.* ORY-1001, a Potent and Selective Covalent KDM1A Inhibitor, for the Treatment of Acute Leukemia. *Cancer Cell* **33**, 495-511.e412 (2018).

256. Regensteiner, J.G., *et al.* Sex Differences in the Cardiovascular Consequences of Diabetes Mellitus: A Scientific Statement From the American Heart Association. *Circulation* **132**, 2424-2447 (2015).

257. Tabas, I. & Bornfeldt, K.E. Macrophage Phenotype and Function in Different Stages of Atherosclerosis. *Circ Res* **118**, 653-667 (2016).